Accuracy and precision of stroke volume and left ventricular ejection fraction quantification with handheld echocardiography

Frederique M. de Raat, BSc

October 2021

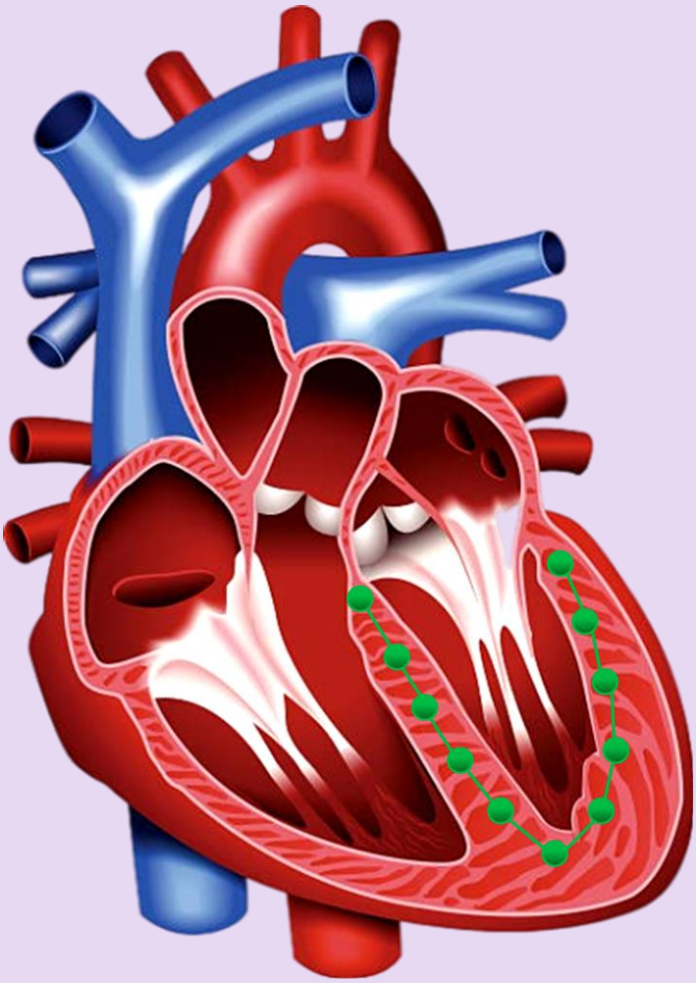

Home institution:
University of Twente
Technical Medicine
Medical Sensing and Stimulation
Netherlands, Enschede

UNIVERSITY OF TWENTE.

Host institution:
Catharina hospital Eindhoven
Department of Anesthesiology
Netherlands, Eindhoven

catharina
een santeon ziekenhuis

Graduation Committee

Prof. dr. ir. C.L. de Korte	Chairman & technical supervisor
Dr. R.A. Bouwman, MD	Medical supervisor
PhD E.C. de Boer	Technical supervisor
Prof. dr. ir. M. Mischi	Technical supervisor
Drs. J. van Houte, MD	Daily and medical supervisor
Drs. R. Krol	Process supervisor

Master Thesis

Accuracy and precision of stroke volume and left ventricular ejection fraction quantification with handheld echocardiography

Frederique M. de Raat

I. List of abbreviations

2DCPA	Two-dimensional cardiac performance analysis
2DE	Two-dimensional echocardiography
3DE	Three-dimensional echocardiography
A2CH	Apical two chamber
A4CH	Apical four chamber
AI	Artificial intelligence
AS	Auto strain
ARP	Absolute refractory period
B-mode	Brightness mode
CMR	Cardiac magnetic resonance
CNN	Convolutional neural network
CO	Cardiac output
CV	Coefficient of variation
CT	Computed tomography
DHM	Dynamic heart model
DICOM	Digital imaging and communication in medicine
ECG	Electrocardiogram
ED	Emergency department
ED frame	End-diastolic frame
EDV	End-diastolic volume
ES	End-systolic
ESV	End-systolic volume
FOV	Field of view
HHE	Handheld echocardiography
HFrEF	Heart failure accompanied by reduced left ventricle ejection fraction
ICC	Intra class correlation
ICU	Intensive care unit
LOA	Limits of agreement
LV	Left ventricle
LVEDD	Left ventricle end-diastolic diameter
LVEDP	Left ventricle end-diastolic filling pressure
LVEF	Left ventricle ejection fraction
LVESD	Left ventricle end-systolic diameter
LVivo	LVivo-EF software is a fully automatic online solution for quantification of cardiac function designed by DIA (*DIA imaging Analysis Ltd., Israel)*
M-mode	Motion-mode
NFC	Near field clutter
NN	Neural network
OR	Operation room
PAC	Pulmonary artery catheter
RC	Repeatability coefficient
SD	Standard deviation
SE	Standard echocardiography
SV	Stroke volume
TEE	Transoesophageal echocardiography
TTE	Transthoracic echocardiography
V_{bi}	Left ventricle volume according to biplane method
V_{2CH}	Left ventricle volume according to the two-chamber view
V_{4CH}	Left ventricle volume according to the four-chamber view

Table of Contents

II. Preface

Beste lezer,

Met trost presenteer ik u mijn master thesis. Hopelijk weet ik u te informeren en te amuseren met het geschreven stuk. Zes jaar geleden ben ik begonnen aan de bachelor technische geneeskunde aan de University of Twente. Hierna heb ik gekozen voor de master medical sensing and stimulation. De afgelopen 10 maanden heb ik stage gelopen in het Catharina ziekenhuis te Eindhoven op de afdeling Anesthesiologie. Het zijn plezierige en leerzame maanden geweest die ik niet had kunnen bewerkstellen zonder de mensen om mij heen. Daarom wil ik graag de volgende mensen bedanken voor hun bijdrage.

Ten eerste Arthur Bouwman voor de tijd en moeite die hij niet alleen heeft gestopt tijdens deze stage maar ook daarvoor. Het verwezenlijken van mijn M3 stage in het Catharina was niet vanzelfsprekend en daarvoor heb ik jouw te danken. Hoe druk jouw agenda ook was, jij maakte tijd. Daarom wil ik jou bedanken voor je tijd en expertise, hier is namelijk heel veel moois uit voortgekomen. Verder wil ik Joris van Houte bedanken voor zijn dagelijkse supervisie. Zowel vakkundig als op persoonlijk vlak heb ik veel van jou kunnen leren. Je deur stond altijd open. Ik vond de samenwerking zeer prettig, jouw visie en aanmoediging gaf rust en vertrouwen, dankjewel daarvoor. Ook wil ik Esmée de Boer bedanken voor haar technisch geneeskundige begeleiding. Jouw kennis en kunde als technisch geneeskundige waren zeer waardevol, feedback bracht mij dan ook altijd op ideeën. Maar naast vakkundige toevoeging waren de wandelingen samen ook altijd gezellig en een bron van ontspanning. Daarnaast wil ik, Chris de Korte bedanken voor zijn rol als technisch begeleider en voorzitter. We hebben elkaar niet vaak gesproken maar jouw ervarenheid en kennis brachten inzichten en hielden me scherp, dankjewel daarvoor. Verder wil ik ook Massimo Mischi bedanken, het inplannen van een gezamenlijk moment was niet altijd een gegeven maar toch werd er tijd gemaakt, dankjewel voor het delen van je kennis. Tevens wil ik Ruby Krol, als proces begeleider bedanken. Ook al ben je midden in het proces gevallen, vanaf het begin af aan heb ik mij gehoord gevoeld. Dankjewel voor je open en eerlijkheid. Daarnaast wil ik ook Maurice Keulen bedanken voor zijn tijd en moeite als buitenlid van de commissie.

Verder zijn er nog een aantal mensen die ik wil bedanken die niet deel uitmaken van mijn afstudeer commissie maar wel degelijk toevoeging hebben gehad aan mijn leerproces. Om te beginnen, wil ik Peter Bingley bedanken voor alle tips en hulp die je mij hebt aangeboden. Jouw gezelschap hielp mij niet alleen verder in het denkproces maar bovenal bracht het mij ook een stuk gezelligheid en dat mag zeker niet ontbreken. Daarnaast wil ik ook de cardiologen Suzanne Felix en Sjoerd Bouwmeester bedanken. Alle echo's die jullie samen met de laboranten hebben gemaakt, het zijn er bijna te veel om op te noemen. Dus ook richting de laboranten, bedankt! Ondanks jullie drukke planning op een dag, was er tijd en ruimte, dankjewel daarvoor. Verder wil ik Sjoerd bedanken voor de tijdrovende inclusie die heeft plaatsgevonden en het betrekken van de Lumify in zijn eigen studie. Ook jouw wil ik bedanken voor de tijd en de moeite die je hierbij hebt gedaan om mij te helpen. Mijn intervisie groepje wil ik bedanken voor alle leuke wandelingen en etentjes waarin we elkaar hielpen om te reflecteren op zowel de leuke als mindere momenten. De afgelopen twee jaar hebben jullie mij geholpen om verder te komen, dankjewel voor het luisterende oor en de nieuwe inzichten.

Tenslotte wil ik mijn familie en vrienden bedanken, met name mijn vader en moeder, jullie hebben mij het vertrouwen en de steun gegeven die ik nodig had, heel erg bedankt.

Ik wens jullie veel lees plezier,
Met vriendelijk groet,

Frederique de Raat

III. Abstract

Background: Reliable quantification of stroke volume (SV) and left ventricle ejection fraction (LVEF) for assessment of left ventricle (LV) function is essential for point of care assessment in hemodynamically compromised patients. However, user-independent non-invasive bedside quantification of SV and LVEF is yet not feasible. By incorporating an online quantification tool (LVivo, DIA) in a handheld echocardiography (HHE) device (Lumify, Philips Healthcare), bedside quantification of LV function is among the possibilities.

Methods: Thirty-six patients were scanned with HHE, standard echocardiography (SE) and three-dimensional echocardiography (3DE). HHE and SE images were analysed with three different quantification tools: LVivo, Auto Strain (AS) and two-dimensional cardiac performance analysis (2DCPA). Segmental endocardial border delineation was scored (2 = good, 1 = poor, 0 = invisible) to assess HHE and SE image quality. Assessments of LV volumes and ejection fraction were compared.

Results: The mean endocardial visibility grades were 10.49 ± 1.7 with SE and 9.42 ± 2.0 with HHE ($P < 0.001$). Correlation, bias, and LOA between SE (AS) and HHE (AS) for ejection fraction, and SV assessment was r = 0.71, bias = 1.60%, LOA = 8.84% and r = 0.85, bias = 1.32 ml, LOA = 15.54 ml respectively. LVivo (HHE) showed the highest correlation with AS (HHE) (r = 0.89; 0.84; 0.84; 0.69 for EDV, ESV, SV and LVEF, respectively). There was no agreement between any quantification tool or between HHE and SE measurements in comparison to 3DE measurements.

Conclusion: Lumify shows great potential for LVEF quantification and monitoring of SV in point of care settings. Quantification comparisons showed no agreement between any of the three quantification tools.

IV. Rationale

At the intensive care unit (ICU) of the Catharina hospital, patients with various severe medical conditions are taken care of. Some of the more frequent cases are patients who show sepsis, shock, heart failure, trauma or respiratory distress. Most of these patients need evaluation of their hemodynamic status. Left ventricular (LV) systolic function is an essential clinical parameter in hemodynamically and respiratory compromised ICU patients to guide fluid therapy and the administration of inotropes and vasopressors.[1] Indices used to assess LV performance are based on the capacity of the heart to pump blood, its ability to generate force and the degree of chamber shortening. Based on these concepts, devices to estimate stroke volume (SV) and LV ejection fraction (LVEF) have been developed over the last several decades to quantify LV performance.

For decades, the clinical reference standard for cardiac output (CO) monitoring has been the use of a transpulmonary artery catheter (PAC) based on the concept of thermodilution.[2] However, SV monitoring with PAC requires central venous access, with the risk of complications such as catheter-related infections, haemorrhage or, pneumothorax.[3] As not all ICU patients require an arterial and/or central venous line, the need for a reliable, non-invasive, readily available, accurate, and time-efficient LV function monitoring technique for the ICU, operation room (OR) and emergency department (ED) is growing. Moreover, the invasiveness of the technique should always be kept minimal for quick and easy information extraction. Particularly in situations in which rapid patient assessment is required, such as in point of care situations.

The first-choice technique to quantify LV function is two-dimensional echocardiography (2DE). It is considered the standard echocardiography (SE) approach since it is fully integrated into routine clinical practice. Besides 2DE, there is cardiac magnetic resonance (CMR) and cardiac computed tomography (CT), which are less frequently used due to high costs and prolonged acquisition time. However, both provide non-user dependent and reproducible estimates of LVEF. Nevertheless, none of those mentioned above methods is feasible as point of care examination since they are both time inefficient and not available at the bedside due to the size of the device. Estimation of LVEF during point of care treatment requires a quick, efficient, non-invasive, and reliable method.

Handheld echocardiography (HHE) is one of the most promising imaging techniques in point of care for critically ill patients.[4] Cardiac function and hemodynamics could be assessed non-invasively at the bedside using an HHE device and provide information that helps clinicians in adequate clinical decision making in ICU patients. According to previous literature, HHE devices correlate well with SE devices when assessing LVEF. [5]

There are various HHE devices on the market. However, there is a lack of information about the actual performance of quantifying cardiac volumes such as end-diastolic volume (EDV), end-systolic volume (ESV) and SV. For a few years, the Lumify S4-1 probe (*Philips, Health Care*) has been on the market. For clinical implementation at the ICU or for routine use at the OR, or ED in the future, it would be valuable to have quantitative data about the performance of the Lumify HHE device. Therefore, we pose the following research question:

How does quantification of LVEF, EDV, ESV and SV with the Lumify HHE device correlate and agree with SE?

To answer this question, we designed a study in which an HHE device (Lumify, Philips Healthcare) is evaluated against a high-quality reference SE device (*EPIQ, Philips Healthcare*). Therefore, the following sub-questions were formulated to answer this question:

- *How does HHE perform compared to a high SE device? Performance will be assessed by determining the correlation, accuracy, and precision of EDV, ESV, SV and LVEF measurements.*

- *How is the image quality of HHE compared to a high SE device?*

Bedside quantification of SV and LVEF with HHE devices is not yet possible. It is conducted through visual estimation (eyeballing), with clinical experience levels varying across point of care settings.[6] Therefore, achieving reliable LVEF estimations in point of care settings can be challenging.

The newly designed LVivo-EF software (*DIA imaging Analysis Ltd., Israel*) for HHE devices addresses this challenge by quickly and efficiently providing clinicians with LVEF- and volume measurements at the bedside (online) via advanced artificial intelligence (AI) technology and advanced pattern recognition algorithms. The algorithm combines image processing and a Deep Learning Neural Network (NN) for the LV function analysis.

Conventional interpretation of echocardiographic images relies heavily on the process of pattern recognition by the human brain. Deep learning NN can be trained with this pattern recognition from large data sets and make accurate predictions on newly unknown input data. Deep learning NN can also overcome the human limitations of fatigue or distraction and inter- and intra-observer variability. Besides the heavy reliance on pattern recognition by the human brain, interpretation of echocardiograms can be very subjective. AI tackles this problem as it has the potential to extract information that is not apparent to the observer. AI-based solutions such as the LVivo software are increasingly being adopted to automate workflows and assist clinicians with objective clinical indications to support their decision-making process. However, the performance of the newly designed LVivo software compared to other conventional quantification tools used at the office (offline) is unknown. Therefore, we came up with the following research questions:

How does LVivo perform compared to other echocardiographic quantification tools?

The following sub-questions were formulated to answer this question:

- *How does LVivo perform compared to a high standard **automatic offline** cardiac quantification tool? Performance will be assessed by determining the correlation, accuracy and precision of EDV, ESV, SV and LVEF measurements for both quantification tools.*
- *How does LVivo perform compared to a high standard **manual offline** cardiac quantification tool? Performance will be assessed by determining the correlation, accuracy and precision of EDV, ESV, SV and LVEF measurements for both quantification tools.*

It is known that SE derived LV chamber sizes are consistently underestimated compared to the gold standard CMR derived values.[7] In contrast, three-dimensional echocardiography (3DE) has the advantages of full-volume acquisition with established accuracy and reproducibility and has shown superior correlation with CMR.[7] Therefore, it is interesting to know how the HHE device correlates based on its consistency and agreement with 3DE. Resulting in the following research question:

How does HHE perform based on correlation, accuracy and precision compared with 3DE?

To answer this question, the results of the quantification of EDV, ESV, SV and LVEF for HHE images with all three quantification tools are compared with 3DE quantifications.

With these three main research questions, we strive to gain more insight into the functioning of the Lumify HHE device for the quantification of LV function. Hence, this graduation research contributes to optimizing point of care treatment for patients at the ICU, OR and ED.

This thesis consists of several chapters. In the first section, the theoretical background (VI.), several relevant concepts are elaborated to get more insight into the research problem. The first part of the theoretical background focuses on the cardiovascular system's anatomy, physiology, and pathophysiology. The second part describes the technical aspects, such as ultrasound physics and the basics of artificial intelligence. With this knowledge, the reader should understand the relevant concepts to continue onwards to the introduction (VII.). With the introduction, the main problem and the proposed solution are explained. Subsequently, the study design and results are described in the methods (VIII.) and results (IX.) section, respectively. Next, based on the results and previous literature, a summary analysis regarding the clinical implementation is given in the discussion (X.) section. Finally, the thesis ends with a conclusion (XI). Supplemental material can be found in the appendices (XIII. till XV.).

V. Theoretical background

In this chapter, the theoretical framework is described. With the theoretical framework, an understanding of relevant concepts to the topic of research is demonstrated. The goal of this chapter is to define concepts and evaluate relevant theories and models.

A. Cardiac vascular anatomy and physiology

The cardiovascular system maintains the delivery of nutrients and oxygen to all body organs and ensures homeostasis at the cellular level. The heart is a crucial component of the cardiovascular system. The heart has nearly the same size as the fist of an adult and weighs around 300g.[8], [9] It is embedded in the mediastinum between the lungs and continues downwards on the left lateral side between the second and fifth intercostal space. The heart is enfolded in the pericardium, which protects the heart. At the fifth intercostal space on the left side, rhythmic pumping of the heart can be heard and felt. The heart's rhythmic pumping has the purpose of maintaining a continuous blood flow through the human body. The heart itself is supplied by rich oxygenated blood through the coronary circulation. The major vessels of the coronary circulation are the left main coronary artery, which divides into the left anterior descending and circumflex artery and the right coronary artery.[10] The right and left coronary arteries emerge from vascular openings at the base of the aorta, called the coronary Ostia.[11] Figure 1 shows a schematic illustration of the perfusion territories of the three major coronary arteries. The small arteries and arterioles are the primary sites of vascular resistance and, therefore, the primary site for blood flow regulation. Eventually, the arterioles branch into numerous capillaries close to the cardiac myocytes. Adequate oxygen delivery to the myocytes and the removal of waste products from the cell are enabled by a high capillary-to-cardiomyocyte ratio and short diffusion.

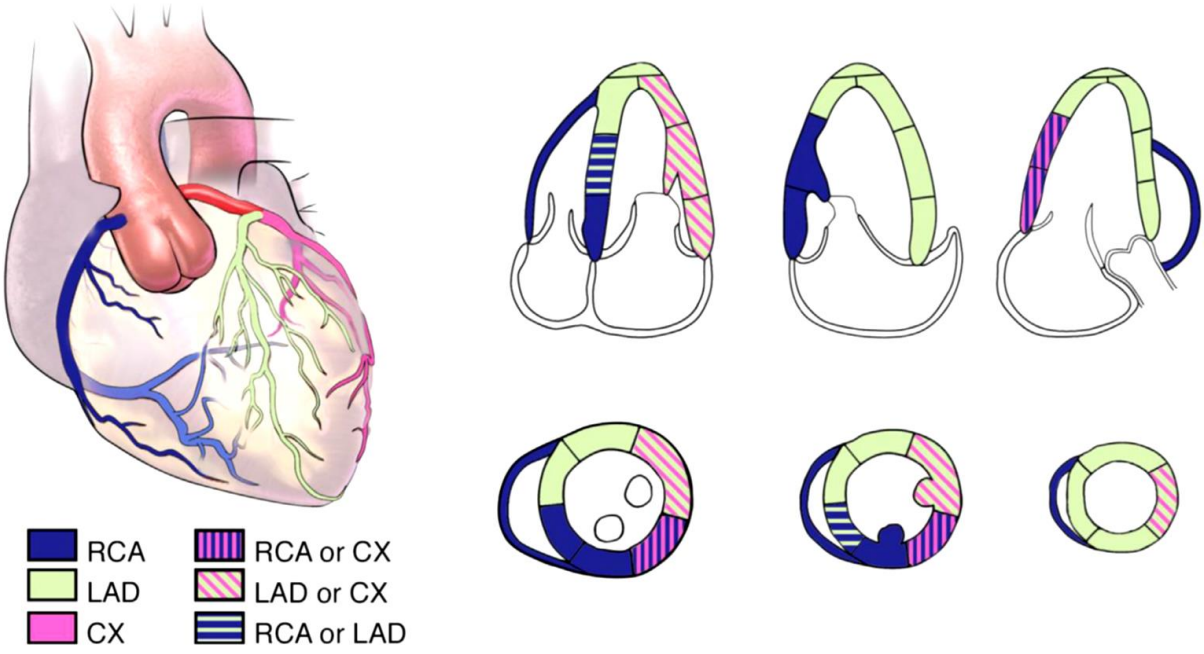

Figure 1. Typical distributions of the right coronary artery, the left anterior descending coronary artery, and the circumflex coronary artery. The arterial distribution varies among patients. Some segments have variable coronary perfusion. [49]

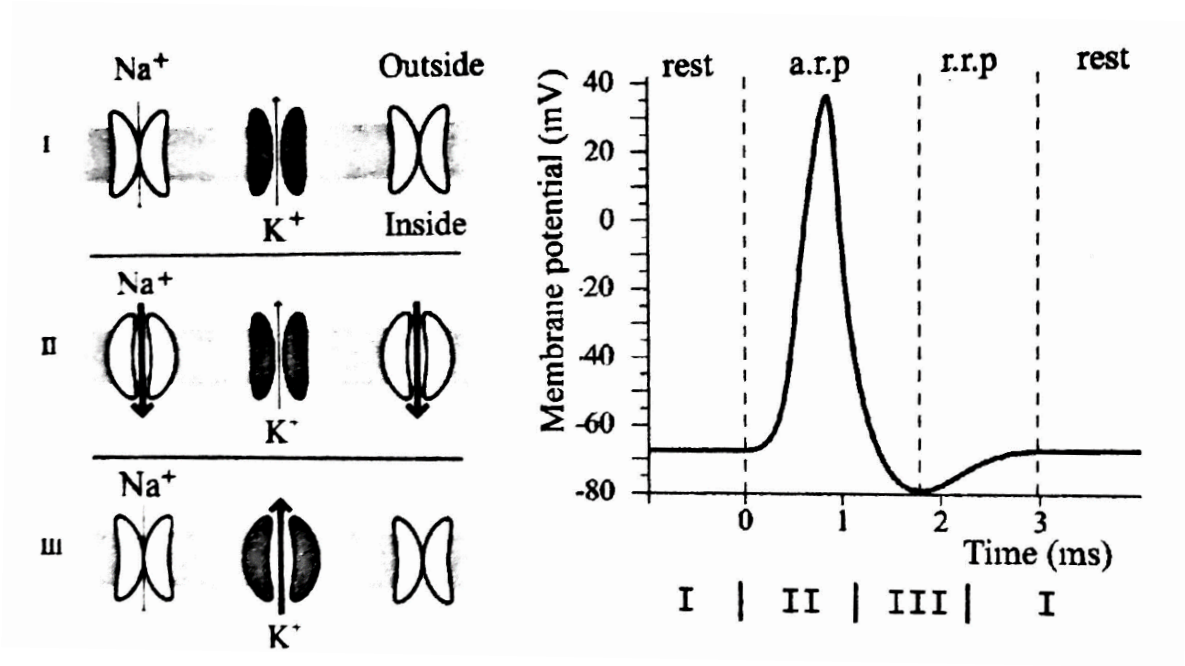

Figure 2. Left: Illustration of the action potential generation, with concurrent changes in the permeability of sodium and potassium. Right: corresponding change in transmembrane voltage. In rest, the potassium conductance is about a hundred times larger than the sodium conductance, which explains why the cell in rest is near the Nernst potential of Potassium (I). At the start of the action potential, the sodium permeability strongly increases (II). There is an undershoot in the membrane voltage during repolarization due to a temporary increase in potassium conductance (III). Immediately following the beginning of the action potential, the cell membrane is in the absolute refractory period, during which the cell is insensible for any stimulus. The absolute refractory period is followed by the relative refractory period, during which a new action potential can be generated only with a stimulus strength much larger than the threshold during the rest membrane potential.

Cardiac contraction is regulated by an electrical conduction system that coordinates the contraction of the atria and ventricles of the heart. The cardiac conduction pathway starts with the spontaneous generation of an action potential generated by the sinoatrial node. First, the atria contract and then the electrical stimulus travels down through the atrioventricular (AV) node. Next, the action potential is slowed down at the AV node before travelling along with the bundle of His, which divides into the left and right bundle branches. Finally, the bundle branches divide into the Purinkje fibres, which allow the ventricles to contract simultaneously. The Purinkje fibres are located in the sub endocardium and consist of electrically excitable cells.

$$(1)\ V_{GHK} = \frac{kT}{q} ln \frac{P_K[K^+]_o + P_{Na}[K^+]_o + P_{Cl}[K^+]_i}{P_K[K^+]_i + P_{Na}[K^+]_i + P_{Cl}[K^+]_o}$$

As can be seen with the Goldman-Hodgkin-Katz equation (1), the main factors that determine the value of the cell membrane potential are the concentration gradients of sodium, potassium and chloride. Excitable cells, such as cardiac myocytes, have the property that they can quickly change the permeability for certain ion species after applying an adequate stimulus. This leads to a depolarization of the cell membrane and the generation of an action potential. The process can be described as follows. After applying an adequate stimulus, the permeability of the cell membrane for sodium ions increases and, if the strength of the stimulus is sufficient, the threshold is reached. This causes the permeability for sodium ions to increase quickly further, to a value many orders of magnitude larger than the permeability's of the other ions species, especially potassium. Due to this process, the cell membrane potential will reach a value close to the Nernst potential of Sodium, which is about + 60 [mV].[12] After about 0.3-1 [ms], the increase in the permeability for potassium leads to repolarization of the cell membrane.[12] This cycle is illustrated in Figure 2.

Cellular depolarization leads to the excitation and contraction coupling of actin and myosin in the sarcomere.[13] This reciprocal action of actin and myosin together results in the shortening of thousands of sarcomeres and eventually into macroscopically cardiac contraction. The three-dimensional (3D) arrangement of myocardial fibre bundles in the ventricular myocardium is complex, with fibres arranged to optimize the efficiency of cardiac contraction. [15] Most cardiac myofibers are oriented in the circumferential direction, with a proportionally smaller number oriented in a longitudinal direction (Figure 3).[16] The circumferential to longitudinal fibres ratio is approximately 10:1, with a higher proportion of circumferential fibres at the base and a lower proportion at the cardiac apex.[16] The orientation of cardiac fibres permits the heart to contract in the radial direction and shorten its length.[15] Normal functioning of these mechanics is essential for systolic and diastolic function, and disturbed function can lead to many pathologies that affect the left ventricular function. It is known that impairment of longitudinal function is an early marker of left ventricular dysfunction.[17] Reduced LV function can lead to reduced CO as SV decreases, formula (2).

$$(2)\ CO = SV \times HR$$

$$(3)\ SV = EDV - ESV$$

SV is calculated as the difference between EDV and ESV, formula (3). High-pressure baroreceptors in the left ventricle, aortic arch, and carotid sinus detect reductions in CO and respond by increasing their afferent signalling to the vasomotor centre in the central nervous system.[18] Activation of the vasomotor centre results in increased activity in efferent sympathetic pathways. Increased activity of the sympathetic pathways leads to, among others, increased secretion of aldosterone, renin and consequently increased concentrations of angiotensin II.[18] This results in elevated blood pressures and retention of salt and water. This subsequently results in increased cardiac preload and, in the long term, volume load and an increased heart rate to maintain a sufficient CO.

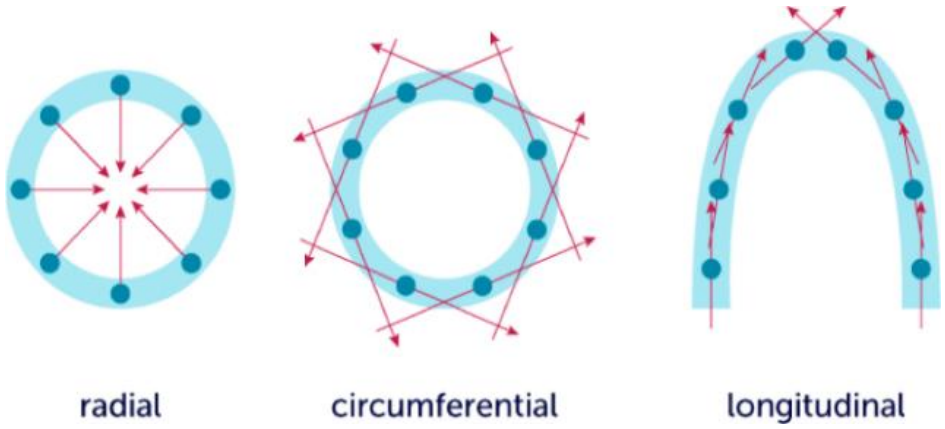

Figure 3. Three different orientation patterns of myocardial contraction

1. Cardiac output & Stroke Volume

CO is a well-established hemodynamic parameter at the Intensive Care Unit (ICU) for monitoring global cardiac function.[19] As shown in formula (2), the CO depends on the SV and heart rate. The SV is determined by the preload and afterload of the heart and the contractility. Afterload is described as the heart's pressure to eject blood during systole and is proportional to the mean arterial pressure (MAP). If aortic and pulmonary pressures increase, the afterload will also increase for the left and right ventricle, respectively. Preload is the amount of sarcomere stretch at the end of ventricular filling during diastole. Myocardial contractility, also known as the inotropy of the heart, represents the cardiac muscle's ability to contract. The effect of afterload, preload and contractility on the SV can be further explained by the Frank-Starling curves, shown in Figures 4A and 4B.[20]

The strength of ventricular contraction increases due to increased stretching of the ventricle prior to contraction, caused by an increased venous return.[21] If venous return increases, the ventricular filling (EDV) also increases, leading to increased left ventricular end-diastolic pressure (LVEDP). This leads to the stretching of cardiac myocytes, increasing the sarcomere length. This causes an increase in force generation prior to contraction, enabling the heart to eject the additional venous return, thereby increasing SV.

With the Frank-Starling curve, the effect of changes in preload on the isometric tension development is illustrated. The magnitude and slope of the active tension curve at a given preload depend upon the muscle's inotropic state and vascular resistance.[20] For example, the tension curve shifts upwards if the inotropy is increased by administering dobutamine (Figure 4A). The force-velocity relationship describes how an isolated muscle fibre contraction is affected by afterload.[23] Experiments have shown that the greater the afterload, the slower the length of shortening due to increased vascular or pulmonary resistance. In combination with the length-tension relationship, it can be found that if preload increases at a given afterload, cardiac muscle fibres will have an increased velocity.[24] So, if preload increases, the maximal isometric force and the shortening velocity increase.[24] Changes in inotropy also alter the force-velocity relationship. If inotropy increases of the cardiac muscles, the maximal fibre shortening velocity and the maximal isometric force increase.

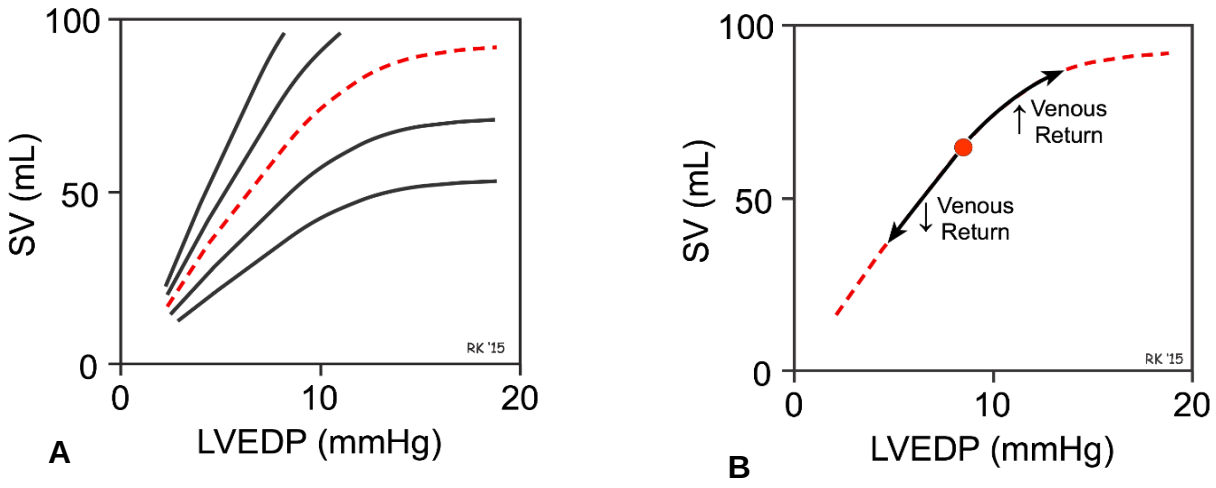

Figure 4. A) Frank-Starling curve for different afterload and inotropy states. The red dashed curve represents a "normal" ventricular Frank-Starling curve. Increasing afterload or decreasing inotropy shifts the curve down and to the right. Therefore, at a given LVEDP, depressing the curve will result in a lower SV. Decreasing afterload and increasing inotropy shifts the curve up and to the left. Therefore, at a given LVEDP, shifting the Frank-Starling curve up and to the left will result in a greater SV at a given LVEDP. B) Frank-Starling curve influenced by venous return, the ventricle responds to changes in venous return and ventricular filling based on the unique curve for those conditions.[21]

2. Left ventricular ejection fraction

Assessment of the LV function is essential for driving various treatment strategies in point of care settings, particularly at the ED, ICU, and perioperative care.[25] Studies have shown that LV function correlates with symptoms, prognosis, events, and complications in many conditions.[26] LVEF is the fundamental measure of left ventricular systolic function.[27] LVEF is the fraction of chamber volume ejected in systole (SV) in relation to the total volume of the blood in the ventricle at the end of diastole (EDV). Quantitative evaluation of the LVEF requires the measurement of ESV and EDV. LVEF quantification traditionally relies on tracing the endocardial boundaries at the two phases of the cardiac cycle, followed by model-based calculations. LVEF is calculated by the following formula (4):

$$(4)\ Left\ ventricular\ ejection\ fraction\ (\%) = \frac{EDV - ESV}{EDV} \times 100$$

B. Pathophysiology

Heart failure is a common cardiovascular disease that affects more than 5 million people in the US and covers $10-38 billion of medical costs per year.[28] Heart failure is a clinical syndrome characterized by certain symptoms (e.g. shortness of breath, ankle swelling and fatigue) that can be accompanied by clinical signs (e.g. elevated jugular venous pressure and peripheral oedema) caused by impairment of cardiac function, resulting in a reduced CO.[29] In the early stages of heart failure, several compensatory mechanisms (LV wall thickening, reduced systemic afterload, increased heart rate) occur, leading to minimal symptoms encountered by patients. Although beneficial at heart failure onset, each compensatory mechanism will eventually fail, leading to symptomatic heart failure. There are two main categories of heart failure, diastolic- and systolic heart failure. Systolic heart failure occurs when the heart is unable to contract effectively. Systolic heart failure is accompanied by a reduced EF. The leading cause of heart failure accompanied by reduced left ventricle ejection fraction (HFrEF) is coronary artery disease.[30] The reduced oxygenation of the myocardium caused by coronary artery disease results in ischemia. Cardiac ischemia causes direct damage to the myocardium. This results in inadequate relaxation in diastole and impaired contraction in systole, which decreases contractility, SV and CO. Another cause of HFrEF is valvular heart disease. Aortic- and mitral valve stenosis and/or insufficiency can lead to persistent left-sided volume- or pressure overload, which may lead to HFrEF.[31]

On the contrary, diastolic heart failure occurs when the heart is unable to relax during diastole. The leading cause of diastolic heart failure is chronic hypertension.[32] This leads to hypertrophy of the LV and increases the formation of fibrous tissue, both leading to a decrease in cardiac compliance.[32] Because of the formation of fibrous tissue, the heart gets stiff and bulky, and it cannot fill completely, resulting in a lower SV and CO. However, the systolic function remains, and therefore LVEF is not affected.

C. Cardiovascular monitoring

Cardiovascular monitoring refers to the monitoring of the heart and circulatory functions. In the case of perioperative hemodynamic instability, cardiovascular monitoring is of great importance.[19] Hemodynamic instability in cardiac surgery patients at the OR and ICU is associated with an increased risk of complications and mortality.[25], [33] To improve patient outcomes, clinicians focus on adequate hemodynamic monitoring and management. The goal is to optimize the balance between oxygen transport (DO_2) and oxygen consumption (VO_2). In the case of hypoperfusion, tissue oxygenation decreases, and the patient is at risk of entering a state of shock which can lead to organ failure. Therefore, cardiovascular monitoring in critically ill patients is essential for diagnostic and therapeutic management. Assessing LVEF, SV, and CO are vital components in this. Several cardiovascular monitoring devices are on the market to obtain these variables, ranging from fully invasive to completely non-invasive.

1. Cardiovascular monitoring techniques

Many devices are currently available for monitoring CO. The technique of choice depends on the patient's conditions, the clinical setting, and the local infrastructure. Moreover, the invasiveness of the technique should always be kept to a minimum for quick and easy information extraction and for minimizing patient discomfort and risk. Particularly in situations in which rapid assessment of the patient is required.

Invasive methods

Since 1970, the thermodilution method with the Pulmonary Artery Catheter (PAC) has been regarded as the golden standard for measuring CO.[2], [33], [34] However, this method is not an actual continuous CO monitoring device as it presents the CO of five minutes ago. Besides CO measurements, the PAC enables to obtain the pulmonary artery pressure, systemic and pulmonary vascular resistance and the DO_2 and VO_2. Nevertheless, usage of the PAC thermodilution method has decreased because of its invasiveness and associated complications.

Semi-invasive methods

For estimating CO in a semi-invasive way, transpulmonary thermodilution and pulse wave analysis have been established. Transpulmonary thermodilution is a variant of the PAC method in which a saline bolus is given through a central venous catheter. A temperature change is detected by a sensor placed in the femoral artery. However, the use of this method in patients with body temperature variations or intracardiac shunts is questionable.[3] The information that is extracted from the blood pressure wave form is calculated into a beat-to-beat SV. Besides CO monitoring, the pulse pressure variation or SV variation can be calculated, which helps to guide fluid therapy. The main disadvantage of a transpulmonary thermodilution system is that precision and reliability decrease in patients characterized by changes in volume and vascular tone.[34]

Non – invasive methods

There are several non-invasive methods to monitor CO, among which is the volume clamping method. With the volume clamping method, a cuff is placed around the middle phalanx of a finger, and the arterial blood pressure is measured.[35] From the arterial finger pressure, the brachial pressure is reconstructed. Finally, the pulse contour method is used to estimate CO. However, previous studies have shown that the volume clamping method is not very precise nor accurate.[36], [37] A more frequently used non-invasive method is echocardiography. Echocardiography is considered the first-line standard technique for estimating the LV function at the bedside of the patient.[38] It allows minimally invasive (transesophageal echocardiography, TEE) or non-invasive (transthoracic echocardiography, TTE) assessment of cardiac function. Moreover, echocardiography provides the physician with a rapid and accurate diagnosis of hemodynamic instability in critically ill patients.[39] In the following chapters, the ultrasound technique is further explained.

D. Echocardiography

In 1947 the first diagnostic ultrasound image was made of a living human being, recorded by Karl Theo Dussik. Inge Edler and C. Hellmuth Hertz first described the possibility of using ultrasound imaging to visualize the heart.[40] To be able to interpret an ultrasound image, a physical understanding of acoustic wave reflection is valuable. Ultrasound uses acoustic waves with a frequency around 2-15 MHz and is produced by so-called transducers. An acoustic wave is a travelling pressure disturbance that produces alternating compression and expansion of the tissue. The compression and expansion displace the incremental volumes of the tissue and in this way the wave propagates via transfer of momentum among different incremental volumes.[41] Each incremental volume of the tissue undergoes small oscillations around its original position but does not travel with the pressure wave.[42]
A pressure plane wave, p(x,t), moving along one spatial dimension, x, through a homogenous, non-attenuating fluid medium can be formulated starting from Euler's equation (5) and the equation of continuity (6). Combining the Euler equation and the equation of continuity results in the acoustic wave equation (7).[43]

$$(5)\ \frac{\partial}{\partial x}p(x,t) + \rho_0 \frac{\partial}{\partial t}u(x,t) = 0$$

$$(6)\ \frac{\partial}{\partial t}p(x,t) + \frac{1}{\kappa}\frac{\partial}{\partial x}u(x,t) = 0$$

$$(7)\ \frac{\partial^2}{\partial x^2}p(x,t) - \frac{1}{c^2}\frac{\partial^2}{\partial t^2}p(x,t) = 0$$

$$(8)\ speed\ of\ sound, c(m/s) = \frac{1}{\sqrt{\rho_0}\kappa}$$

Where $\rho_0(kg/m^3)$ is the density of the medium, and κ (N/m) is the coefficient of stiffness.

The intensity of an acoustic wave characterizes the strength of the wave, which is the average power calculated over a surface perpendicular to the propagation direction.[43] For acoustic plane waves, the intensity, I (W/m^2) is related to the pressure amplitude (P) by:

$$(9)\ I = \frac{P^2}{2\rho_0 c}$$

1. Reflection and transmission of ultrasound waves

An ultrasound transducer can both emit ultrasound waves and detect the ultrasound waves reflected by the tissue. In most cases the elements in ultrasound transducers are made of unique ceramic crystal materials called piezo-electric materials. The piezo-electric effect is described as the process in which crystal deformation causes electrical energy to be generated. In this way, transducers receive ultrasound waves. The inverse piezoelectric effect is described as the process of realignment of the internal dipole structures inside the piezoelectric material caused by applying an electric field to the piezoelectric element.[42] The realignment of the dipole structures results in crystal lengthening or contracting, converting the electrical energy into mechanical energy. In this way the transducer produces ultrasound waves. Using the speed of sound and the time passed between transmitting and receiving the reflected ultrasound wave, the distances between the organ and the transducer is calculated. The bandwidth (frequency spread of an ultrasound pulse) and transducer sensitivity are improved by sandwiching the piezoelectric crystal between a backing layer (or damping layer) and a matching layer.[44] The backing layer absorbs ultrasound waves radiated from the back face of the crystal and damps the reverberations within the crystal, see Figure 5.[40] The matching layer is at the front face of the crystal and reduces the reflection coefficient between the transducer and the tissue. The reflection coefficient will be explained in further detail in the following section.

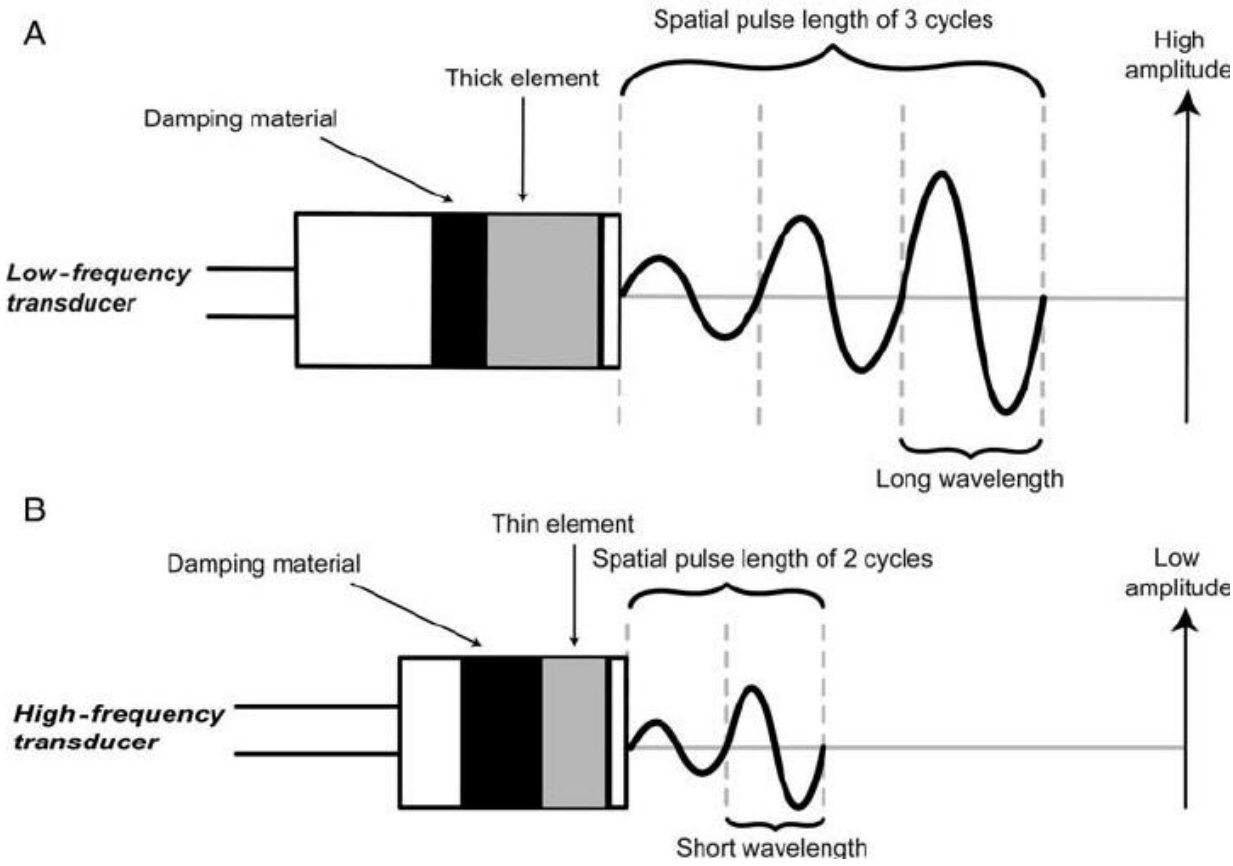

Figure 5. Effect of high vs low frequency transducers on the spatial pulse length (A) Low frequency transducer with long spatial pulse length and low axial resolution. (B) High frequency transducer with short pulse length and high axial resolution.[45]

Acoustic Impedance

Acoustic impedance (Z) is a physical property of tissue defined by the density, ρ $[kg/m^3]$, and the speed of the sound wave, c $[m/s]$.[42] It describes how much resistance an ultrasound beam encounters as it travels through the tissue and can be described with the following formula:

$$(10)\ Z = \rho \times c$$

Acoustic impedance plays a crucial role in medical imaging because the ability of ultrasound to move from one tissue to another entirely depends on the difference in acoustic impedance of the two tissues. A substantial difference will cause the acoustic wave to be reflected. The extent of reflection is formulated by the reflection coefficient[43]:

$$(11)\ Reflection\ coefficient = \left(\frac{Z_2 - Z_1}{Z_2 - Z_1}\right)^2$$

Z_1 and Z_2 represent the acoustic impedance in tissue one and tissue two, respectively.
In Figure 6, the ultrasound wave transmitted into the second tissue medium bents towards the normal if $c1 > c2$ and away from the normal if $c1 < c2$. The latter is called refraction and can be a fundamental source of artefacts in clinical imaging (see section: *limitations and artefacts of ultrasound imaging).* The amount of reflected sound waves determines the brightness of the depicted tissue. The more incoming soundwaves are reflected, the more hyperechogenic (whiter) the tissue is imaged. The image will be more hypoechogenic with a reduced reflection or anechogenic if there is no reflection (visualized as black on an ultrasound image). High-density tissue generates hyperechogenic images (e.g., bone/calcareous structures). On the contrary, fluids are anechogenic.

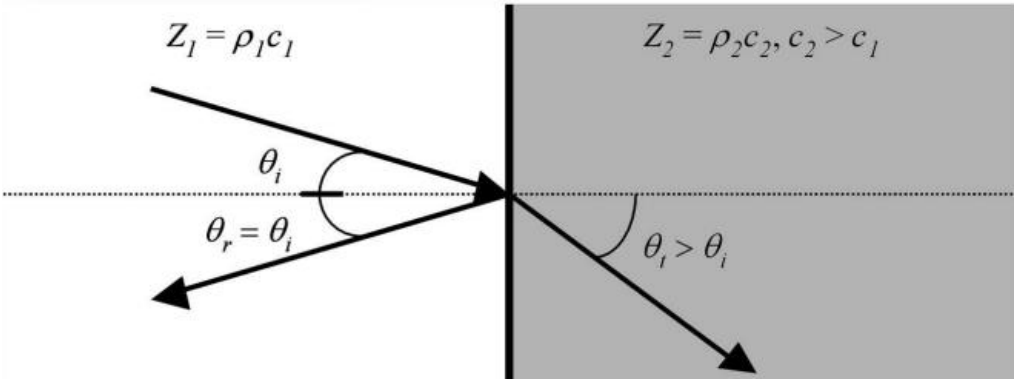

Figure 6. Shows how the acoustic impedance of tissue affects the direction of an ultrasound wave

Non-Linear Propagation

Nonlinearity arises in acoustic propagation because the pressure wave alters the density of the medium, and the speed of sound depends on density, according to *formula 8*. Every ultrasound device assumes that the acoustic velocity is constant at 1540 [m/s]. The result of this assumption is that in an actual body with non-uniform tissues, the beam becomes partially defocused, which leads to reduced image resolution.

Impedance matching

With impedance matching it is tried to design an input impedance of an electrical source in such a way as to have a maximal power transfer. If the acoustic impedance of the two media is very different, most sound energy will be reflected (or absorbed) rather than transferred across the border. An example of impedance matching is gel application on the ultrasound transducer since this prevents the formation of air pockets between the transducer and the skin. Air sacs block ultrasound waves from entering the body. So, in order to get a high-quality image, a gel is applied to the skin of the patient.

Acoustic attenuation

Even with gel application visualizing deep structures in the human body with ultrasound is difficult. This is due to a loss of energy described by acoustic attenuation.[42] When ultrasound propagates through tissue there is always thermal absorption of energy caused by viscosity. Acoustic attenuation can also be the result of specular reflections, divergence or scattering from inhomogeneity. Scattering occurs when the wave encounters dimensions similar to or smaller than the wavelength of the transmitted wave. Attenuation and frequency are directly related, causing sound waves with a higher frequency to attenuate faster than sound waves with a lower frequency. In this way, attenuation limits the maximum depth of penetration. Furthermore, waves with a higher frequency result in images with a better spatial resolution. Therefore, there is a trade-off between spatial resolution and penetration depth, as shown with the following formula (12):

$$(12)\ A(z) = A_0 e^{-\mu \cdot z}$$

Where A(z) is output amplitude, A_0 is the input amplitude, μ_z is the attenuation coefficient.

2. Spatial resolution

To understand how an ultrasound image is created on a screen, it is necessary to understand how the quality of the image is affected by the physical properties of the transducers and the ultrasound waves emitted and detected by the transducer.

Axial resolution

The axial resolution of an ultrasound system is defined as the ability to differentiate between two separate structures that are located parallel with reference to the ultrasound beam. Axial resolution is defined as the following:

$$(13)\ \ Axial\ resolution = {}^{1}/_{2} \times spatial\ pulse\ length$$

Spatial pulse length is determined by the wavelength of the ultrasound beam and the number of cycles within a pulse.[45] To improve axial resolution, a shorter spatial pulse length should be used. This can be achieved with: 1) high damping material within the transducer, which reduces the number of cycles within a pulse (Figure 5B), or 2) use high frequency pulses.[45] However, as discussed, high frequency pulses result in a lower penetration depth and excessive damping is accompanied by loss of amplitude.

Lateral resolution

Lateral resolution is the ability of the ultrasound system to differentiate anatomical structures positioned perpendicular to the ultrasound beam. The lateral resolution is primarily determined by the width of the ultrasound beam. So, the lateral resolution is improved by decreasing the beam diameter, that is, by focusing. At the surface of the transducer, the width of the ultrasound beam converges to its narrowest at the near-zone length (Fresnel's zone). Beyond the near zone the beam diverges. Hence lateral resolution decreases: this zone is called the far-field zone (Fraunhofer's zone). So, the lateral resolution is depth-dependent and high when near-zone lengths are long, which is defined by the following formula:

$$(14)\ \ near\ zone\ length = \frac{diameter\ of\ beam^2}{4\ \times \lambda}$$

Where λ symbolizes wavelength.

Another aspect of an ultrasound beam is that the energy is not confined to a single primary lobe but radiates off at various angles to the transducer. These off-axis lobes are called side-lobes and contain approximately 1% of the total energy. Side lobes are created by contraction and expansion of the piezoelectric element in the radial direction. Side lobes are minimised as far as possible by the manufacturer during the design process by using apodization. Apodization is a widely used signal filtering method that reduces the amplitude of side lobes with the use of windowing, such as a Hann of Hamming filter. The high spatial frequency components of the side lobes of the received ultrasound are suppressed by the windowing. Hence, a downside of apodization is widening of the main lobe, thereby reducing spatial resolution.

Focusing

Beam focusing is defined as creating a focal point where the lateral resolution is most excellent. There are two types of focusing: fixed and adjustable. Fixed focusing was used in old ultrasound machines and will therefore not be discussed.

Adjustable focusing can be applied for either transmission or receiving. With transmit focusing, the outer piezoelectric elements are activated first and the centre elements last. In this way, the focal depth is determined by the extent of the activation time delay. The more significant the difference in time delay, the shallower the focal depth. Dynamic receiving focusing is used if the signals received by the outer elements have travelled a longer distance, and therefore time delay is necessary to compensate and prevent loss of resolution. The greater the depth of the received signal, the less time delay is needed between the receiving elements.

Temporal resolution

Temporal resolution defines the capability of the ultrasound device to detect deformations in structures over time. The temporal resolution is solely determined by the frame rate, which depends on the penetration depth, number of focal points and the number of scan lines per frame. This can be explained with the following formula:

$$(15)\ c = 2 \times depth\ of\ penetration \times pulse\ repetition\ frequency$$

Where pulse repetition frequency is defined as:

$$(16)\ pulse\ repetition\ frequency = frame\ rate \times number\ of\ foci \times number\ of\ scan\ lines\ per\ frame$$

Investigating the above mathematical relationships demonstrate that a high frame rate, hence a high temporal resolution is inversely proportional to the depth of penetration, number of foci and the number of scan line per frame.

3. Broadband beamforming

The transducer in combination with the beamformer determine the ultimate contrast resolution, spatial resolution, sensitivity and accuracy of the system, referred to as beamforming. The process of beamforming begins with pulsing the transducer elements. Subsequently, sound waves reflected by the target return to the elements of the transducer, generating an un-focused beam. The broadband beamformer focuses the beam with the help of time delays. So, when all the channels are properly summed together the exact tissue characteristics are obtained. The critical design requirement of the beamformer is to preserve the entire bandwidth which contains all the acoustic information.

The time delays required for beamforming can be accomplished by broadband digital beamforming (Figure 7).[46] With broadband beamforming all the information content of the tissue signal is preserved. Broadband beamforming can preserve all the tissue signature information for optimum spatial and contrast resolution as well as true dynamic focusing to provide optimum resolution at each point of the image.

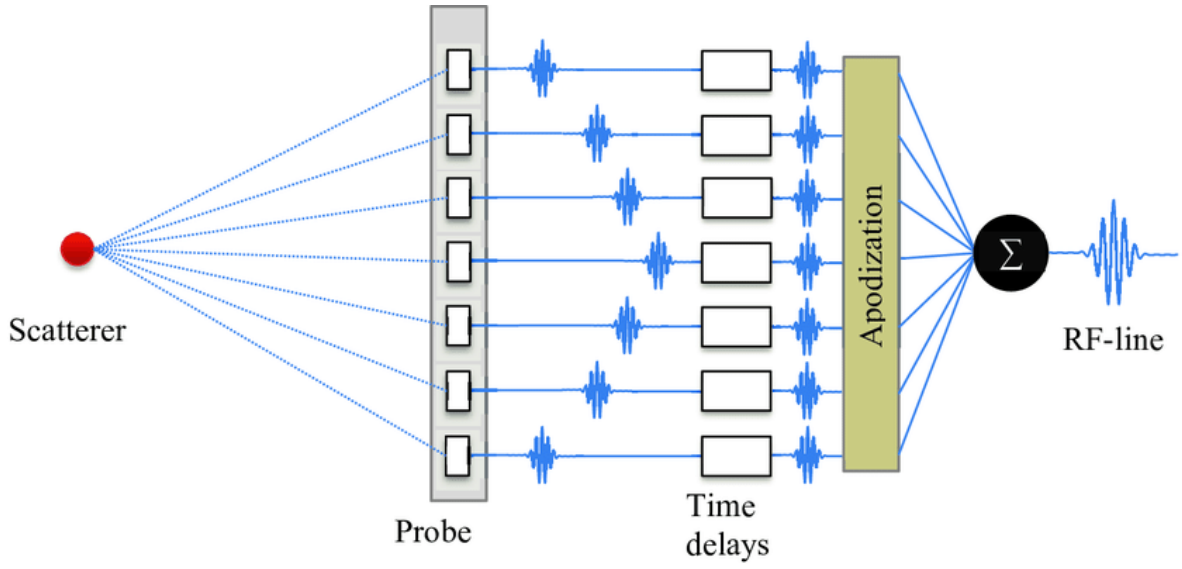

Figure 7. Illustration of the digital broadband beamforming concept.[46]

4. Linear and phased array beamforming

The piezoelectric elements functioning as the sensors and sources of the ultrasound probe are generally grouped in sub-apertures, when considering linear beamforming, see Figure 8. [47] For ultrasound transmission, the elements that belong to the same sub-aperture can either be excited by signals with the same phase, called un-focused linear beamforming or have different phases as in the linear focused case. When using focused beams, higher pressures compared to un-focused beamforming can be achieved. Furthermore, the beams are narrow so the lateral resolution, signal to noise ratio and penetration depth are improved.[47] However, the field of view (FOV) is narrowed, so more transmissions are needed to achieve the same FOV which may decrease the frame rate.

On the contrary, with phased array beam forming the entire array aperture, so no sub-apparatus is used for each transmission, see Figure 8. Again, the beam can be used focused or un-focused. The phases of the transmitted waves are adjusted for every element at each transmission. So, to steer the beam, different sets of phases are used to obtain different steering directions. When comparing linear and phased array probes there are several pros and cons for each technique. For instance, the linear probe can only visualize what is in front of the probe, while a phased array probe can visualize a broader part of its surroundings since the beam can be steered. A second advantage of the phased array probe is the capability of visualizing structures through a small imaging window such as with TTE. However, a disadvantage of the phased array probe is that the pitch, the distance between the centre of two adjacent elements, needs to be smaller than half the wavelength to avoid grating lobes.[47] These are additional lobes, which can further degrade the image quality. Therefore, using phased-array probes in combination with high frequencies needs to be avoided.

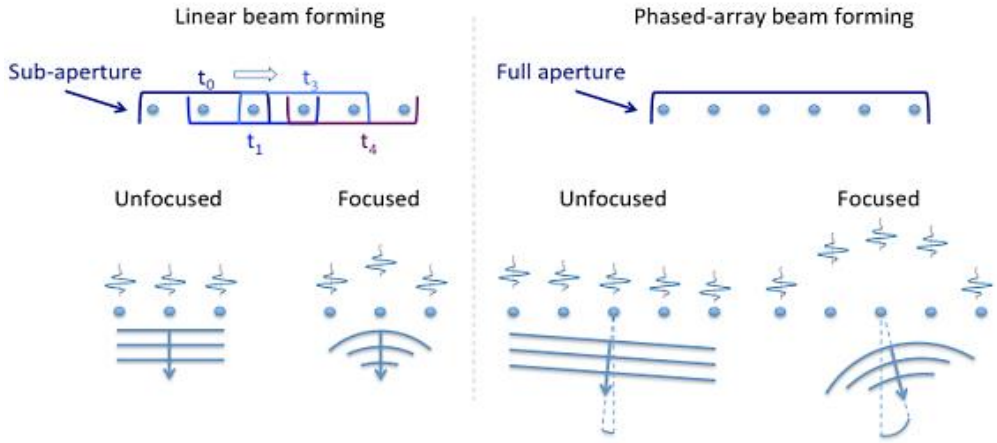

Figure 8. Schematic representation of linear beam forming and phased-array beam forming.[47]

In general, three different transducers are used in clinical practice (Figure 9): the sector, linear and convex transducers. The sector array transducer uses the phased-array beamforming technique. The linear and convex transducers emit linear high frequency beams, achieving high-resolution images. The convex probe has a convex shaped surface and therefore emits a fan-shaped beam pattern.

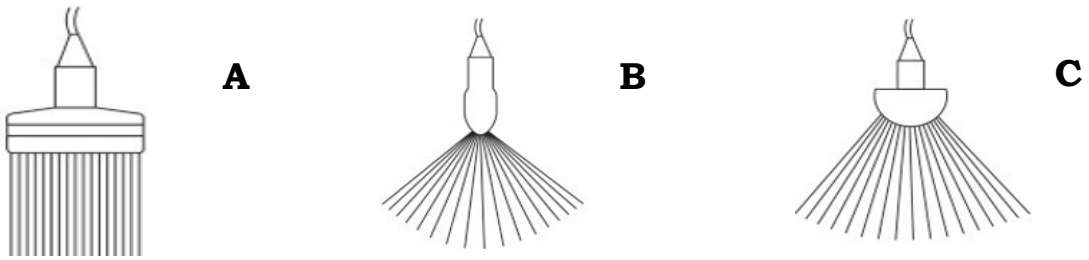

Figure 9. A) shows a linear array probe which has a high frequency range around 8-15 MHz. B) shows a sector or phased array probe emitting frequencies around 2-6 MHz. C. is a convex or curved linear array probe emitting frequencies between 2-12 MHz.

Spatial compounding

Spatial compounding is another method of beamforming in which information is obtained by transmitting beams in different angles, typically within 20 degrees from the perpendicular, shown in Figure 10.[47] In this way, the information from different angles is combined to create a single image. This is different from conventional Brightness-mode (B-mode) beamforming, in which an image is created by transmitting beams from a single angle. A benefit of the use of spatial compound imaging is the reduction of angle-dependent artefacts such as speckle artefacts. Speckle artefacts result from the scattering of the ultrasound beam from small tissue reflectors. Improved image quality compared to conventional imaging can be obtained by using spatial compound imaging.

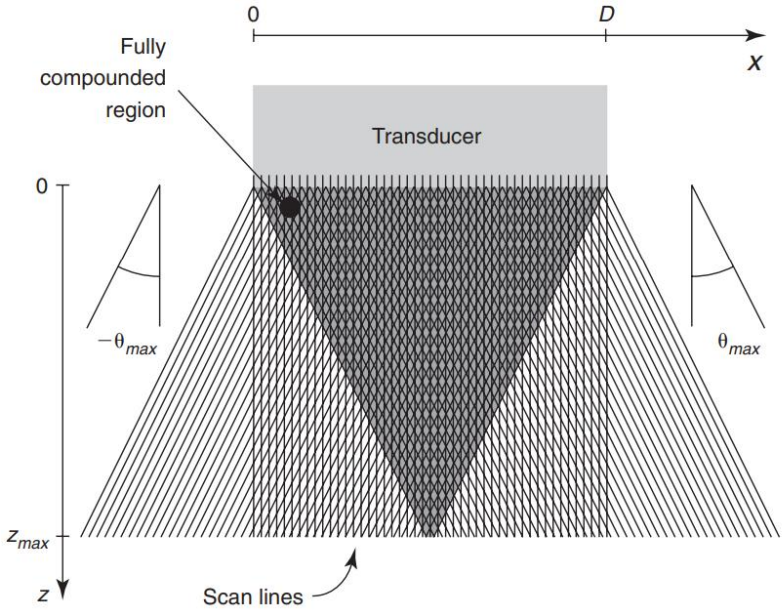

Figure 10. Illustration of transducer and associated scan lines for recording of three single-angle images. (Adapted from Jespersen SK, Wilhjelm JE, Sillesen H. In vitro spatial compound scanning for improved visualization of atherosclerosis. Ultrasound Med Biol. 2000;26:1357–1362.)

5. Limitations and artefacts of ultrasound imaging

Ultrasound creates artefacts that may significantly alter image quality and falsely display structures or tissue. Some types of artefacts are explained below: acoustic shadowing, near-field clutter, reverberations, refraction and side lobe artefacts.

Acoustic shadowing results from an ultrasound wave that encounters tissue with a large attenuation coefficient, such as bone tissue or fibrous tissue. As a result, the ultrasound waves cannot pass through; consequently, there is less intensity behind the reflector (shadow).

Near field clutter (NFC) is a mechanism explained by high amplitude oscillations of piezoelectric elements.[48] If the piezoelectric elements are not well dampened, the pulse length increases, and the axial resolution reduces. This results in a cloudy artefact directly beneath the transducer. However, modern ultrasound machines have improved damping material inside their probes, resolving this issue almost entirely. Nevertheless, with TTE, NFC can still occur due to reverberations in the transthoracic tissue because of reflectors in the near field of the probe.[48]

Reverberations occur when echoes are reflected several times before reaching the transducer. In Figure 12, the mechanisms of reverberations (12A) and NFC (12B) are shown. Identifying structures close to the transducer may be harder to identify, such as the apex in the apical four-chamber (A4CH) view. This could lead to confusion, e.g. when trying to diagnose if a patient has an apical thrombus or not.

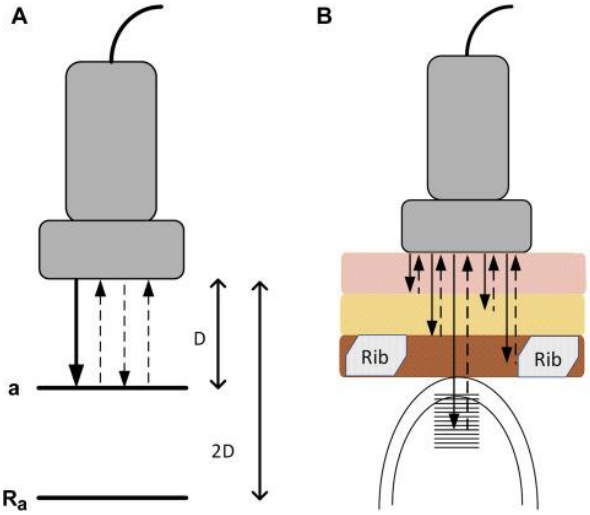

Figure 12 A) The mechanism of reverberation artifact. Ultrasound waves are reflected multiple times between the reflector (a) and the transducer resulting in the projection of r (Ra) being twice as far projected as the real distance (d), (B) The mechanism of NFC. The same principle as for reverberations applies for NFC, however the reverberations occur abundantly in the chest wall, creating stepladder reverberations located closely to the transducer, resulting in a hazy projection (multiple lines in the images).[48]

Refraction is referred to as a change in the direction of the sound wave when it strikes a boundary between two tissue types with different propagation velocities. If the first medium's propagation velocity is greater than the second medium, the resultant angle will be greater than the angle of incidence. As a result, refraction may cause a reflection that is projected laterally from the real object.

A beam pattern of a simple transducer appears as in Figure 13 and shows that the energy is not confined to a single primary lobe but radiates off at various angles to the transducer. These off-axis lobes are called sidelobes. Since a transducer assumes that all returning ultrasound beams arise from the primary lobe, the echoes are falsely displayed.

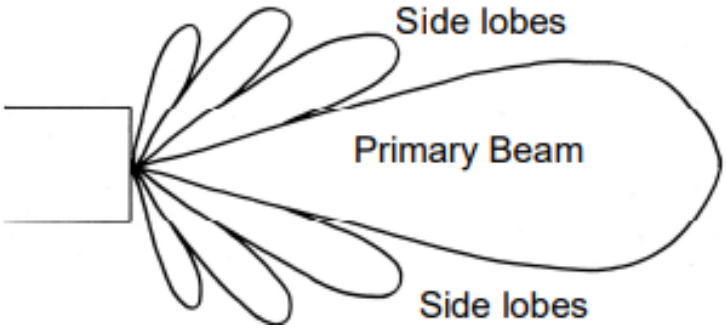

Figure 13. Basic illustration of an synthetic beam pattern with side lobes.

6. Two-dimensional echocardiography

Echocardiography is a well-established technique and the most commonly used technique for cardiac diagnostic imaging.[49][50] The non-invasive nature and free of ionization make ultrasound a very appealing technique for cardiovascular monitoring. The method enables clinicians to analyse multiple cardiac variables such as the size of the ventricular chambers, contractility and valvular function. With visual examination of the 2DE cardiac images, LV function can be assessed subjectively based on regional wall motion and myocardial thickening, also known as eyeballing. However, objective quantification of the LVEF and CO to evaluate the circulatory system is essential during the examination of any hospitalized patient.[51] Both fractional shortening and the Simpsons biplane method are commonly used at the cardiology department to quantify and evaluate heart function.

Motion-mode (M-mode) ultrasound imaging is often utilized because of its excellent axial and temporal resolution due to its high sampling frequency and pulse transmission rate.[52] In M-mode, a one-dimensional image is created by emitting a single scan line which enables to measure a range of motion. Using M-mode, the left ventricular end-systolic diameter (LVESD) and the left ventricular end-diastolic diameter (LVEDD) can be derived. These parameters refer to the size of the ventricle at the end of systole and diastole. By using the formula, the fractional shortening can be calculated:

$$(17)\ Fractional\ Shortening\ (\%) = \frac{LVEDD - LVESD}{LVEDD} \times 100$$

Fractional shortening gives the percentage change in size of the LV due to contraction. This value does not express LVEF because we are not computing volumes but distances (diameters). Theoretically, LVEF can be derived from the LVEDD and LVESD with the cube method, which assumes that the LV is spherical:

$$(18)\ Left\ ventricular\ ejection\ fraction\ (\%) = \frac{LVEDD^3 - LVESD^3}{LVEDD^3} \times 100$$

Some important pitfalls need to be addressed when it comes to assessing LV function with M-mode measurements. One limitation is that the measurement of the ventricular diameter must be correct, for which the M-mode line needs to cut the ventricle perpendicularly, and the endocardial borders need to be clearly delineated. Furthermore, estimating global LV function from an M-mode image can lead to inaccurate measurements with over- or underestimation of LV function. Volume calculations derived from M-mode measurements rely on the assumption of a fixed geometric LV shape such as a spherical geometry. However, this assumption is not valid in various cardiac pathologies. Therefore, volume assessments based on linear measurements are not recommended anymore in the current clinical guidelines.[53]

Another commonly used method is Simpson's biplane method. Simpson's biplane method is based on B-mode imaging. With B-mode imaging a phased array of elements in a transducer simultaneously scan a plane that can be viewed as a 2D image. In the "monoplane Simpson method", only the A4CH view is employed to calculate volume. In the biplane Simpson method volume calculation is also based on the apical two-chamber (A2CH) view. The biplane Simpson method requires delineation of the endocardial border based on tracings of the blood tissue interface in the A2CH and A4CH view. The LV is then subdivided into a series of elliptical discs, which are summated to determine LV volume (Figure 14).

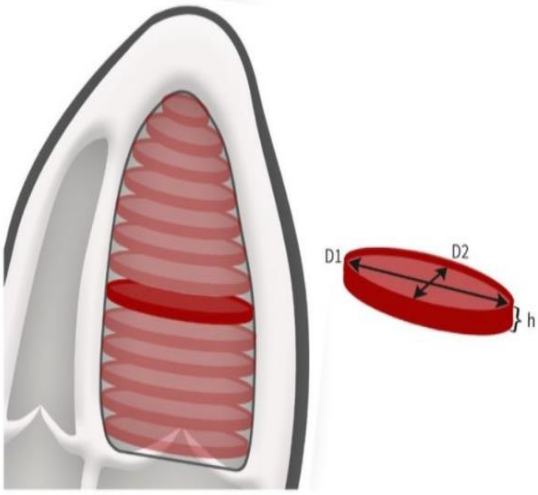

Figure 14. Calculation of ejection fraction (LVEF) with Simpson's biplane method.

$D1 =$ *diameters in apical 2CH view*
$D2 =$ *diameter in apical 4CH view*
$h =$ *disk height*

Table 1 *Normal values for 2DE parameters of LV size and function according to gender* [49]

	Male		Female	
parameter	Mean ±SD	2-SD range	Mean ±SD	2-SD range
LV volumes (biplane)				
LV EDV (ml)	106 ± 22	62–150	76 ± 15	46–106
LV ESV (ml)	41± 10	21–61	28 ± 7	14–42
LV volumes normalized by BSA				
LV EDV (ml/m2)	54 ± 10	34–74	45 ± 8	8 29–61
LV ESV (ml/m2)	21 ± 5	11–31	16 ± 4	8–24
LV EF (biplane)	62 ± 5	52–72	64 ± 5	54–74

BSA = body surface area, EDV = End-diastolic volume, ESV = End-systolic volume, LV = left ventricle, LVEF = Left ventricle ejection fraction, SD = Standard deviation, SV = Stroke volume, ml = millilitres

LVEF is assessed by measuring the difference in ventricular size between the end-diastolic and end-systolic phases, divided by the EDV. The end-diastole frame is the first frame after mitral valve closure or the frame in the cardiac cycle where the respective LV dimension or volume measurement is the largest. The end-systole frame is best defined as the frame after aortic valve closure and when the ventricular size is the smallest. Table 1 shows the average values for biplane 2DE parameters of LV size and function according to gender, obtained from biplane views. Compared to the fractional shortening method, fewer geometric assumptions of the LV shape are necessary for the biplane method. The biplane method directly measures the contribution of longitudinal contraction. However, since not an entire 3D delineation is done still some geometric assumptions are made. The main limitation of Simson's biplane method is when poor image quality does not allow reliable tracing of the endocardial borders.[27] Furthermore, the apex is frequently foreshortened, which refers to the situation where the plane of the ultrasound device does not cut through the true apex. This causes the need for extensive training of physicians to provide reliable measurements. Nevertheless, the biplane method is widely used for clinical application, either manually or incorporated in an integrated software application.

TOMTEC 2DCPA analysis

Echocardiographic determination of the LVEF can often be time-consuming, requiring manual tracing of multiple images. Therefore, several commercial automatic LV quantification software algorithms are available, one of which is the TOMTEC Arena 2D two-dimensional cardiac performance analysis (2DCPA) algorithm. This is an operator semi-independent, offline solution for the quantification of cardiac function. Detailed analysis of myocardial velocity, displacement and strain is performed based on 2D speckle tracking in A4CH or A2CH views. Basic volumetric measures such as the EDV, ESV, SV and LVEF are made from routine digital imaging and communication in medicine (DICOM) images. Due to advanced cardiac motion assessment, the AS software can calculate a semi-automatic initial contour proposal. Advanced cardiac motion assessment can be explained as the following: a grey-scale image from echocardiography is composed of several bright speckles produced due to the scatter of the ultrasound beam by the tissue. The AS software identifies these speckles and tracks them frame-by-frame using a 'sum-of-the absolute differences' algorithm. In image processing, the sum of absolute differences measures the correlation between two images. It is calculated by taking the absolute difference between each pixel in the original matrix and the corresponding pixel. For LV

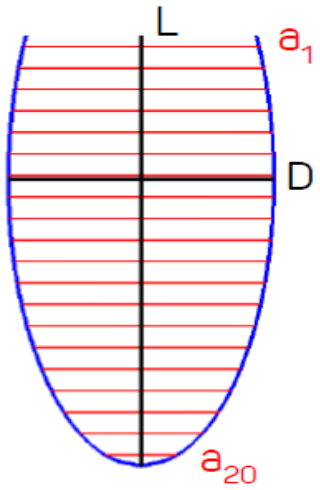

Figure 15. Schematic representation of the calculation of the left ventricular volume with the biplane method.

a_i=diameter; L = maximal longitudinal axis obtained from A4CH and/or A2CH. D = maximal chamber diameter obtained from A4CH and/or A2CH

function assessment with the 2DCPA software, several steps need to be followed. Firstly, if the DICOM file doesn't include an electrocardiogram (ECG) signal, the ED and ES frame of the cardiac cycle need to be selected in the A2CH view using an incorporated M-mode tool. Secondly, the entire endocardial border of the ESV frame needs to be traced either manually or by tracing the mitral valve and apex with three clicks, and the rest is done automatically by the algorithm. Thirdly, the algorithm automatically generates the tracing of the endocardial border in the EDV frame due to cardiac motion assessment. Afterwards, the operator can choose to make adjustments. Finally, the volumetric measurements and strain analysis are made. Figure 15 gives a schematic representation of the 2DCPA calculations. Dependent on the ratio of long axis lengths (*l*) for the A2CH (L_{2CH}) and A4CH (L_{4CH}) view, there is a small diameter (*D*) interval for which the biplane volume becomes larger than any single plane volume. In formulas 19, 20, 21, 22 and 23, the calculations for the volume from the A2CH (V_{2CH}) and A4CH (V_{4CH}) and biplane (V_{bi}) method are shown, respectively. This is explained by the three cases shown in Figure 16.

$$(19)\ V_{2CH} = \frac{\pi}{4} \cdot \frac{L_{2CH}}{20} \sum a_i^2$$

$$(20)\ V_{4CH} = \frac{\pi}{4} \cdot \frac{l \cdot L_{2CH}}{20} \sum (k a_i)^2 = V_{2CH} \cdot l \cdot k^2$$

$$(21)\ V_{2CH} = \frac{\pi}{4} \cdot \frac{L_{2CH}}{20} \sum a_i^2$$

$$(22)\ V_{4CH} = \frac{\pi}{4} \cdot \frac{l \cdot L_{2CH}}{20} \sum (k a_i)^2 = V_{2CH} \cdot l \cdot k^2$$

$$(23)\ V_{bi} = \frac{\pi}{4} \cdot \frac{L_{2CH}}{20} \sum (k a_i) a_i = V_{2CH} \cdot k^2$$

Where k is the ratio of the diameter (*D*) between the A2CH and A4CH view.

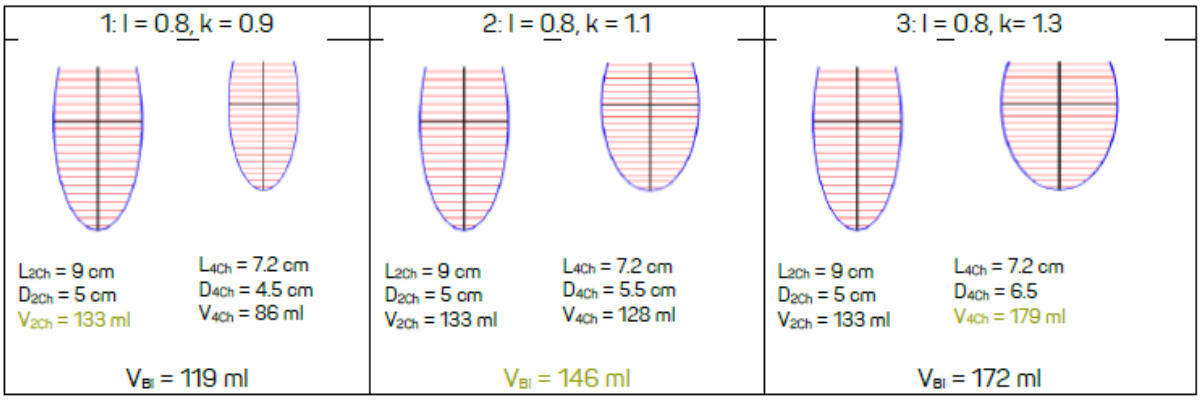

Figure 16. A. shows case 1 for which k<1 $V_{4Ch} < V_{Bi} < V_{2Ch}$, B. shows case 2 for which 1< k<1/ $V_{Bi} > [V_{2Ch}, V_{4Ch}]$ C. shows case 3 for which 1/k $V_{2Ch} < V_{Bi} < V4$
V_{Bi} = volume biplane, V_{2CH} = volume A2CH view, V_{4CH} = volume A4CH view

7. Three-dimensional echocardiography

The main disadvantage of quantifying LV volume with 2DE is that geometric assumptions are needed. These assumptions cause inaccuracies in several cases, such as in patients with dilated ventricles or regional wall motion abnormalities. These limitations can be overcome with 3DE.[54]

In the early 1990s, two biomedical engineers invented the 3DE ultrasound prototype.[55] The 3DE prototype reconstructed 3DE images from parallel stacked 2D images.[55] Spatial resolution was poor due to interpolation that was needed to fill in the missing voxels. In the early 2000s, 3DE was first used inside ultrasound laboratories, where labour-intensive offline analysis took place to reconstruct 3D structures from 2D images.[55] Subsequently, real-time 3DE was invented, which made it possible to observe movement of cardiac structures. 3DE became clinically available and is currently used daily by cardiologists to study complex anatomical cardiac structures. The main advantage of real-time 3DE is the in-depth visualization of heart structures and quantification of cardiac parameters without using geometric assumptions.[56] Furthermore, 3DE is unaffected by foreshortening and is more accurate and reproducible compared to 2DE.[54] 3DE enables us to accurately and precisely understand the pathophysiologic nature of cardiac diseases. 2DE-derived LV sizes are shown to consistently underestimated LV size compared to the golden standard CMR.[7], [57] In contrast, 3DE has the advantages of full-volume acquisition with established accuracy and reproducibility and has shown superior correlation with CMR compared to 2DE.[7] For LV volume quantification, multiple-beat 3DE is applied in which different narrow angles are merged to create a full-volume image of a heartbeat. This means that the final LV volume quantification is based on an average volume over multiple heartbeats.

Table 2 *Normal values for 3DE parameters of LV size and function according to gender* [58]

	Total		**Male**		**Female**	
Parameters	Mean ± SD	2-SD	mean ± SD	2-SD	mean ± SD	2-SD
LV EDV (ml)	115.6 ± 29.6	93.1–132.3	133.3 ± 30.5	114.2–150.2	102.5 ± 20.8	87.4–114.2
LV ESV (ml)	47.1 ± 13.7	36.6–55.3	55.4 ± 13.9	45.4–63.0	41.0 ± 9.9	33.6–48.5
LVEF (%)	59.4 ± 4.6	55.9–62.5	58.5 ± 4.3	54.9–61.6	60.1 ± 4.6	56.7–63.2
SV (ml)	68.5 ± 17.6	55.8–77.4	78.0 ± 18.6	63.7–92.2	61.5 ± 13.0	53.1–69.3
Normalized to BSA						
LV EDV (ml/m^2)	63.9 ± 12.9	54.8–72.0	68.7 ± 14.0	58.6–77.2	60.4 ± 10.8	52.7–67.1
LV ESV (ml/m^2)	26.0 ± 6.2	21.3–29.7	28.5 ± 6.5	24.4–32.6	24.1 ± 5.3	20.4–27.5
SV (ml/m^2)	37.9 ± 7.9	32.0–43.0	40.1 ± 8.7	34.1–46.5	36.3 ± 6.9	31.4–40.3

BSA = body surface area, EDV = End-diastolic volume, ESV = End-systolic volume, LV = left ventricle, LVEF = Left ventricle ejection fraction, SV = Stroke volume, ml = millilitres

Several studies have published 3DE reference values for healthy normotensive subjects, which are summarized in Table 2.[58] The main disadvantage of 3DE is a lower temporal resolution. Often, 3DE images lack contrast or contain artefacts that lead to missing data in the image to be segmented. Furthermore, regional homogeneity could impede automatic algorithm endocardial border detection. On the contrary, cardiac sonographers or cardiologists are able to identify the endocardial border in the presence of regional homogeneity because they have a-priori knowledge about the shape and appearance of the heart. Several algorithms are on the market for 3DE cardiovascular parameter quantification that aim to translate this knowledge into AI algorithms. Philips Dynamic HeartModel$^{A.I.}$ (Philips Health care, United States) is such an algorithm.

The Philips Dynamic HeartModel$^{A.I.}$

The Philips Dynamic HeartModel (DHM) incorporates automated analysis software that detects the LV and left atrial endocardial border using a 3D model-based segmentation algorithm. First, the EDV frame is defined using the ECG signal. Secondly, the ESV frame is determined by using motion analysis to identify the smallest LV cavity. Motion analysis can also be described as speckle tracking, discussed in the previous chapter (*TOMTEC 2D strain analysis*). With the information and training from a 3DE database consisting of approximately 1000 ultrasound images from a wide variety of heart shapes, sizes and image qualities, end-systolic and end-diastolic models of the LV and left atrium are built.[54] A 17 segments model is incorporated to determine if the image quality is sufficient to accurately estimate chamber volumes. For accurate chamber volume calculations, at least 14 to 15 LV segments are necessary (Figure 17). Fourthly, the left atrium and LV endocardial contours are displayed on end-diastolic and end-systolic A4CH, A3CH and A2CH cut planes. Because of the fully automated nature of the algorithm, it has a deterministic convergence response, thus yielding the same result when repeating the analysis on the same dataset. However, manual corrections of the resultant LV and left atrial endocardial surfaces are possible when the operator judges the automatically detected surface to be inadequate. Finally, cardiac parameters such as the ESV, EDV, SV and LVEF, are automatically quantified. Automatic cardiac image segmentation is a demanding task because the anatomical structure and visualization of the heart are highly variable, and the 3DE images have relatively low resolution compared to 2DE.[56]

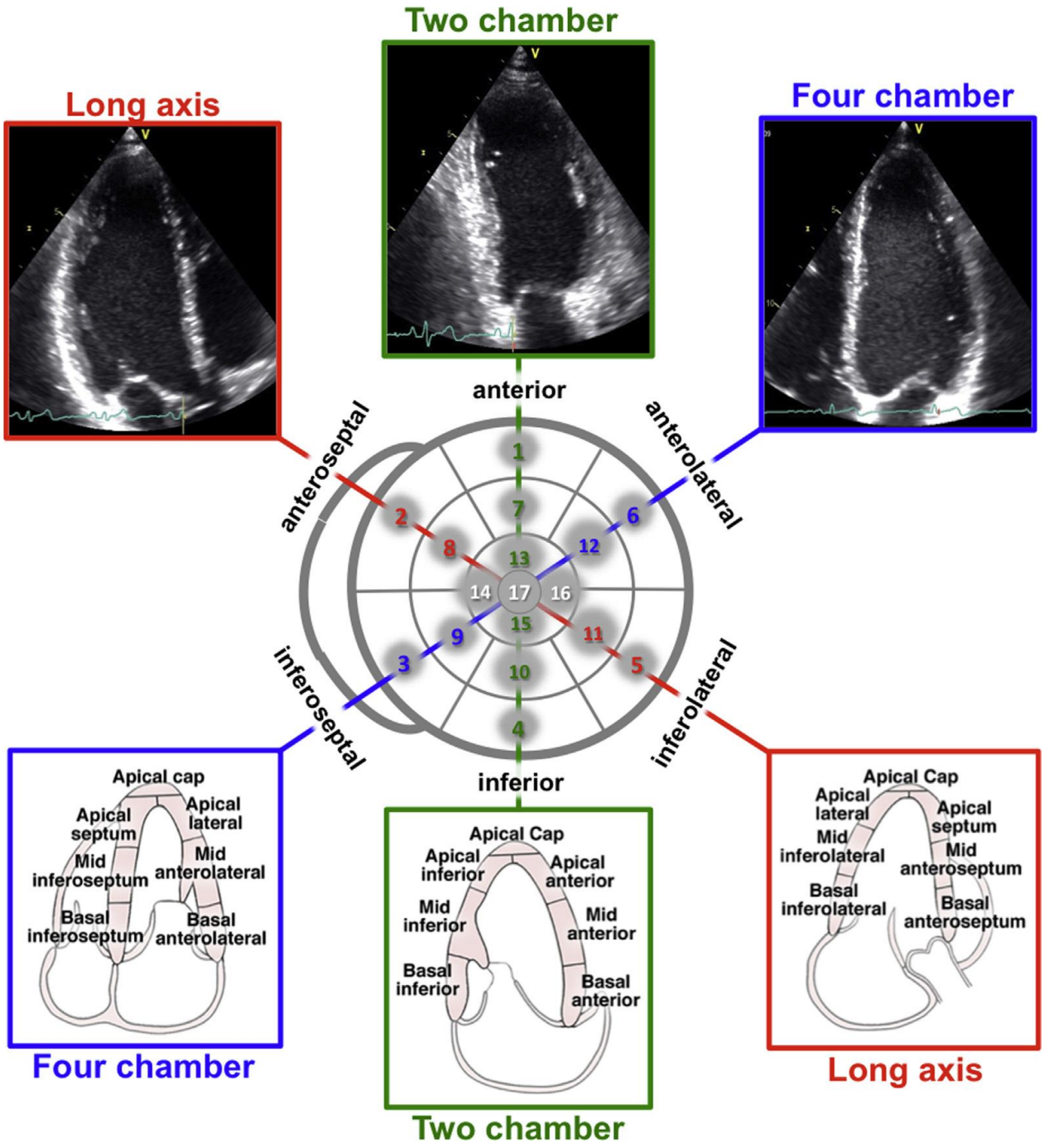

Figure 17. Orientation of apical four-chamber (A4CH), apical two-chamber (A2CH), and apical long-axis views in relation to the bull's-eye display of the LV segments (center). Top panels show actual images, and bottom panels schematically depict the LV wall segments in each view.[49]

The model-based segmentation method, incorporated in the DHM software, aims to translate a-priori knowledge about the heart into AI algorithms. The model-based segmentation method can be qualified as top-down and usually consists of a first stage in which the appearance and location of the heart are based on artificial models. The goal of image segmentation is to simplify the presentation of an image that is easier to analyze. With image segmentation, it is easier to detect and locate boundaries. During image segmentation, each pixel is labelled such that a contour is extracted from the image. In recent years, the success of deep convolutional neural networks (CNN) has influenced the field of automatic image segmentation for endocardial border detection.[59] With the combination of image processing and neural networks (NN), the DHM model makes a volumetric analysis of the LV.[60]
A NN comprises four main components: inputs (x), weights (w), a bias or threshold and an output.[61] The algebraic formula would look like this:

$$(24)\ \sum_{i=1}^{m} w_i x_i + bias = w_1 x_1 + w_2 x_2 + w_3 x_3 + bias$$

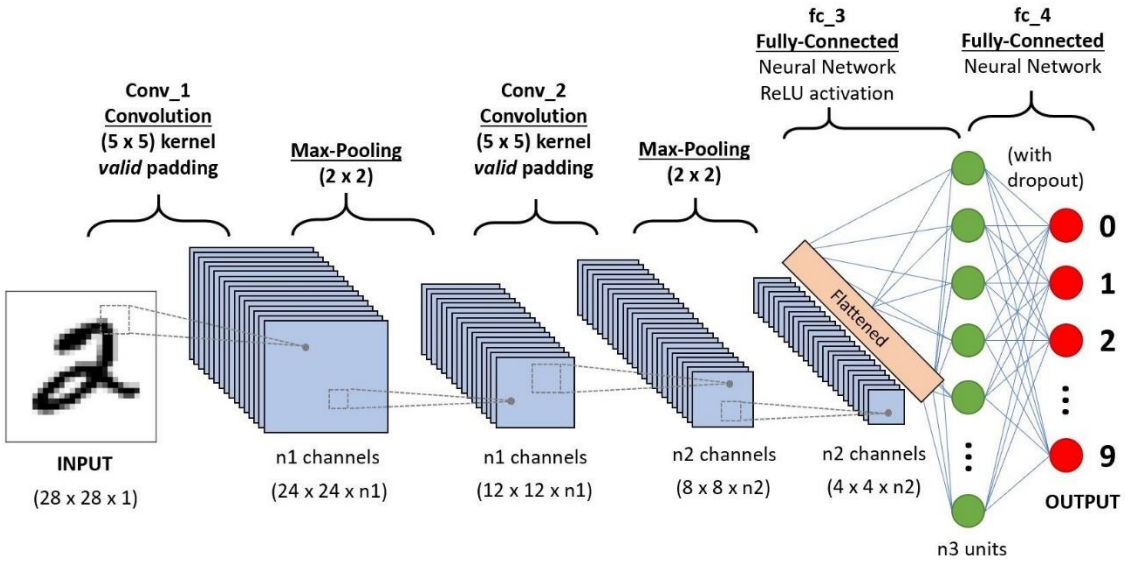

Figure 18. An schematic representation of a CNN sequence

The weights and biases can be identified as the importance of various aspects in the image. In this way, objects and aspects in the image can be differentiated from one another. The architecture of a NN is comparable with the connectivity patterns of neurons in the human brain. A CNN model is a specific kind of NN and is predominately used for image processing. A CNN model processes data through many layers of nonlinear transformations of the input data to calculate the output. If the output of a node has reached a value above the specified threshold the node is activated and data is sent to the next layer of the NN. This process is repeated multiple times because a neural network usually has multiple “hidden” layers (Figure 14). Each hidden layer has its own activation function. Once all the outputs from the hidden layers are generated, they are used as inputs to calculate the neural network's final output. A neural network that consists of more than three layers can be considered a deep learning model.[61] The objective of a CNN is to simplify an image without losing critical features for a good prediction. A CNN consists of a convolution layer and a pooling layer. A convolution layer is a set of filters, also known as kernels, applied to a matrix of pixels (image). Using the kernel, a 2D matrix of features is converted into a new 2D matrix of features (Figure 18). The new matrix can be reduced in dimensionality compared to the input, or the dimensionality is either increased or remains the same. The reduction of dimensionality is caused by the application of valid padding, while the latter two cases are achieved by using same padding. The objective of the convolution operation is to extract high-level features, such as boundaries, from the input image.
The pooling layer intends to reduce the dimensionality of the matrix of pixels after the convolution layer, trying to decrease the computational power required to process the data.

Furthermore, it helps to extract dominant features that are constant, thus maintaining an effective training model. There are two types of pooling: average pooling and max pooling. With average pooling, the average value covered by the kernel is returned. With max pooling the maximal value is returned. Max pooling performs better than average pooling because the max pooling kernel also serves as a noise suppressant. The convolutional layer and the pooling layer, together from a layer in the CNN. Depending on the complexity of the image the number of layers inside the CNN is increased. With the process described above the model can extract and understand the features of the image. In the last part the final output is flattened into a vector and fed into a regular NN for classification.
The conventional interpretation of echocardiographic images relies heavily on the process of pattern recognition by the human brain. Deep learning CNN can train this pattern recognition from large data sets and make accurate predictions on newly unknown input data. Deep learning CNN also have the potential to overcome human limitations such as fatigue or distraction, inter- and intra-observer variability. Besides the heavy reliance on pattern recognition by the human brain, interpretation of echocardiograms can be very subjective. AI tackles this problem as it has the potential to extract information that is not apparent to the observer. The endocardial boundaries and the location of the annulus of the mitral valve are automatically identified by the NN model. In this way, the chance of encountering the limitation of the Simpson biplane method of not permitting reliable tracing of the endocardial contour is decreased. The algorithm provides measurements of LV size, LVEF, CO and SV. AI-based solutions such as the DHM software are increasingly being adopted to automate workflows and assist clinicians with objective clinical indications to support their decision-making process.

E. Point of care Cardiovascular monitoring

Cardiovascular monitoring is an essential component in adequately managing a critically ill patient present at the ED or ICU, as mentioned before. Ideally, a cardiovascular monitoring device should be reliable, validated, safe, easy to use, readily available, non-invasive, time-efficient, feasible and cost-effective.[62] Previous studies have shown clinical assessment combined with echocardiography to be a proper initial guiding method for cardiac point of care assessment.[38], [63] In recent years, point of care ultrasound imaging has been widely considered as the method for cardiovascular status objectification.[64] The fact that it is non-invasive, free of ionization, safe and easy to use at the bedside qualifies ultrasound as a very appealing technique for cardiovascular monitoring.[64] With the development of HHE devices, time efficiency and accessibility of echocardiography have significantly improved.[65] Despite having a high operator-dependency, echocardiography is the most practical method for cardiovascular monitoring and fluid therapy guidance.
The newly designed HHE device by Philips, called the Lumify, is a high-quality ultrasound imaging tool that can be connected to a smart device such as a tablet or phone. The Lumify S4-1 probe works on the principle of digital broadband beamforming and can be used for performing cardiac exams.

1. Online echocardiography quantification algorithms

HHE is an attractive and feasible imaging tool for critical care physicians, as mentioned in previous paragraphs. However, automatic operator-independent bedside quantification of CO, SV and LVEF with HHE devices is not available yet and needs to be performed at the office (offline). Bedside interpretation of LVEF is mainly done by visual estimation. As experience levels vary over clinicians, objective and accurate estimation of LVEF is challenging in clinical practice. The LVivo-EF software of DIA for HHE devices addresses this challenge by providing clinicians with LVEF and LV volume measurements using AI technology and pattern recognition algorithms on the bedside of the patient (online).

VI. Introduction

In critically ill patients point of care assessment of the cardiac function plays a valuable role in early diagnosis and treatment of hemodynamic and respiratory instability. It supports the clinician in clinical decision making by guiding adequate fluid therapy or administration of vasoactive and inotropic medication.[50], [66] LV function is an essential clinical parameter in hemodynamically and respiratory compromised ICU patients in order to guide fluid therapy and administer inotropes and vasopressors.[19] Indices used to assess LV performance are based on its ability to generate force and the degree of chamber shortening. Based on these concepts SV and LVEF have been used to quantify LV function over the last several decades. Echocardiography has been the primary device used for the quantification of SV and LVEF. 2DE is considered the standard echocardiography (SE) method since it is fully integrated into the routine clinical practice. Another type of echocardiography is 3DE which has become an integral part of the echocardiography landscape as well because of its proven advantages over SE. Nonetheless, both SE and 3DE cannot be used as point of care device since they are not readily available at the beside of the patient due to cost inefficiency and size.

Over the past years, technological advancements have resulted in the emergence of miniaturized handheld ultrasound equipment that is compact and battery operated. The simplicity of use, availability at the patient's bedside, easy transportability, and relatively low cost have encouraged physicians to use these HHE devices for prompt medical decision making in point of care treatment.[67], [68] As a consequence, the use of HHE is on the rise even among non-echocardiographers, such as intensivists and emergency care physicians).[69] However, there is a lack of information about the actual performance of HHE devices for the quantification of SV. Moreover, bedside quantification of SV and LVEF with HHE devices is yet not feasible and needs to be performed offline.

In this observational study, the performance of a clinically certified HHE device (Lumify, Philips) in combination with an online automatic cardiac quantification tool (LVivo, DIA) is evaluated in clinical practice. By incorporating LVivo in Lumify, bedside measurements of SV and LVEF are among the possibilities.
It is hypothesized that SV and LVEF measurements with the Lumify/LVivo system correspond with SE measurements. To test this hypothesis, the present study was designed to: 1) validate measurements of EDV, ESV, SV and LVEF with the HHE probe against SE measurements; 2) Validate the LVivo tool against a manual and a fully automatic quantification tool; 3) compare EDV, ESV, SV and LVEF measurements made with HHE and SE with 3DE measurements.

VII. Methods

This prospective observational study was approved by the institutional review board of the University Medical Centre Utrecht, The Netherlands 5th of March 2021. This study was conducted from January to September 2021 at the Cardiology department of the Catharina hospital (Eindhoven, the Netherlands). Written informed consent was obtained from all patients. Patients were included if they were above 18 years, in sinus rhythm and agreed to participate. Exclusion criteria were: poor delineation of the endocardial border on 2D echocardiography images, supraventricular arrhythmias (atrial fibrillation, atrial flutter), moderate to severe valvular disease, and moderate to severe pulmonary hypertension. Patients baseline characteristics, including age, gender, BMI, and comorbidities, were collected.

Study design

Forty-three consecutive patients who were referred to the echo lab of the Catharina Hospital in Eindhoven for a 2D TTE examination were screened for participation. An expert cardiologist blinded to the results conducted all acquisitions. Spontaneously breathing patients, lying in left lateral position, were asked to perform an expiratory hold maneuverer during image acquisition. Image quality was optimized to improve endocardial visualization by adjusting gain and depth settings.

Data acquisition

(i, SE) Two-dimensional, single beat images of the A2CH and A4CH view were acquired with a harmonic EPIQ ultrasound system (Philips Medical Systems, Best, the Netherlands) equipped with an X5-1 phased array transducer (3040 piezoelectric elements,1–5 MHz). Storage and looping of cardiac cycles were ECG triggered.

(ii, 3DE) A real-time, single beat, wide-angled 'full volume' 3DE image was acquired from the A4CH view position, with a harmonic EPIQ ultrasound system (Philips Medical Systems, Best, the Netherlands). Storage and looping of cardiac cycles were ECG triggered.

(iii, HHE) Because storage and acquisition with the HHE device could not be ECG triggered, single beat recordings were not be acquired. Instead, a recording of 8 seconds of the A2CH and A4CH view was acquired with the Lumify S4-1 phased array transducer (Philips Health care, USA).

Data acquisition was done sequentially by one expert cardiologist on the same patient. Total acquisition time was approximately 5-10 minutes. The acquisitions were saved as DICOM files and were exported to a personal computer for subsequent offline post-processing. Offline post-processing was done by one blinded observer which performed the image quality assessment and data analysis described in the following section.

2DE quantification software

From the HHE recordings only the second beat was evaluated. The following software tools were used to quantify the EDV, ESV, SV and LVEF from SE and HHE images.

1. *2DCPA - Offline 2DE manual*

First, with 2DCPA (2DCPA *TOMTEC – ARENA* lot 41, *TOMTEC Imaging Systems GmbH),* the LV ED and ES frames were chosen manually, with the largest (the first frame after mitral valve closure) and smallest (the frame after aortic valve closure) LV cavity, respectively. Second, the blood-tissue boundaries of the LV were manually traced for the ES frame. Then the endocardial border tracing of the ED frame was determined automatically by using cardiac motion analysis. Last, the EDV, ESV, SV and LVEF were generated by the software system using the Simpson biplane method.

2. *AS - Offline 2DE automated*

The Auto Strain (AS) software (Auto Strain *TOMTEC - ARENA lot 41, TOMTEC Imaging Systems GmbH*) automatically identifies the ED and ES frame according to the ECG signal. The SE data included an ECG signal, and the HHE data did not. So, the ED and ES frame for an HHE image needed to be selected manually with the help of the M-Mode tool incorporated in the AS tool. With an M-mode tracing through the annulus, the ED and ES frame was selected for the HHE recording. Secondly, EDV, ESV, SV and LVEF are calculated based on the Simpson biplane method.

3. *LVivo - Online 2DE automated*

The LVivo tool (*LVivo EF, ver 3.6.1, DIA imaging Analysis Ltd., Israel*) was able to automatically trace the endocardial border. Hence, no manual input or adjustments were needed. However, quantification of EDV, ESV, SV and LVEF was done according to the Simpon's monoplane method. Hence, LVivo was not able to quantify the A4CH and A2CH views, solely A4CH.

3DE quantification software

3DE LV volume and LVEF quantification was performed using the Philips Dynamic Heart-Model$^{A.I.(Anatomical\ Intelligence)}$ (*Philips Health care, United States*), referred to as DHM in this study. The software automatically identifies the ED and ES frames of the cardiac cycle based on the acquired ECG signal and creates ED and ES 3D projections of the LV cavity, from which LV parameters are derived directly. No manual corrections of the derived LV endocardial border tracings were allowed to make. When the operator judged automatically detected endocardial borders to be incorrect, images were deleted from the data set.

Data analysis

The data analysis was subdivided into three sections: (Figure 19).

Section1. Inter-technique comparison: HHE vs SE

EDV, ESV, SV and LVEF measurements derived from HHE are compared against SE measurements by using the 2DE quantification software described previously. The image quality of HHE and SE recordings were compared using the advised 17 segment model from the American Heart Association. However, the model used in this study didn't include the apical three-chamber view, so only thirteen segments were assessed. Segmental endocardial border delineation was scored (2 = good, 1 = limited visibility, 0 = invisible) for each segment to describe SE and HHE image quality.

Section 2. Intra-technique comparison of quantification methods

In this section, three different 2DE quantification software tools (2DCPA, AS, LVivo) were compared for HHE, and SE derived data.

Section 3. Inter-technique comparison (SE vs 3DE)

This section compares HHE, and SE derived recordings, analysed with three quantification software (2DCPA, AS, and LVivo) with 3DE measurements analysed with DHM.

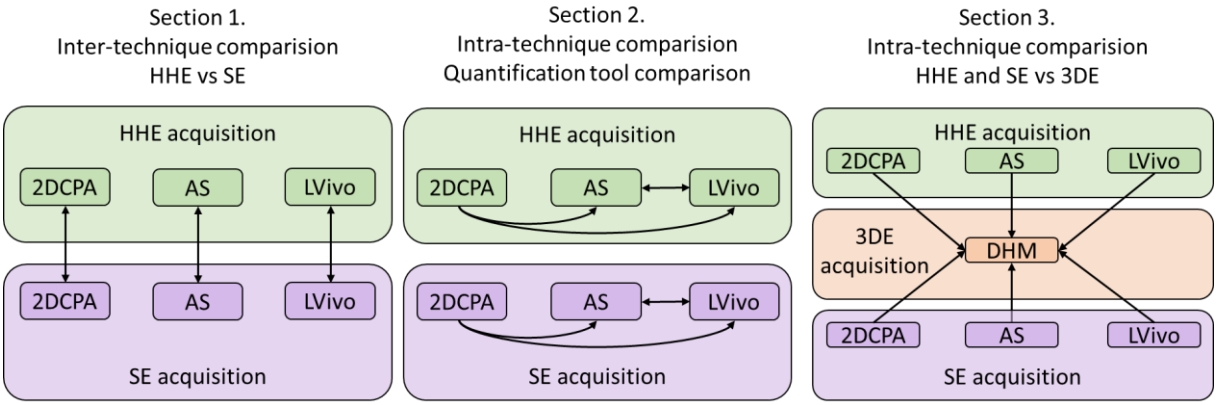

Figure 19. Schematic representation of the data analysis

Repeatability

Repeatability was assessed in all patients by repeating the measurements described in the *data acquisition section*. This means that after acquiring the first SE recording of the A2CH and A4CH view, the sonographer kept the probe in place and obtained a second and third recording. This procedure was also applied for HHE and 3DE data acquisition. Hence, in total three SE, HHE and 3DE recordings were acquired of the A2CH and A4CH view for each patient. All recordings were analysed with corresponding quantification software, as described in the sections *2DE quantification software* and *3DE quantification software.*

Statistical analysis

A sample size calculation was performed to limit the width of the 95% confidence interval (CI) around the standard deviation (SD) of the bias to 10%. Based on a mean SV of 60 ml and a mean error of 30%, a sample size of 32 patients was calculated to be sufficient.[70][71]
Statistical analysis and data visualization was performed using IBM SPSS statistics (*version 22, IBM Corp, USA*) and MATLAB (*MATLAB 2020a, MathWorks, Inc. United States*). Data were described as mean ± SD, and the assumption of normality was tested using the Shapiro-Wilk normality test. The statistical analysis compared EDV, ESV, SV and LVEF values of HHE vs SE, HHE vs 3DE and SE vs 3DE, but also intra-technique comparison of 2DCPA vs AS, 2DCPA vs LVivo and AS vs LVivo was performed. Image quality comparison focused on SE vs HHE and 2CH vs 4CH for both SE and HHE. Correlation calculations were performed using linear regression with Pearson correlation coefficients for normally distributed and Spearman correlation was used for non-normally distributed data. Correlation coefficients below 0.4 were considered low, between 0.4 and 0.7 was considered moderate, between 0.7 and 0.9 was considered strong, above 0.9 was considered very strong.
Bland-Altman analysis was performed to assess the bias and limits of agreement (LOA). The presence of proportional bias in the Bland–Altman plot is checked with regression analysis. To verify the significance of the biases, an ANOVA test was performed. Values of $p < 0.001$ were considered significant according to the Bonferroni correction. A bias of SV below 10% and a mean error below 30% are considered clinically acceptable and define agreement. For EDV, ESV and LVEF, the clinically acceptable bias was set to 10% and the clinically acceptable mean error to 15%.[72] Based on these percentages, the clinical acceptable LOA^- and LOA^+ were calculated with the following formulas:

$$(25)\ Mean\ error\ (\%) = 100\% \times 2 \times \frac{SD}{mean\ SV}$$

$$(2)\ LOA = bias \pm 2 \times SD$$

The LOA and mean error are influenced by the precision of the used reference technique. The formula of Critchley and Critchley can explain this:

$$(26)\ Mean\ error\ (\%) = \sqrt{experimental\ precision^2 + reference\ precision^2}$$

As formula 26 shows, the use of imprecise reference techniques will lead to wide LOA and high ME's. This emphasizes the need for the evaluation of reference precision in addition to experimental precision. Therefore, the repeatability coefficient (RC) was calculated for both the reference and experimental techniques. The RC is defined as:

$$(27)\ Repeatability\ coefficient\ (RC) = 2 \times \sqrt{1{,}96} \times SD_{\ within\ subject}$$

To calculate the within-subject SD for all three quantification tools and all three acquiring techniques, one-way ANOVA was performed with EDV, ESV, LVEF and SV values as dependent factors and the subject as independent. This was used to determine the RC. Second, the coefficient of variation (CV) was calculated for LVEF (CV_{LVEF}), SV (CV_{sv}), EDV (CV_{EDV}) and ESV (CV_{ESV}) for each measurement method. The CV is also a valuable metric to get insight into the precision performance of an experimental technique. The ratio is given between the within-subject SD and the mean measured value with the CV. A high within-subject SD and a relatively low mean will give a high CV. In the literature, a CV below 10% is considered clinically acceptable.[73]
To determine the reliability for the quantification of LVEF, SV, EDV, and ESV, the intraclass correlation coefficient (ICC's) was calculated. The ICC relates the size of the within-subject measurement error to the variability between subjects.[74], [75] The ICC has a value between 0 and 1, where a value of 1 corresponds to no measurement error and a value of 0 all the variability in measurements was caused by measurement error. ICC values below 0.75 were interpreted as moderate reliability, values ranging from 0.76 to 0.9 were interpreted as good reliability and values above 0.9 represent excellent reliability.[76]

VIII. Results

Baseline characteristics are presented in Table 3. Forty-three patients participated, seven patients were excluded because of poor endocardial delineation in SE images. In total 36 patients were included for analysis. Due to changes in the protocol, for four patients only one SE image was acquired, and for ten patients only two SE images were acquired instead of three. EDV ranged from 60 to 145 ml. ESV ranged from 26 to 74 ml, LVEF ranged from 40% to 71%, SV ranged from 26 to 127 ml. LVivo was unable to quantify 15/102 of the SE images and 7/102 of the HHE images. For AS endocardial border tracings, 0/102 were categorized as incorrect. For DHM endocardial border tracings, 4/102 were categorized as incorrect. Data were normally distributed.

1. Inter-technique comparisons - HHE vs SE

There was a strong correlation for the EDV, ESV, SV and LVEF between HHE and SE when quantified with 2DCPA, AS and LVivo. (Table 4, Figure 20) Except the correlation for LVEF with LVivo was moderate. The 95% CI for the LOA and bias were acceptable for LVEF measurements with 2DCPA and AS but not for LVivo (Table 4, Figure 21). The 95% CI for the LOA was acceptable for EDV and SV with all quantification tools. A4CH image quality was significantly ($p<0.001$) different between SE and HHE (10,49 ± 1,72 and 9,42 ± 1,96, respectively), as was A2CH image quality (9,82 ± 1,99 and 8,49 ± 2,07, respectively).The image quality of A2CH recordings was not significantly different from A4CH recordings for HHE and SE.

Table 3. Baseline demographic characteristics

	Mean
Total number of participants (N)	*36*
Male (%)	*16 (44%)*
Female (%)	*20 (56%)*
Age (yrs.)	*55.87 ± 14.85*
Body length (cm)	*172.56 ± 8.78*
Body weight (kg)	*76.76 ± 13.50*
BMI (kg/ $m^{2)}$	*25.71 ± 3.81*
Body surface area (m^2)	*1.87 ± 0.34*
Creatinine (µmol/L)	*82.31 ± 13.78*
Diabetes	*8%*
Hypertension	*33%*
Myocardial infarction	*8%*
Revascularization	*8%*
Valvular disease	*0%*
Peripheral disease	*11%*
COPD	*0%*

Values are presented as mean ± SD
COPD = chronic obstructive pulmonary disease.
BMI = Body mass index. BSA = body surface area

Table 4. Inter-technique comparison of HHE Versus SE

	N	Averaged SE (I)	Averaged HHE (J)	Corr	Bias (I-J)	95% CI of Bias	LOA	95% CI of LOA-	95% CI of LOA+
LVEF, %									
2DCPA	*36*	*57.46 ± 5.13*	*57.08 ± 4.68*	*0.78*	*0.38* ♦	*[-3.40:4.16]* ♦	*5.70* ♦	*[-6.96; -3.70]* ♦	*[4.45; 7.71]* ♦
AS	*36*	*62.56 ± 5.77*	*60.96 ± 5.57*	*0.71*	*1.60* ♦	*[-2.18:5.38]* ♦	*8.84* ♦	*[-9.79: -4.69]* ♦	*[7.89: 12.99]* ♦
LVivo	*34*	*56.43 ± 5.27*	*54.21 ± 6.22*	*0.68*	*2.22* ♦	*[-1.64:6.08]*	*7.23* ♦	*[-13.36: -6.16]*	*[10.59: 17.79]*
EDV, ml									
2DCPA	*36*	*106.94 ± 5.13*	*108.04 ± 25.96*	*0.85*	*-1.10* ♦	*[-21.71:19.51]*	*19.95* ♦	*[-26.83: -15.28]* ♦	*[13.08:24.62]* ♦
AS	*36*	*118.16 ± 5.77*	*120.20 ± 25.60*	*0.88*	*-2.04* ♦	*[-22.65:18.56]*	*23.32* ♦	*[-32.07: -18.63]* ♦	*[14.54:27.98]* ♦
LVivo	*34*	*103.06 ± 5.27*	*103.61 ± 27.63*	*0.86*	*-0.55* ♦	*[-21.60:20.51]*	*25.09* ♦	*[-37.84: -20.60]* ♦	*[19.51:36.73]* ♦
ESV, ml									
2DCPA	*36*	*45.93 ± 5.13*	*46.49 ± 12.06*	*0.90*	*-0.56* ♦	*[-10.68:9.57]*	*8.95* ♦	*[-12.10: -6.94]* ♦	*[5.82:10.98]* ♦
AS	*36*	*43.83 ± 5.77*	*47.20 ± 13.00*	*0.85*	*-3.37* ♦	*[-13.49:6.76]*	*14.55*	*[-22.14: -13.72]*	*[6.99:15.41]*
LVivo	*34*	*44.59 ± 5.27*	*47.60 ± 15.14*	*0.78*	*-2.47* ♦	*[-1.82:8.20]*	*20.44*	*[-26.13: -13.43]*	*[16.01:28.71]*
SV, ml									
2DCPA	*36*	*61.01 ± 5.13*	*58.45 ± 11.06*	*0.85*	*2.56* ♦	*[-9.07:14.18]*	*11.47* ♦	*[-18.81: -9.24]* ♦	*[-14.35:23.93]* ♦
AS	*36*	*74.53 ± 5.77*	*73.21 ± 15.61*	*0.85*	*1.32* ♦	*[-10.30:12.94]*	*15.54* ♦	*[-18.70: -9.74]* ♦	*[12.38:21.35]* ♦
LVivo	*34*	*57.95 ± 5.27*	*56.08 ± 15.31*	*0.82*	*1.87* ♦	*[-10.00:13.74]*	*16.55* ♦	*[-19.49: -9.58]* ♦	*[13.32:23.23]* ♦

Values are presented as mean ± SD. * p < 0.001
♦ Within the clinical acceptable LOA or bias range
Corr = Correlation Coefficient; CI = confidence interval; EDV = end-diastolic volume; ESV = End-systolic volume; LVEF = left ventricle ejection fraction; LOA = limits of agreement; SV = Stroke volume

2. Intra-technique Comparison of quantification methods

HHE - For HHE, there was a strong correlation between the three quantification software tools for the variables EDV, ESV and SV, except ESV quantification of LVivo vs 2DCPA (Table 5, Figure 22). The correlation for LVEF was moderate. The correlations of AS vs LVivo were the highest. The average SV and LVEF quantifications were significantly (p<0,001) larger for AS than for LVivo (Table 5, Figure 18).

SE – For SE, there was a moderate to strong correlation between the three quantification software tools for the variables EDV, ESV, SV and LVEF (Table 6, Figure 23). Correlations were overall lower compared to HHE. The SV and LVEF quantifications were significantly (p<0,001) larger for AS than for LVivo (Table 6, Figure 20).

3. Inter-technique comparison against 3DE measurements

HHE vs 3DE
For HHE compared to 3DE, there was a strong correlation for EDV, ESV and LVEF, except for SV and ESV quantification with LVivo. The correlation was moderate for LVEF (Table 7, Figure 24). EDV, SV and LVEF were significantly (p<0,001) lower for SE (LVivo) compared to 3DE (DHM) (Table 7, Figure 22). SV was significantly lower for SE (2DCPA) compared with 3DE (DHM). LOA and bias were acceptable for LVEF measurements with AS but not for LVivo and 2DCPA.

SE vs 3DE
For SE compared to 3DE showed strong correlations for all variables, except for EDV (2DCPA) and ESV (LVivo) quantification (Table 8, Figure 25). The correlation for LVEF was moderate. SV quantified with 2DCPA and LVivo, was significantly (p<0,001) lower than 3DE (DHM). LOA and bias were acceptable for LVEF measurements with AS but not for LVivo and 2DCPA.

Figure 20 Correlation of the HHE and SE technique with AS software

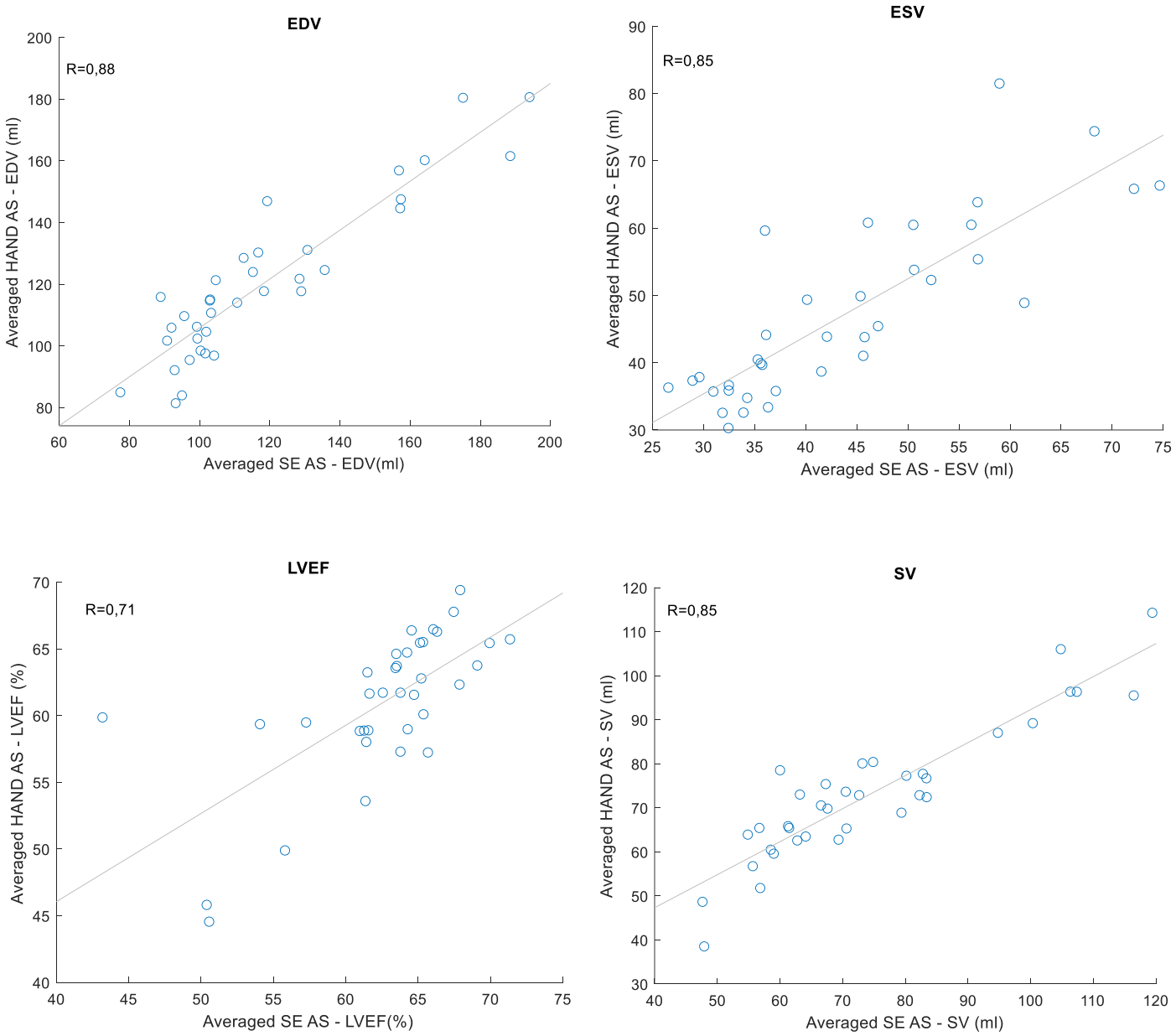

Correlation analysis of **(A)** End-diastolic volume (EDV), **(B)** End-systolic volume (ESV), **(C)** left ventricular ejection fraction (LVEF), **(D)** Stroke Volume (SV),
AS = Auto Strain; 3DE = three-dimensional echocardiography; EDV = end-diastolic volume; ESV = end-systolic volume; HAND = HHE measurements; LVEF = left ventricle ejection fraction; SV = stroke volume; R = Correlation coefficient

Figure 21 Bland-Altman plots of the HHE versus the SE technique with AS software

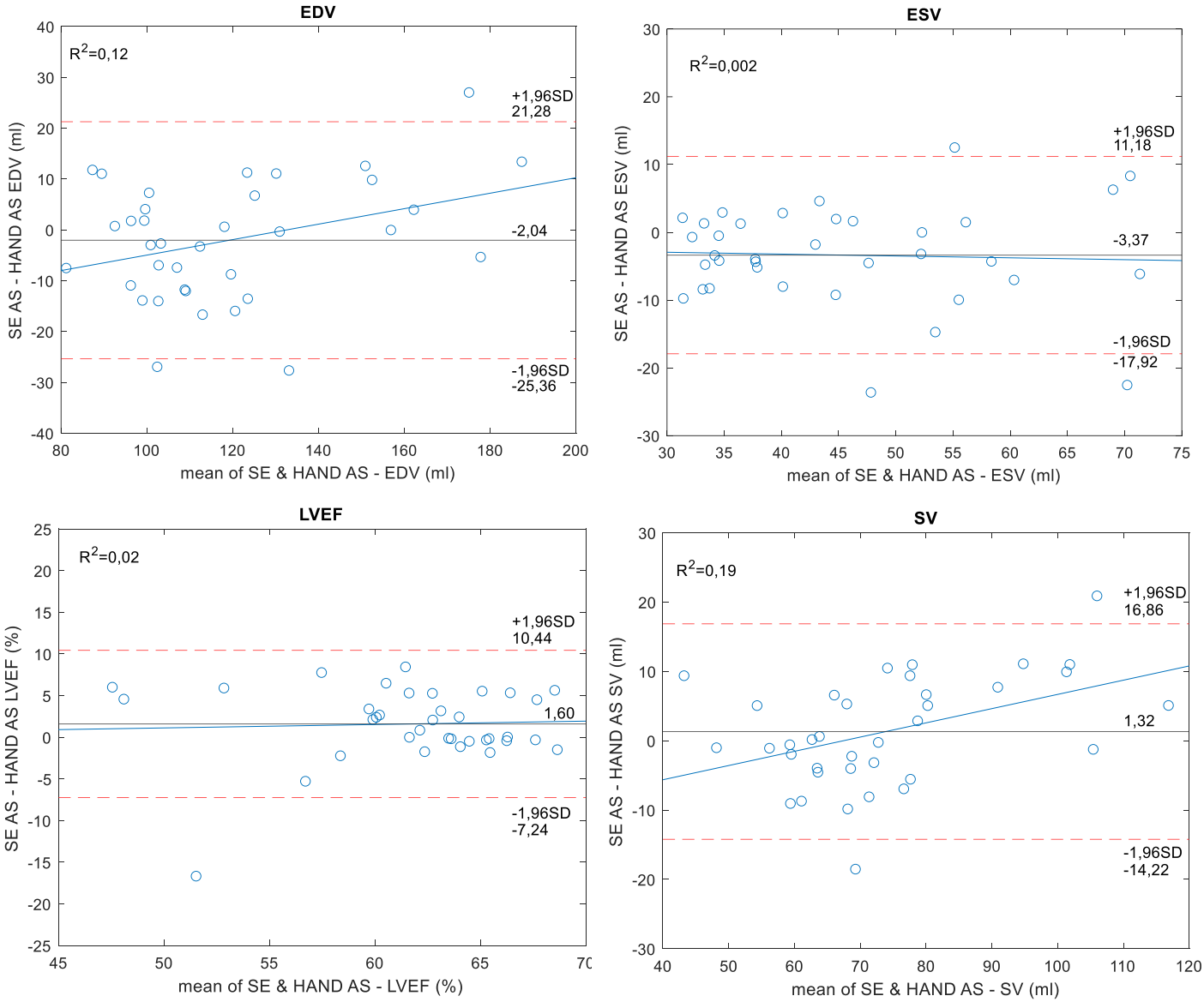

Bland-Altman analysis of **(A)** EDV, **(B)** ESV, **(C)** LVEF, **(D)** SV. R^2 = Regression coefficient. Other abbreviations as in Figure 20

Table 5. **Intra-technique quantification method comparison for HHE**

	N	Corr	Bias	95% CI of Bias	LOA	95% CI of LOA-	95% CI of LOA+
LVEF, %							
2DCPA - AS	*36*	*0.52*	*-3.88*	*[-7.66: -0.10]*	*9.15*	*[-15.68: -10.38]*	*[2.63:7.92]*
2DCPA - LVivo	*35*	*0.61*	*2.87♦*	*[-0.94:6.68]*	*10.06*	*[-9.97: -4.13]*	*[9.87:15.71]*
AS - LVivo	*35*	*0.69*	*6.75**	*[2.94:10.55]*	*8.82♦*	*[-4.63:0.53]*	*[12.97:18.13]*
EDV, ml							
2DCPA - AS	*36*	*0.83*	*-12.16*	*[-32.77:8.45]*	*30.15*	*[-50.99: -33.61]*	*[9.30:26.68]*
2DCPA - LVivo	*35*	*0.79*	*4.43♦*	*[-16.33:25.88]*	*33.78*	*[-39.38: -19.55]*	*[28.40:48.23]*
AS - LVivo	*35*	*0.89*	*16.58*	*[-4.17:37.34]*	*27.01*	*[-17.44: -2.03]*	*[35.20:50.61]*
ESV, ml							
2DCPA - AS	*36*	*0.74*	*-0.71♦*	*[-10.84:9.42]*	*20.06*	*[-26.57: -14.95]*	*[13.54:25.15]*
2DCPA - LVivo	*35*	*0.66*	*-1.10♦*	*[-11.30:9.09]*	*19.61*	*[-26.23: -14.82]*	*12.62:24.02]*
AS - LVivo	*35*	*0.84*	*0.40♦*	*[10.59:9.80]*	*16.65*	*[-21.09: -11.72]*	*[10.93:20.30]*
SV, ml							
2DCPA - AS	*36*	*0.83*	*-14.75*	*[-26.37: -3.13]*	*16.29♦*	*[-35.76: -26.32]*	*[-3.18:6.25]*
2DCPA - LVivo	*35*	*0.75*	*2.37♦*	*[-9.33:14.08]*	*20.35*	*[-23.25: -11.64]*	*[16.38:27.99]*
AS - LVivo	*35*	*0.84*	*17.12**	*[5.42:28.83]*	*18.32♦*	*[-6.30:4.29]*	*[29.96:40.55]*

Values are mean. *p < 0.001
♦LOA within the clinical acceptable LOA
Abbreviations as in Table 4

Table 6. **Intra-technique quantification method comparison for SE**

	N	Corr	Bias	95% CI of Bias	LOA	95% CI of LOA-	95% CI of LOA+
LVEF, %							
2DCPA - AS	*36*	*0.62*	*-5.10*	*[-8.88: -1.32]*	*8.81*	*[-16.45: -11.36]*	*[1.15:6.25]*
2DCPA - LVivo	*34*	*0.64*	*1.03♦*	*[-2.81:4.86]♦*	*11.42*	*[-13.46: -6.83]*	*[8.88:15.52}*
AS - LVivo	*34*	*0.53*	*6.13**	*[2.30:9.97]*	*12.87*	*[-10.34: -2.80]*	*[15.06:22.60]*
EDV, ml							
2DCPA - AS	*36*	*0.72*	*-11.22*	*[-31.82:9.39]*	*34.04*	*[-55.07: -35.45]*	*[13.02:32.64]*
2DCPA - LVivo	*34*	*0.65*	*3.87*	*[-17.04:24.78]*	*36.07*	*[-45.19: -22.72]*	*[30.46:52.93]*
AS - LVivo	*34*	*0.77*	*15.09*	*[-5.82:35.99]*	*29.64*	*[-25.42: -6.89]*	*[37.06:55.60]*
ESV, ml							
2DCPA - AS	*36*	*0.72*	*2.10*	*[-8.03:12.22]*	*17.26*	*[-20.16: -10.18]*	*[14.38:24.36]*
2DCPA - LVivo	*34*	*0.49*	*0.81*	*[-9.46:11.08]*	*24.23*	*[-31.92: -16.91]*	*[18.53:33.54]*
AS - LVivo	*34*	*0.69*	*-1.29*	*[-11.56:8.99]*	*20.74*	*[-29.15: -16.93]*	*[13.81:26.58]*
SV, ml							
2DCPA - AS	*36*	*0.69*	*-13.51*	*[-25.14: -1.90]*	*22.87*	*[-42.98: -29.80]*	*[2.77:15.94]*
2DCPA - LVivo	*34*	*0.74*	*3.06*	*[-8.73:14.85]*	*16.85♦*	*[-19.79: -9.33]*	*[15.45:25.91]*
AS - LVivo	*34*	*0.82*	*16.58**	*[4.78:28.37]*	*18.98♦*	*[-9.47:2.48]*	*[30.67:42.62]*

Values are mean. *p < 0.001
♦LOA within the clinical acceptable LOA
Abbreviations as in Table 4

Figure 22 Correlation of AS and LVivo quantification for HHE derived variables

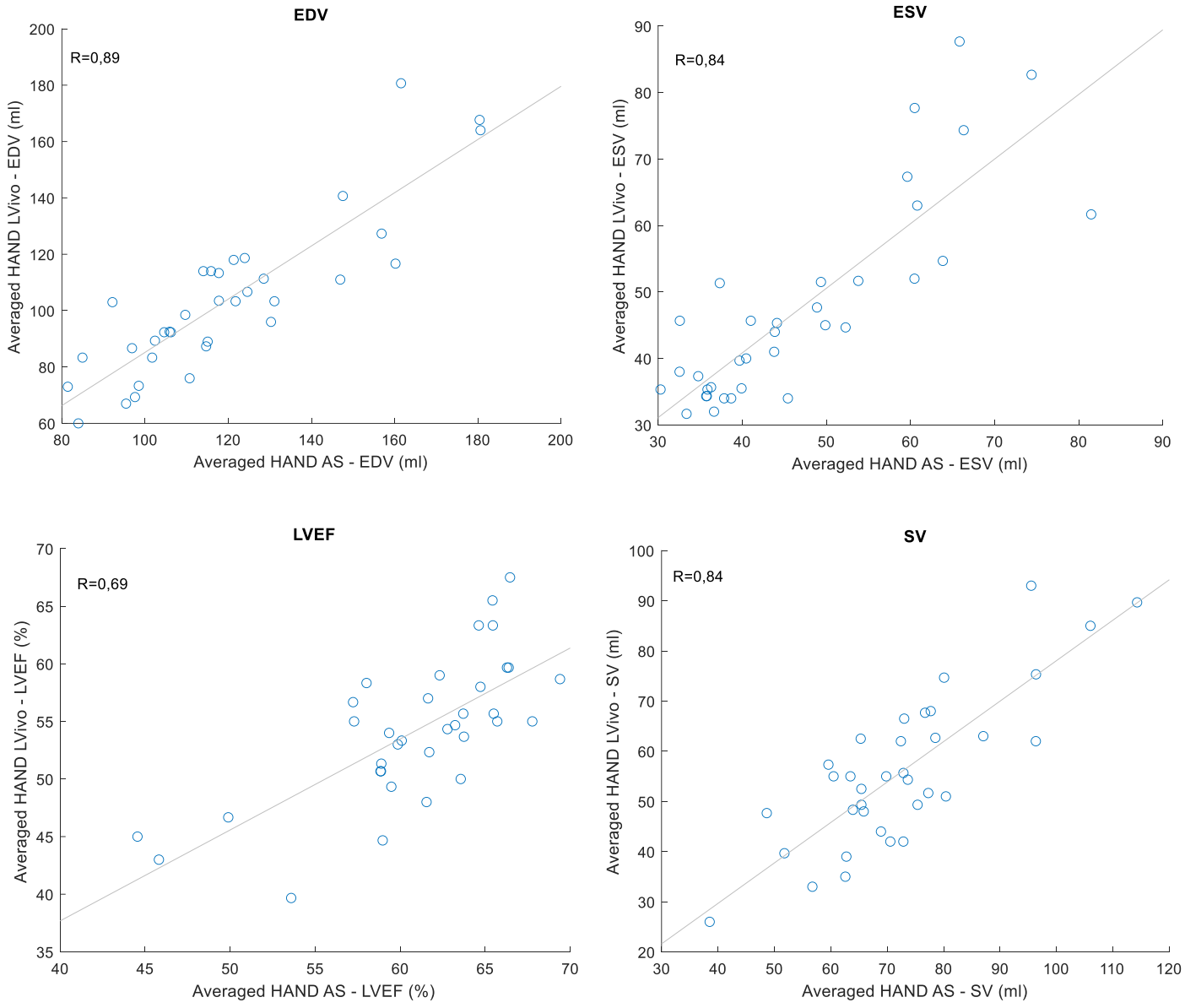

Correlation analysis of **(A)** EDV, **(B)** ESV, **(C)** LVEF, **(D)** SV. Abbreviations as in Figure 20

Figure 23 Bland-Altman plots of AS versus LVivo quantification for HHE derived variables.

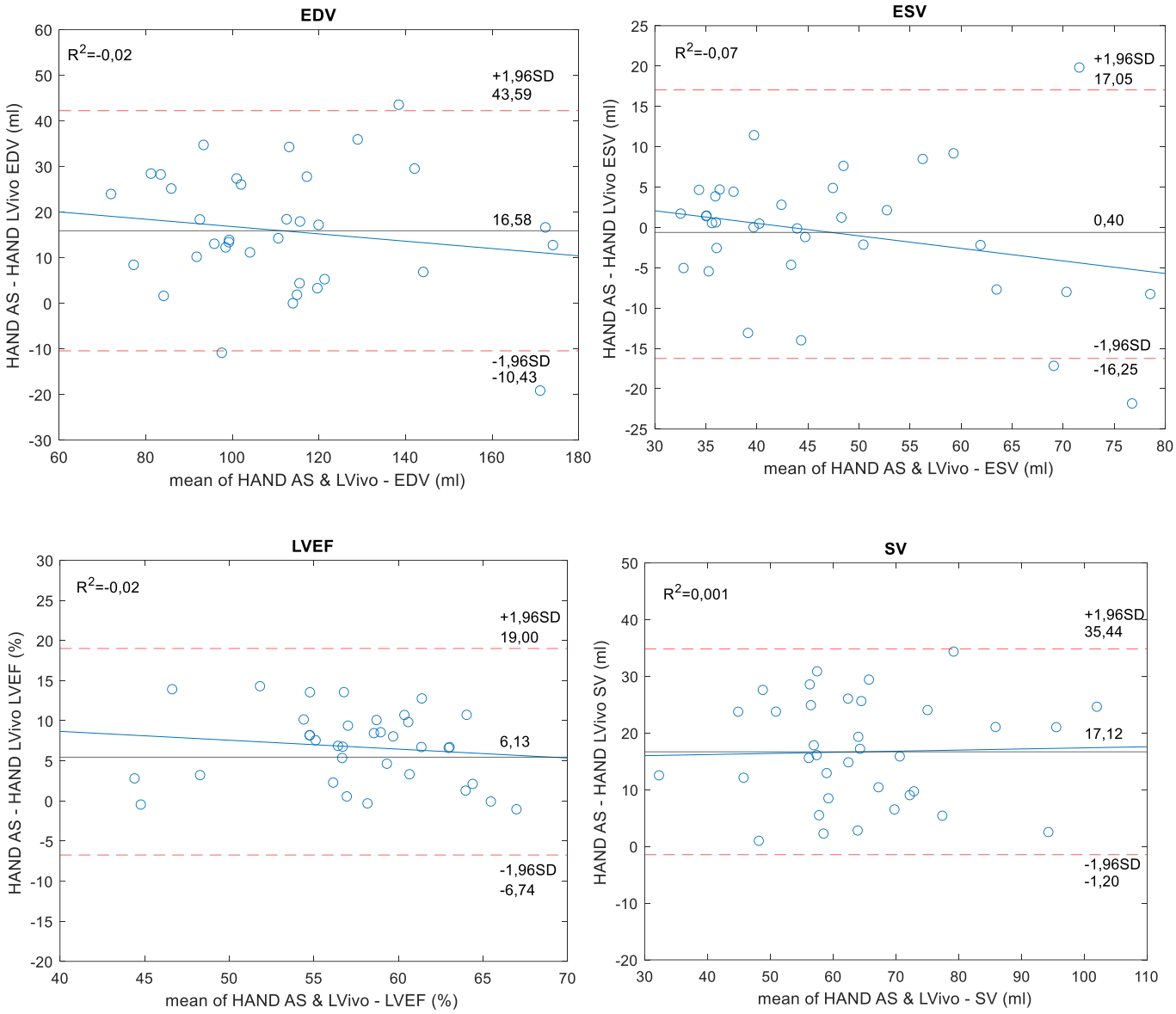

Bland-Altman analysis of **(A)** EDV, **(B)** ESV, **(C)** LVEF, **(D)** SV. Abbreviations as in Figure 20

Table 7. Inter-technique quantification method comparison of HHE versus 3DE

	N	Averaged Lumify (J)	Averaged 3DE (I)	Corr (I J)	Bias (I-J)	95% CI of Bias	LOA	95% CI of LOA-	95% CI of LOA+
LVEF, %									
DHM	*36*		*60.39 ± 4.98*						
2DCPA	*36*	*57.08 ± 4.68*		*0.56*	*3.31*	*[-0.47:7.09]*	*8.49♦*	*[-7.62: -2.73]♦*	*[9.36:14.25]♦*
AS	*36*	*60.96 ± 5.57*		*0.55*	*-0.56♦*	*[-4.34:3.22]♦*	*9.88♦*	*[-13.29: -7.59]♦*	*[6.46:12.17]♦*
LVivo	*35*	*54.21 ± 6.22*		*0.51*	*6.18**	*[2.38:9.99]*	*11.12♦*	*[-8.19: -1.67]*	*[14.04:20.56]*
EDV, ml									
DHM	*36*		*134.61±36.83*						
2DCPA	*36*	*57.08 ± 4.68*		*0.78*	*26.57*	*[-5.96:47.17]*	*38.28*	*[-28.14: -3.63]*	*[56.76:81.28]*
AS	*36*	*60.96 ± 5.57*		*0.88*	*14.41*	*[-6.20:35.01]*	*40.47*	*[-37.74: -14.39]*	*[43.20:66.56]*
LVivo	*35*	*54.21 ± 6.22*		*0.76*	*31.00**	*[1024:51.75]*	*44.46*	*[-23.73:1.05]*	*[60.94:85.72]*
ESV, ml									
DHM	*36*		*52.70± 17.50*						
2DCPA	*36*	*57.08 ± 4.68*		*0.71*	*6.21*	*[-3.91:16.34]*	*18.77*	*[-18.00: -7.13]*	*[19.56:30.42]*
AS	*36*	*60.96 ± 5.57*		*0.83*	*5.50*	*[-4.62:15.63]*	*23.27*	*[-24.48: -11.04]*	*[22.05:35.49]*
LVivo	*35*	*54.21 ± 6.22*		*0.68*	*5.11*	*[-5.09:15.31]*	*20.36*	*[-20.14: -8.73]*	*[18.95:30.35]*
SV, ml									
DHM	*36*		*79.98± 21.17*						
2DCPA	*36*	*57.08 ± 4.68*		*0.84*	*21.53**	*[9.91:33.15]*	*26.73*	*[-13.39:2.23]*	*[40.83:56.44]*
AS	*36*	*60.96 ± 5.57*		*0.79*	*6.78*	*[-4.85:18.40]*	*12.14♦*	*[-26.32: -11.52]*	*[25.07:39.87]*
LVivo	*35*	*54.21 ± 6.22*		*0.64*	*23.90**	*[12.20:35.61]*	*31.21*	*[-14.73:2.79]*	*[45.01:62.53]*

Values are mean ± SD. *p < 0.001
♦LOA or bias within the clinical acceptable boundaries
3DE= three-dimensional echocardiography; DHM = Heart Model; Other abbreviations as in Table 4

Table 8. Inter-technique quantification method comparison of SE versus 3DE

	N	Averaged 2D EPIQ (I)	Averaged 3DE HM (J)	Corr	Bias (J-I)	95% CI of Bias	LOA	95% CI of LOA-	95% CI of LOA+
LVEF, %									
DHM	*36*		*60.39 ± 4.98*						
2DCPA	*36*	*57.46 ± 5.13*		*0.61*	*2.94*	*[-0.84:6.72]*	*8.51♦*	*[-8.01:-3.12]♦*	*[9.00:13.89]♦*
AS	*36*	*62.37 ± 5.77*		*0.60*	*-2.16*	*[-5.94:1.62]♦*	*11.31♦*	*[-16.73: -10.21]♦*	*[5.89:12.40]♦*
LVivo	*34*	*56.43 ± 5.27*		*0.55*	*-3.97*	*[0.13:7.80]*	*18.27*	*[-9.85: -3.54]*	*[11.47:17.79]*
EDV, ml									
DHM	*36*		*134.61±36.83*						
2DCPA	*36*	*57.46 ± 5.13*		*0.67*	*27.67*	*[7.06:48.27]*	*42.45*	*[-27.04: -2.53]*	*[57.87:82.38]*
AS	*36*	*62.37 ± 5.77*		*0.85*	*16.45*	*[-4.15:37.06]*	*34.95*	*[-28.58: -8.41]*	*[41.32:61.48]*
LVivo	*34*	*56.43 ± 5.27*		*0.83*	*31.54**	*[10.63:5245]*	*38.50*	*[-20.78:3.18]*	*[59.89:83.86]*
ESV, ml									
DHM	*36*		*52.70 ± 17.50*						
2DCPA	*36*	*57.46 ± 5.13*		*0.70*	*6.77*	*[-3.36:16.34]*	*18.07*	*[-16.53: -6.07]*	*[19.61:30.07]*
AS	*36*	*62.37 ± 5.77*		*0.74*	*8.87*	*[-1.26:19.00]*	*19.83*	*[-16.68: -5.21]*	*[22.95:34.42]*
LVivo	*34*	*56.43 ± 5.27*		*0.68*	*7.59*	*[-2.69:17.86]*	*20.40*	*[-20.19: -7.49]*	*[22.66:35.35]*
SV, ml									
DHM	*36*		*79.98 ± 21.17*						
2DCPA	*36*	*57.46 ± 5.13*		*0.73*	*18.97 **	*[7.35:30.59]*	*26.54*	*[-15.24:0.10]*	*[37.84:53.18]*
AS	*36*	*62.37 ± 5.77*		*0.81*	*5.45*	*[-6.17:17.08]*	*23.14♦*	*[-24.38: -11.01]*	*[21.91:35.29]*
LVivo	*34*	*56.43 ± 5.27*		*0.75*	*22.03 **	*[10.24:33.82]*	*26.80*	*[-13.65:2.71]*	*[41.35:57.71]*

Values are mean ± SD. *p < 0.001
♦LOA or bias within the clinical acceptable boundaries
3DE= three-dimensional echocardiography; Other abbreviations as in Table 7

Figure 24 Correlation of measurements derived by 3DE (DHM) and HHE (AS) for all variables.

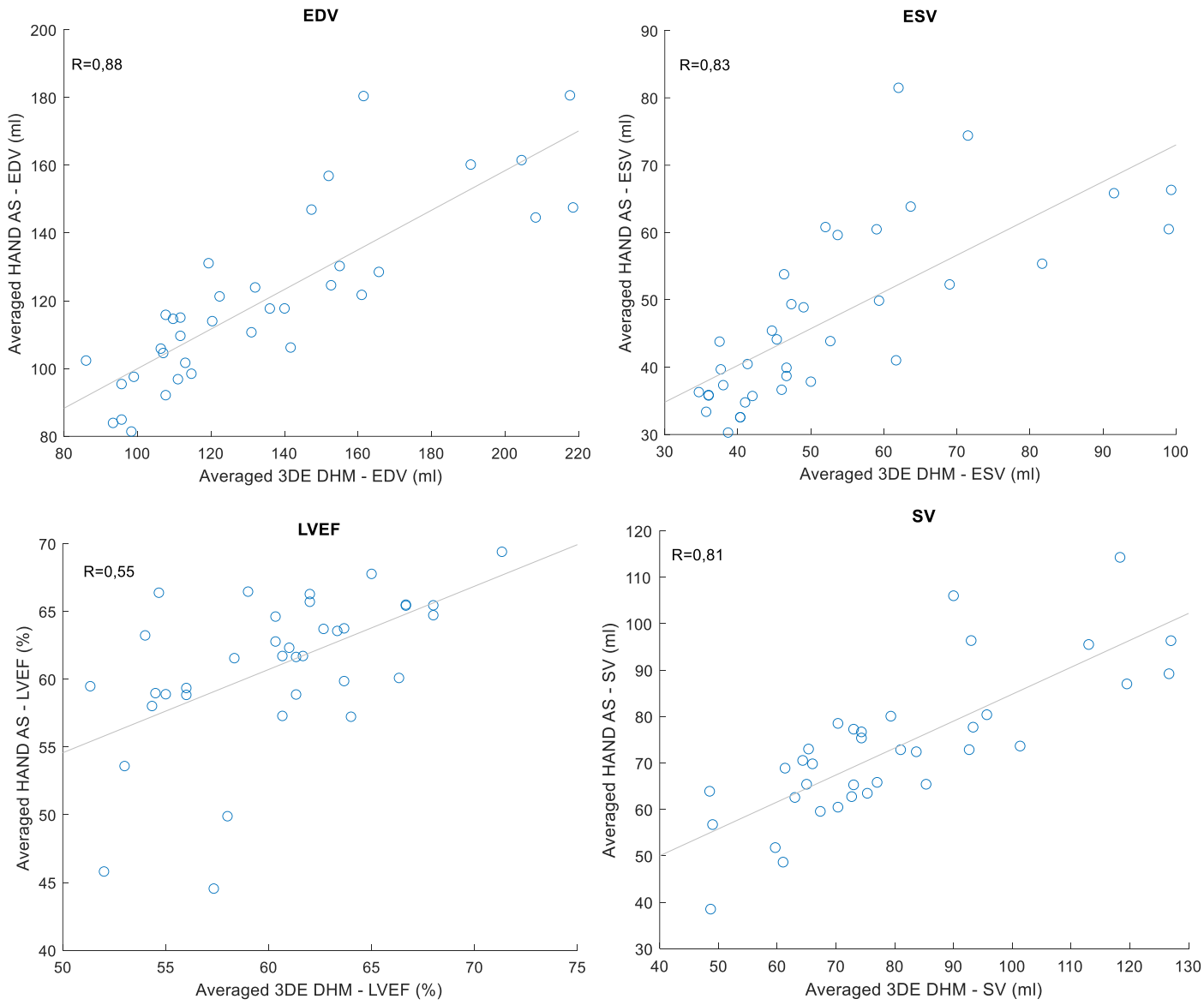

Correlation analysis of **(A)** EDV, **(B)** ESV, **(C)** LVEF, **(D)** SV. 3DE = three-dimensional echocardiography; Other abbreviations as in Figure 20

Figure 25 Bland-Altman plots of 3DE (DHM) versus HHE (AS) derived measurements for all variables.

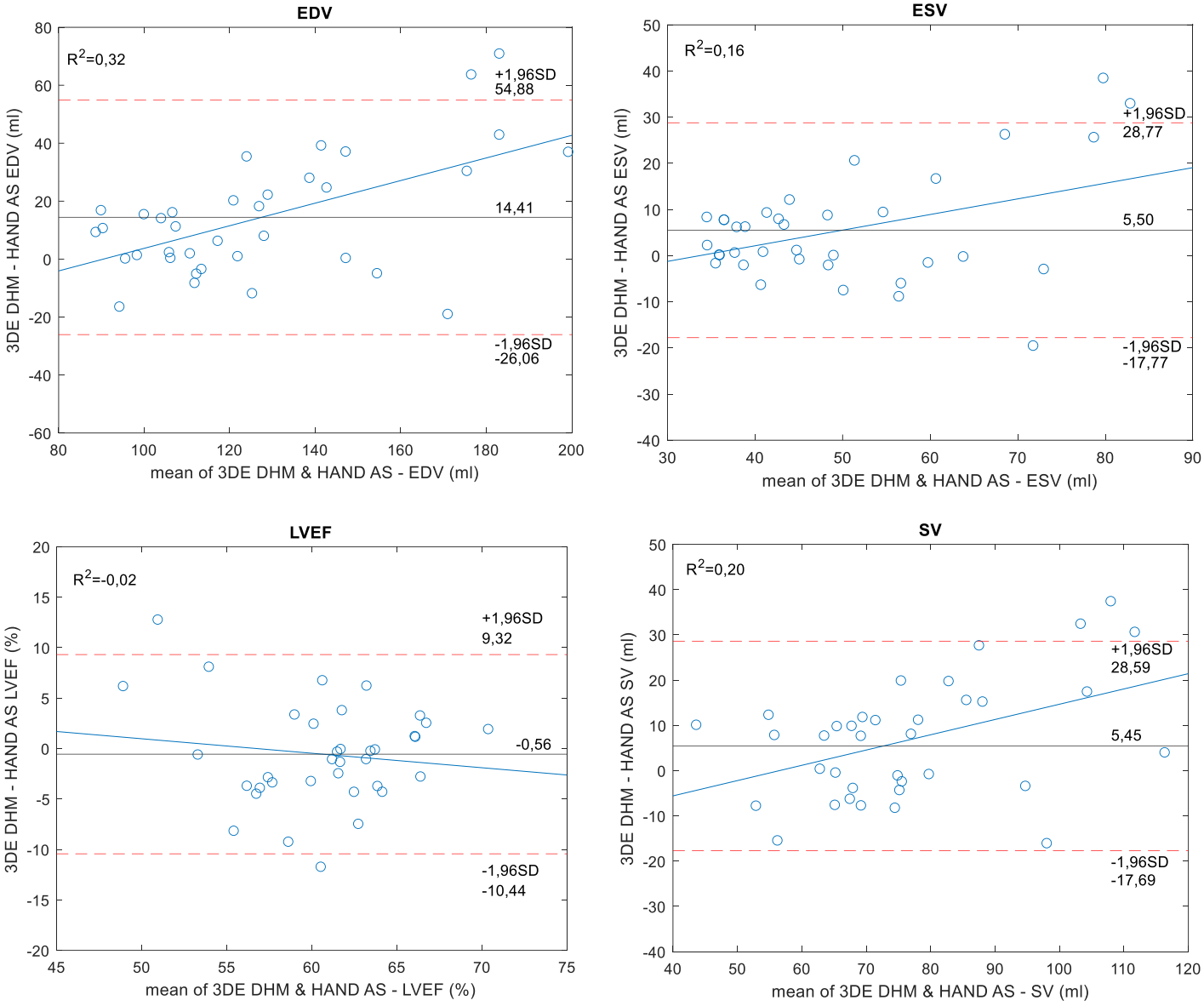

Bland-Altman analysis of **(A)** EDV, **(B)** ESV, **(C)** LVEF, **(D)** SV. 3DE = three-dimensional echocardiography; Other abbreviations as in Figure 20

4. Repeatability and reliability analysis

Results of ICC, CV and RC calculations are presented in table 9, table 10 and table 11, respectively. Because of an incomplete SE dataset, the ICC, CV and RC were calculated for twenty-two patients in the SE category. Moreover, the LVivo tool failed to quantify an additional seven recordings, with as a consequence, the ICC, CV and RC were calculated for fifteen patients in the SE LVivo category. Furthermore, the DHM tool quantified four images incorrectly, resulting in ICC, CV and RC calculations for thirty-two patients in the 3DE (DHM) category.

Table 9. Reliability – Intraclass correlation (ICC)

	N	EDV	ESV	SV	LVEF
HHE					
2DCPA	*36*	*0.983*	*O.967*	*0.778*	*0.899*
AS	*36*	*0.979*	*0.965*	*0.950*	*0.908*
LVivo	*30*	*0.965*	*0.937*	*0.925*	*0.759*
SE					
2DCPA	*22*	*0.982*	*0.959*	*0.967*	*0.879*
AS	*22*	*0.983*	*0.939*	*0.963*	*0.794*
LVivo	*15*	*0.924*	*0.915*	*0.912*	*0.805*
3DE					
DHM	*32*	*0.894*	*0.982*	*0.962*	*0.921*

Values are mean. *p < 0.001
ICC = intraclass correlation; other abbreviations as in Table 4

Table 10. Coefficient of variation (CV)

	N	CV_{EDV}	CV_{ESV}	CV_{SV}	CV_{LVEF}
HHE					
2DCPA	*36*	*4.79±3.49*	*7.13±5.08*	*12.78±8.32*	*3.96±2.31*
AS	*36*	*4.89±2.17*	*7.17±3.70*	*7.24±3.26*	*4.02±2.61*
LVivo	*30*	*7.54±4.16*	*8.53±10.59*	*10.10±6.30*	*7.53±4.55*
SE					
2DCPA	*22*	*4.47±3.00*	*6.29±5.64*	*6.77±4.45*	*4.05±3.07*
AS	*22*	*4.14±2.91*	*6.23±7.65*	*7.42±4.32*	*3.98±1.78*
LVivo	*15*	*7.74±8.18*	*11.56±6.45*	*9.65±9.24*	*4.85±4.86*
3DE					
DHM	*32*	*7.35±9.19*	*6.19±4.03*	*8.08±5.63*	*3.97±2.77*

CV = coefficient of variation; other abbreviations as in Table 4

Table 11. Repeatability coefficient (RC)

	N	EDV (ml)	ESV (ml)	SV (ml)	LVEF (%)
HHE					
2DCPA	36	13.77	9.02	22.09	6.18
AS	36	16.17	9.71	14.76	6.75
LVivo	30	21.81	15.58	16.27	11.05
SE					
2DCPA	22	13.16	7.90	11.47	6.43
AS	22	14.18	7.93	15.35	6.04
LVivo	15	23.75	11.42	15.94	7.43
3DE					
DHM	32	29.81	9.54	18.62	6.49

Values are mean. *p < 0.001
RC = repeatability coefficient; Other abbreviations as in Table 4

IX. Discussion

This study investigated the correlation, accuracy and precision of an HHE device versus a clinical high-end reference technique. The results suggest excellent consistency and a clinically acceptable precision between HHE and SE. However, accuracy exceeds the clinical threshold of 10% for all volumetric variables, except LVEF. Therefore, HHE is not interchangeable with SE for volumetric measurements. The results also indicated that HHE is not interchangeable with 3DE except for LVEF quantification with AS. Furthermore, we evaluated three LV quantification tools. These results show an excellent correlation between the automated AS software and the newly developed online automated LVivo software for quantifying HHE images. However, there was no agreement between any of the three quantification software tools. Additional research with a focus on the dynamic evaluation of hemodynamic variables over time is needed.

SE is currently considered the routinely used technique to evaluate cardiac chamber volumes and function non-invasive and cost-effective. However, the usability and availability of an HHE device make it the best fit for focused examination at the point of care compared to SE. Beyond simplicity of use, our study results showed a good correlation between HHE and SE, which is in line with a previous study.[5] Results show that the HHE device is not interchangeable with high-end SE for volumetric measurements due to inaccuracy likely driven by the lack of ECG timing on the HHE device. 2DCPA and AS software approximate the ED frame by detecting the QRS complex in the ECG signal for SE data. For the definition of ES, there are a variety of solutions, ranging from the detection of the end of the T-wave in the ECG over automatic AI algorithms that process segmental data. Nevertheless, ED and ES frame identification based on the ECG identify ED and ES indirectly. The observer selected the ES and ED frame for HHE image quantification with AS and 2DCPA, making it operator dependent. Because LV volume changes quickly over time depending on the patient's heart rate, slight deviations in ES and ED frame selection can significantly impact cardiac function quantification, as is shown in the study of R. Mada et al.[77] Moreover, it remains completely unclear which approaches are valid and if they allow reproducible results. Hence, the different ED and ES frame identification approaches could have led to inaccuracy of HHE quantifications compared to SE. However, it is obvious from the existing literature that different SV monitoring techniques have their limitations.[35][78] Hence, no single device can meet all clinical requirements. The purpose of application determines whether the comparability of values is clinically more relevant than the degree of concordance between absolute values. For example, for diagnostic purposes, accuracy of absolute values is considered clinically important. In contrast, for monitoring purposes, changes over time and trending are clinically more relevant. Clinical situations at the ICU or OR often demand more information about the dynamic responses to an intervention instead of the absolute value.[70] Besides, to a certain extent, the desirable level of agreement can be adjusted if the device has clear advantages over the reference technique. For example, HHE is a portable, user-friendly device that can be applied at the patient's bedside in a time-sensitive fashion. Results show that HHE performs better as an SV trend monitor instead of providing absolute SV values compared to SE.

Comparison of HHE and SE shows that none of the acquiring techniques or quantification software is interchangeable with 3DE. These results are in concordance with previously published studies, describing that 2DE measurements underestimate LV volumes compared to 3DE.[54][78] Furthermore, considering the size of the device, HHE can acquire high-resolution images. Results show that on average only one segment of the endocardial border in the A4CH of A2CH view has either limited visibility or is invisible on the HHE recording, compared to good or limited visibility on the SE recording. Since most AI algorithms can cope with poor visibility of two to three segments, endocardial border delineation in HHE recordings should not limit the performance of AI-driven quantification tools.[52][75] In line with this, shows appendix B no correlation between the image quality of HHE recordings and the performance of HHE compared to SE, likely due to the high quality of the HHE images.
Moreover, the HHE S4-1 transducer has a slightly larger width of 3mm than the X5-1, making A2CH views harder to obtain transthoracic. However, results did not show a significant difference in image quality between A4CH and A2CH recordings with HHE. Concluding, Lumify

is a well-designed HHE device that shows promising results for future application as LVEF quantification or SV monitoring device for point of care application.

AS and LVivo are demonstrated to be the preferred method compared to the 2DCPA to assess LV systolic function in a point of care setting. However, the M-mode dependency to select ED and ES frames may become a significant limitation of AS software for point of care treatment. According to the analysis shown in Appendix A, the AS tool traces a wider and longer endocardial border than LVivo tracings leading to larger volumes calculated by AS. As a result, LVivo and AS quantifications are not interchangeable. However, neither is LVivo with 2DCPA nor AS with 2DCPA. This can be explained by what is described in previous literature: manual tracings based on the endocardial boundaries of the EDV and ESV phases in the cardiac cycle, followed by model-based calculations, are associated with considerable intra-observer variability. This intra-observer variability stems from individual differences in the perception of the blood tissue interface in the presence of endocardial trabeculae, especially at end-systole.[80] In line with this, reliability showed a low ICC_{SV} for 2DCCPA quantification compared with other ICC's, and repeatability analysis shows a high CV_{SV} value for 2DCPA quantifications. However, literature also describes how endocardial border identification with automatic AI algorithms is also known for making prone errors due to suboptimal image quality and artefacts.[80], [81] This emphasizes that what really matters for all quantification tools, in general, is how the generated data are interpreted by the physicians and nurses.

However, it should be noted that the LVivo tool could not quantify all HHE and SE images. This is highly likely due to incorrect depth settings and poor endocardial delineation, as shown in Figure 26. In addition, according to the manufacturer of the LVivo tool (DIA), the LVivo tool has limited capability to compensate if the recordings are not acquired according to the predefined protocol (Appendix C). So, future research and implementation should focus on acquiring recordings that comply with the acquisition requirements defined by the manufacturer. Nevertheless, despite insufficient agreement compared to the other two quantification tools, the LVivo software is, in our opinion, "the easiest to use" tool and therefore more suited for point of care usage, as it requires only limited user input.

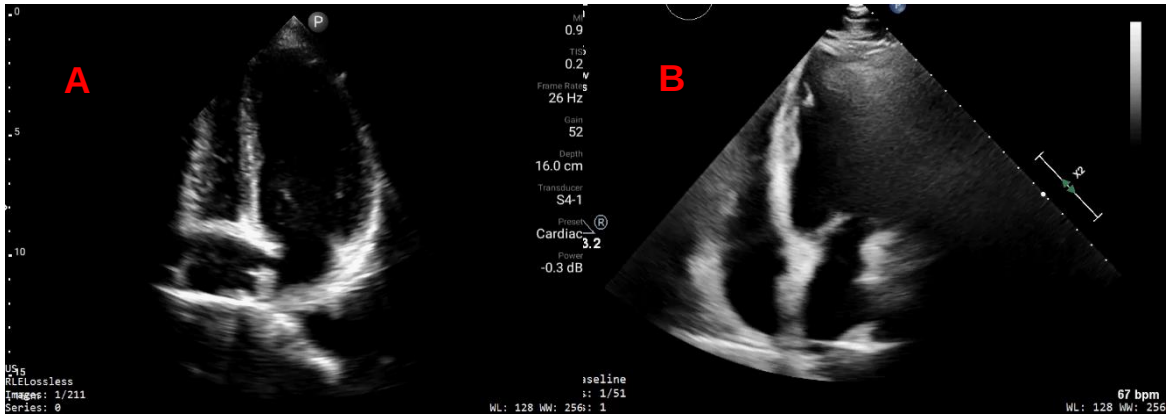

Figure 26. A) shows an HHE acquired image which could not be quantified with LVivo probably due to high depth settings B) shows an SE acquired image which failed to be quantified with LVivo probably due to poor endocardial border delineation on the lateral side.

The evaluation of reference precision in addition to experimental precision shows that the impreciseness of any quantification tool cannot be explained by the individual imprecisions of SE, 3DE, nor HHE measurements. Furthermore, it should be noted that although individual precision of SE was better than HHE for almost every parameter, this does not mean that SE is more precise when compared to the true value, as a true gold standard was not available. It solely indicates that SE measurements were consistent, which led to the repeated measurements being closer to each other. In addition, the precision of HHE measurements is considered clinically acceptable based on the clear advantages at the point of care over the reference techniques (SE, 3DE). The same applies to software comparisons since LVivo is compared to

2DCPA and AS, the only online fully automatic quantification tool that can be used efficiently at the patient's bedside.

The clinical implication of this study is that the first steps are made towards non-invasive and time-efficient quantification and monitoring of left ventricle function for hemodynamic point of care assessment in critically ill patients with HHE. In this way, quick actions can be made accordingly, such as fluid therapy or administration of vasopressors, leading to an improved clinical patient outcome.

Future prospects

For HHE to be acknowledged and thriving at the point of care, it must be affordable, easy to use and provide reliable imaging. Although it is relatively easy for already trained physicians in echocardiography to acquire and interpret A2CH and A4CH recordings, non-echocardiographers need to be trained to meet high standards consistently. Especially since the A4CH and A2CH views are challenging to acquire without training, education should teach physicians how to discern images from an HHE device as diagnostically sufficient or as suboptimal quality that merits a complete echocardiographic examination by an expert with a SE device. Training is therefore critically important and needs standardization. However, this training could be time-intensive. Therefore a universally online available platform for training should be designed to stimulate the developments and implementation of HHE devices.

The design and implementation of HHE are targeted toward cost-effective and high-quality care. Newer designs of miniaturized cardiac ultrasound systems currently being evaluated include wireless transducers capable of continuously monitoring hemodynamic parameters. A critical component of this development is the application of AI. Self-learning machine systems can assist the optimization of the acquisition and interpretation of ultrasound images. In this way, diagnostic accuracy, intra/inter-rater variability can be improved.

Moreover, the application of AI may even allow clinical experts to examine a patient from a distance, such as in an ambulance. In this study, the LVivo tool is validated as an online AI tool. However, a vital component for further success is missing: a grading system for image quality. By providing this, a non-echocardiographer does not need to differentiate between optimal and sub-optimal quality to interpret the acquired image correctly. If, for example, the quality is insufficient for correct quantification and interpretation, the software could give this feedback to the user and suggest a new acquisition.

Furthermore, the diversity of HHE applications will be comprehensive, varying from an additional diagnostic tool to obtaining information at the patient's bedside in a time and cost-effective way. For example, vital signs could be uploaded wirelessly into the electronic patient record system. Moreover, applying an HHE device, such as the Lumify, for pre-and post-operative screening is also one of the many possibilities. With the emergence of new devices for continuous cardiac monitoring, research increasingly focuses on evaluating the trending ability rather than the absolute accuracy. The change in SV over time can be more interesting than its absolute value, especially during cardiac surgery because of an increased risk of cardiovascular comorbidity or during the ICU stay of a patient.[70][82] Therefore, future research should focus on evaluating the trending ability to make bedside cardiac monitoring with HHE feasible. Furthermore, HHE should be validated on patients who are less optimally positioned and mechanically ventilated to evaluate how this affects the performance of the HHE device since these are factors are known for interfering with ultrasound image quality.[83]

Limitations

Our study had several limitations. First of all, cardiac parameters were based on single beat analysis. If multiple beats had been used, results would have been more reliable, considering SV variation due to respiration. However, the expiratory hold manoeuvre was performed, minimalizing the effect of respiratory variation. Furthermore, only patients in sinus rhythm were studied. Therefore, these results cannot be extrapolated to patients with irregular rhythms. In addition to this, patients had a relatively low BMI, which may not represent the average population. Subsequently, the predefined acceptable range for bias (10%) and mean error (15% or 30%) are a matter of discussion. Depending on the clinical application, the limits can be set to be more or less strict thresholds.[84][85] Moreover, expert sonographers conducted all examinations, and a high reproducibility was obtained in this study. Reproducibility may decrease with less experienced observers. Image quality assessment was performed by a single observer. For more reliable results an additional observer should have also assessed the image quality. Furthermore, we did not perform a dynamic evaluation of hemodynamic variables as participants were not examined over time or during preload challenges. Finally, the use of 3D and SE TTE was used as the reference technique, while CMR is currently considered the gold standard in evaluating cardiac chamber volumes.

X. Conclusion

Assessment of the left ventricular function with HHE is both challenging and promising. The results suggest excellent consistency, high image quality and a clinically acceptable precision for HHE compared to SE. Still, the accuracy exceeds the range of 10% except for SV measurements. Therefore, HHE shows great potential for LVEF quantification and monitoring of SV in point of care settings. However, results also show that LVivo software is not interchangeable with other quantification tools used in this study. Additional studies investigating the application of HHE and LVivo under difficult hemodynamic conditions are still needed for future application as a monitoring device, while studies comparing quantification of LV function from HHE images to CMR can provide more scientific underpinning for using HHE in diagnostic applications.

XI. References

[1] M. L. N. G. Malbrain, J. Huygh, Y. Peeters, and J. Bernards, "Hemodynamic monitoring in the critically ill: An overview of current cardiac output monitoring methods," *F1000Research*, vol. 5. Faculty of 1000 Ltd, p. 2855, 2016, doi: 10.12688/f1000research.8991.1.

[2] S. G. Sakka, K. Reinhart, and A. Meier-Hellmann, "Comparison of pulmonary artery and arterial thermodilution cardiac output in critically ill patients," *Intensive Care Med.*, vol. 25, no. 8, pp. 843–846, 1999, doi: 10.1007/s001340050962.

[3] M. Østergaard, J. Nielsen, J. P. Rasmussen, and P. G. Berthelsen, "Cardiac output - Pulse contour analysis vs. pulmonary artery thermodilution," *Acta Anaesthesiol. Scand.*, vol. 50, no. 9, pp. 1044–1049, Oct. 2006, doi: 10.1111/j.1399-6576.2006.01080.x.

[4] G. N. Andersen, B. O. Haugen, T. Graven, Ø. Salvesen, O. C. Mjølstad, and H. Dalen, "Feasibility and reliability of point-of-care pocket-sized echocardiography," *Eur. Hear. J. - Cardiovasc. Imaging*, vol. 12, no. 9, pp. 665–670, Sep. 2011, doi: 10.1093/ejechocard/jer108.

[5] C. Prinz and J. U. Voigt, "Diagnostic Accuracy of a Hand-Held Ultrasound Scanner in Routine Patients Referred for Echocardiography," *J. Am. Soc. Echocardiogr.*, vol. 24, no. 2, pp. 111–116, Feb. 2011, doi: 10.1016/J.ECHO.2010.10.017.

[6] P. Gudmundsson, E. Rydberg, R. Winter, and R. Willenheimer, "Visually estimated left ventricular ejection fraction by echocardiography is closely correlated with formal quantitative methods," *Int. J. Cardiol.*, vol. 101, no. 2, pp. 209–212, May 2005, doi: 10.1016/j.ijcard.2004.03.027.

[7] H. P. Kühl *et al.*, "High-resolution transthoracic real-time three-dimensional echocardiography: Quantitation of cardiac volumes and function using semi-automatic border detection and comparison with cardiac magnetic resonance imaging," *J. Am. Coll. Cardiol.*, vol. 43, no. 11, pp. 2083–2090, Jun. 2004, doi: 10.1016/j.jacc.2004.01.037.

[8] M. DK and D. VJ, "Normal Organ Weights in Women: Part I-The Heart," *Am. J. Forensic Med. Pathol.*, vol. 36, no. 3, pp. 176–181, Sep. 2015, doi: 10.1097/PAF.0000000000000174.

[9] M. DK and D. VJ, "Normal organ weights in men: part I-the heart," *Am. J. Forensic Med. Pathol.*, vol. 33, no. 4, pp. 362–367, Dec. 2012, doi: 10.1097/PAF.0B013E31823D298B.

[10] I. Ogobuiro, C. J. Wehrle, and F. Tuma, "Anatomy, Thorax, Heart Coronary Arteries," *StatPearls*, Jul. 2021, Accessed: Sep. 06, 2021. [Online]. Available: https://www.ncbi.nlm.nih.gov/books/NBK534790/.

[11] S. D. Joshi, S. S. Joshi, and S. A. Athavale, "Origins of the Coronary Arteries and Their Significance," *Clinics*, vol. 65, no. 1, p. 79, 2010, doi: 10.1590/S1807-59322010000100012.

[12] S. M. Chrysafides, S. Bordes, and S. Sharma, "Physiology, Resting Potential," *StatPearls*, Apr. 2021, Accessed: Sep. 06, 2021. [Online]. Available: https://www.ncbi.nlm.nih.gov/books/NBK538338/.

[13] A. Saxton, M. A. Tariq, and B. Bordoni, "Anatomy, Thorax, Cardiac Muscle," *StatPearls*, Aug. 2021, Accessed: Sep. 06, 2021. [Online]. Available: https://www.ncbi.nlm.nih.gov/books/NBK535355/.

[14] M. N. Berman and A. Bhardwaj, *Physiology, Left Ventricular Function*. StatPearls Publishing, 2019.

[15] T. C. McDevitt *et al.*, "In vitro generation of differentiated cardiac myofibers on micropatterned laminin surfaces," *J. Biomed. Mater. Res.*, vol. 60, no. 3, pp. 472–479, Jun. 2002, doi: 10.1002/jbm.1292.

[16] X. Zhang, P. Haynes, K. S. Campbell, and J. F. Wenk, "Numerical Evaluation of Myofiber Orientation and Transmural Contractile Strength on Left Ventricular Function," *J. Biomech. Eng.*, vol. 137, no. 4, p. 0445021, Apr. 2015, doi: 10.1115/1.4028990.

[17] Y. Nagata *et al.*, "Impact of image quality on reliability of the measurements of left

ventricular systolic function and global longitudinal strain in 2D echocardiography," *Echo Res. Pract.*, vol. 5, no. 1, p. 27, Mar. 2018, doi: 10.1530/ERP-17-0047.
[18] R. A. L. Dampney, "Central neural control of the cardiovascular system: current perspectives," *https://doi.org/10.1152/advan.00027.2016*, vol. 40, no. 3, pp. 283–296, 2016, doi: 10.1152/ADVAN.00027.2016.
[19] M. K. Kerstens, M. Wijnberge, B. F. Geerts, A. P. Vlaar, and D. P. Veelo, "Netherlands Journal of Critical Care Non-invasive cardiac output monitoring techniques in the ICU," 2018. Accessed: Feb. 09, 2021. [Online]. Available: http://www.deltexmedical.com/downloads/clinicaleducationguides.
[20] X. Monnet, P. E. Marik, and J. L. Teboul, "Prediction of fluid responsiveness: an update," *Annals of Intensive Care*, vol. 6, no. 1. Springer Verlag, p. 111, Dec. 01, 2016, doi: 10.1186/s13613-016-0216-7.
[21] A. Hussey, L. Eastaugh, and R. G. Weintraub, "Hemodynamic Adaptive Mechanisms in Heart Failure," *Hear. Fail. Child Young Adult From Bench to Bedside*, pp. 59–74, 2018, doi: 10.1016/B978-0-12-802393-8.00005-3.
[22] J. Ross, "Mechanisms of cardiac contraction. What roles for preload, afterload and inotropic state in heart failure?," *Eur. Heart J.*, vol. 4, no. Suppl. A, pp. 19–28, 1983, doi: 10.1093/eurheartj/4.suppl_a.19.
[23] P. P. de Tombe and H. E. D. J. ter Keurs, "The Velocity of Cardiac Sarcomere Shortening; Mechanisms and Implications," *J. Muscle Res. Cell Motil.*, vol. 33, no. 6, p. 431, Dec. 2012, doi: 10.1007/S10974-012-9310-0.
[24] L. M. Hanft and K. S. McDonald, "Length dependence of force generation exhibit similarities between rat cardiac myocytes and skeletal muscle fibres," *J. Physiol.*, vol. 588, no. Pt 15, p. 2891, Aug. 2010, doi: 10.1113/JPHYSIOL.2010.190504.
[25] R. Salem, F. Vallee, M. Rusca, and A. Mebazaa, "Hemodynamic monitoring by echocardiography in the ICU: The role of the new echo techniques," *Current Opinion in Critical Care*, vol. 14, no. 5. pp. 561–568, Oct. 2008, doi: 10.1097/MCC.0b013e32830e6d81.
[26] I. Gotsman, D. Zwas, C. Lotan, and A. Keren, "Heart Failure and Preserved Left Ventricular Function: Long Term Clinical Outcome," *PLoS One*, vol. 7, no. 7, Jul. 2012, doi: 10.1371/JOURNAL.PONE.0041022.
[27] A. Kosaraju, A. Goyal, Y. Grigorova, and A. N. Makaryus, "Left Ventricular Ejection Fraction," *StatPearls*, Jul. 2021, Accessed: Sep. 06, 2021. [Online]. Available: https://www.ncbi.nlm.nih.gov/books/NBK459131/.
[28] A. Groenewegen, F. H. Rutten, A. Mosterd, and A. W. Hoes, "Epidemiology of heart failure," *Eur. J. Heart Fail.*, vol. 22, no. 8, pp. 1342–1356, Aug. 2020, doi: 10.1002/EJHF.1858.
[29] P. Ponikowski *et al.*, "2016 ESC Guidelines for the diagnosis and treatment of acute and chronic heart failureThe Task Force for the diagnosis and treatment of acute and chronic heart failure of the European Society of Cardiology (ESC)Developed with the special contribution of the Heart Failure Association (HFA) of the ESC," *Eur. Heart J.*, vol. 37, no. 27, pp. 2129–2200, Jul. 2016, doi: 10.1093/EURHEARTJ/EHW128.
[30] S. Hajouli and D. Ludhwani, "Heart Failure And Ejection Fraction," *StatPearls*, Aug. 2021, Accessed: Aug. 26, 2021. [Online]. Available: https://www.ncbi.nlm.nih.gov/books/NBK553115/.
[31] F. R. Heinzel, F. Hohendanner, G. Jin, S. Sedej, and F. Edelmann, "Myocardial Hypertrophy and Its Role in Heart Failure with Preserved Ejection Fraction," *J. Appl. Physiol.*, vol. 119, no. 10, p. 1233, Nov. 2015, doi: 10.1152/JAPPLPHYSIOL.00374.2015.
[32] C. Gutierrez and D. G. Blanchard, "Diastolic Heart Failure: The Challenges of Diagnosis and Treatment," *Am. Fam. Physician*, vol. 69, no. 11, pp. 2609–2616, Jun. 2004, Accessed: Sep. 02, 2021. [Online]. Available: www.aafp.org/afp.
[33] A. Saxena *et al.*, "Value of Hemodynamic Monitoring in Patients with Cardiogenic Shock Undergoing Mechanical Circulatory Support," *Circulation*, pp. 1184–1197, Apr. 2020, doi: 10.1161/CIRCULATIONAHA.119.043080.
[34] Y. J. Cho, C. H. Koo, T. K. Kim, D. M. Hong, and Y. Jeon, "Comparison of cardiac output measures by transpulmonary thermodilution, pulse contour analysis, and pulmonary artery thermodilution during off-pump coronary artery bypass surgery: a subgroup analysis of the cardiovascular anaesthesia registry at a single tertiary

centre," *J. Clin. Monit. Comput.*, vol. 30, no. 6, pp. 771–782, Dec. 2016, doi: 10.1007/s10877-015-9784-6.
[35] M. K. Kerstens, M. Wijnberge, B. F. Geerts, A. P. Vlaar, and D. P. Veelo, "Netherlands Journal of Critical Care Non-invasive cardiac output monitoring techniques in the ICU," *NETH J CRIT CARE*, vol. 26, 2018, Accessed: Sep. 23, 2021. [Online]. Available: http://www.deltexmedical.com/downloads/clinicaleducationguides.
[36] A. K, P. PJ, and M. ML, "The accuracy of noninvasive cardiac output and pressure measurements with finger cuff: a concise review," *Curr. Opin. Crit. Care*, vol. 21, no. 3, pp. 232–239, Jun. 2015, doi: 10.1097/MCC.0000000000000198.
[37] M. X *et al.*, "The estimation of cardiac output by the Nexfin device is of poor reliability for tracking the effects of a fluid challenge," *Crit. Care*, vol. 16, no. 5, Oct. 2012, doi: 10.1186/CC11846.
[38] B. J. Kimura, "Point-of-care cardiac ultrasound techniques in the physical examination: Better at the bedside," *Heart*, vol. 103, no. 13. BMJ Publishing Group, pp. 987–994, Jul. 01, 2017, doi: 10.1136/heartjnl-2016-309915.
[39] P. Mercado *et al.*, "Transthoracic echocardiography: An accurate and precise method for estimating cardiac output in the critically ill patient," *Crit. Care*, vol. 21, no. 1, Jun. 2017, doi: 10.1186/s13054-017-1737-7.
[40] I. Edler and K. Lindström, "The history of echocardiography," *Ultrasound Med. Biol.*, vol. 30, no. 12, pp. 1565–1644, Dec. 2004, doi: 10.1016/S0301-5629(99)00056-3.
[41] F. M. Abu-Zidan, A. F. Hefny, and P. Corr, "Clinical ultrasound physics," *J. Emergencies, Trauma Shock*, vol. 4, no. 4, p. 501, Oct. 2011, doi: 10.4103/0974-2700.86646.
[42] J. Shriki, "Ultrasound Physics," *Crit. Care Clin.*, vol. 30, pp. 1–24, 2014, doi: 10.1016/j.ccc.2013.08.004.
[43] S. W. Rienstra and A. Hirschberg, "An Introduction to Acoustics," 2021.
[44] V. M. Do Nascimento, V. Lúcia, S. Nantes Button, J. M. Maia, E. T. Costa, and E. J. V Oliveira, "Influence of Backing and Matching Layers in Ultrasound Transducers Performance," 2003, Accessed: Sep. 06, 2021. [Online]. Available: http://spiedl.org/terms.
[45] Alexander, "Resolution in ultrasound imaging," *Contin. Educ. Anaesth. Crit. Care Pain*, vol. 11, pp. 186–192, 2011, doi: 10.1093/bjaceaccp/mkr030.
[46] M. Toulemonde, "New beamforming strategy for improved ultrasound imaging : application to biological tissues nonlinear imaging," *undefined*, 2014.
[47] L. Demi, "Practical Guide to Ultrasound Beam Forming: Beam Pattern and Image Reconstruction Analysis," *Appl. Sci. 2018, Vol. 8, Page 1544*, vol. 8, no. 9, p. 1544, Sep. 2018, doi: 10.3390/APP8091544.
[48] L. De Vos, V. De Herdt, and F. Timmermans, "Misdiagnosis or Missed Diagnosis: Digging Out the 'Near-Field Clutter' Artifact in a Patient with Stroke," *CASE*, vol. 4, no. 1, pp. 2–6, Feb. 2020, doi: 10.1016/J.CASE.2019.10.007.
[49] R. M. Lang *et al.*, "Recommendations for cardiac chamber quantification by echocardiography in adults: An update from the American Society of Echocardiography and the European Association of Cardiovascular Imaging," *J. Am. Soc. Echocardiogr.*, vol. 28, no. 1, pp. 1-39.e14, Jan. 2015, doi: 10.1016/j.echo.2014.10.003.
[50] G. H. Gundersen *et al.*, "Adding point of care ultrasound to assess volume status in heart failure patients in a nurse-led outpatient clinic. A randomised study," *Heart*, vol. 102, no. 1, pp. 29–34, Jan. 2016, doi: 10.1136/heartjnl-2015-307798.
[51] S. D. Solomon *et al.*, "Influence of ejection fraction on cardiovascular outcomes in a broad spectrum of heart failure patients," *Circulation*, vol. 112, no. 24, pp. 3738–3744, Dec. 2005, doi: 10.1161/CIRCULATIONAHA.105.561423.
[52] K. L. Mok, "Make it SIMPLE: Enhanced shock management by focused cardiac ultrasound," *Journal of Intensive Care*, vol. 4, no. 1. BioMed Central Ltd., pp. 1–17, Aug. 15, 2016, doi: 10.1186/s40560-016-0176-x.
[53] M. A. Oyama and D. D. Sisson, "ASSESSMENT OF CARDIAC CHAMBER SIZE USING ANATOMIC M-MODE," *Vet. Radiol. Ultrasound*, vol. 46, no. 4, pp. 331–336, 2005, doi: 10.1111/j.1740-8261.2005.00062.x.
[54] Cacciapuoti, "Echocardiographic evaluation of ejection fraction: 3DE versus 2DE and M-Mode," *Hear. Views*, vol. 9, no. 2, p. 71, 2008, Accessed: Feb. 08, 2021. [Online].

Available: https://www.heartviews.org/article.asp?issn=1995-705X;year=2008;volume=9;issue=2;spage=71;epage=79;aulast=Cacciapuoti.
[55] I. Edler and K. Lindström, "The history of echocardiography," *Ultrasound Med. Biol.*, vol. 30, no. 12, pp. 1565–1644, 2004, doi: 10.1016/S0301-5629(99)00056-3.
[56] V. C.-C. Wu and M. Takeuchi, "Three-Dimensional Echocardiography: Current Status and Real-Life Applications," *Acta Cardiol. Sin.*, vol. 33, no. 2, p. 107, Mar. 2017, doi: 10.6515/ACS20160818A.
[57] W. Tsang *et al.*, "Transthoracic 3D Echocardiographic Left Heart Chamber Quantification Using an Automated Adaptive Analytics Algorithm," *JACC Cardiovasc. Imaging*, vol. 9, no. 7, pp. 769–782, Jul. 2016, doi: 10.1016/j.jcmg.2015.12.020.
[58] A. Bernard *et al.*, "3D echocardiographic reference ranges for normal left ventricular volumes and strain: Results fromthe EACVI NORRE study," *Eur. Heart J. Cardiovasc. Imaging*, vol. 18, no. 4, pp. 475–483, Apr. 2017, doi: 10.1093/ehjci/jew284.
[59] M. P. Kulkarni and D. Madathil, "A REVIEW OF ECHOCARDIOGRAPHIC IMAGE SEGMENTATION TECHNIQUES FOR LEFT VENTRICULAR STUDY," vol. 13, no. 10, 2018, Accessed: Jun. 01, 2021. [Online]. Available: www.arpnjournals.com.
[60] R. Samtani *et al.*, "Validation of a Novel Artificial Intelligence Left Ventricular Ejection Fraction Quantification Software (LVivo EF by DIA®) by Cardiac MRI."
[61] A. Davis *et al.*, "Artificial Intelligence and Echocardiography: A Primer for Cardiac Sonographers," *Journal of the American Society of Echocardiography*, vol. 33, no. 9. Mosby Inc., pp. 1061–1066, Sep. 01, 2020, doi: 10.1016/j.echo.2020.04.025.
[62] S. Ali and T. Bushari, "Validation of the accuracy of handheld echocardiography for diagnosis of congenital heart disease," *Ann. Pediatr. Cardiol.*, vol. 11, no. 3, pp. 250–254, Sep. 2018, doi: 10.4103/apc.APC_159_17.
[63] V. Di Bello *et al.*, "Incremental Value of Pocket-Sized Echocardiography in Addition to Physical Examination during Inpatient Cardiology Evaluation: A Multicenter Italian Study (SIEC)," *Echocardiography*, vol. 32, no. 10, pp. 1463–1470, Oct. 2015, doi: 10.1111/echo.12910.
[64] F. Thomas, N. Flint, S. Setareh-Shenas, F. Rader, S. L. Kobal, and R. J. Siegel, "Accuracy and Efficacy of Hand-Held Echocardiography in Diagnosing Valve Disease: A Systematic Review," *American Journal of Medicine*, vol. 131, no. 10. Elsevier Inc., pp. 1155–1160, Oct. 01, 2018, doi: 10.1016/j.amjmed.2018.04.043.
[65] M. A. Chamsi-Pasha, P. P. Sengupta, and W. A. Zoghbi, "Handheld Echocardiography," *Circulation*, vol. 136, no. 22, pp. 2178–2188, Nov. 2017, doi: 10.1161/CIRCULATIONAHA.117.026622.
[66] Y. Stenberg, L. Wallinder, A. Lindberg, J. Walldén, M. Hultin, and T. Myrberg, "Preoperative Point-of-Care Assessment of Left Ventricular Systolic Dysfunction with Transthoracic Echocardiography," *Anesth. Analg.*, pp. 717–725, 2021, doi: 10.1213/ANE.0000000000005263.
[67] I. Cavallari, S. Mega, C. Goffredo, G. Patti, M. Chello, and G. Di Sciascio, "Hand-held echocardiography in the setting of pre-operative cardiac evaluation of patients undergoing non-cardiac surgery: results from a randomized pilot study," *Int. J. Cardiovasc. Imaging*, vol. 31, no. 5, pp. 995–1000, Jun. 2015, doi: 10.1007/s10554-015-0656-4.
[68] S. Giusca *et al.*, "Accuracy of Handheld Echocardiography for Bedside Diagnostic Evaluation in a Tertiary Cardiology Center: Comparison with Standard Echocardiography," *Echocardiography*, vol. 28, no. 2, pp. 136–141, Feb. 2011, doi: 10.1111/j.1540-8175.2010.01310.x.
[69] A. J. Labovitz *et al.*, "Focused cardiac ultrasound in the emergent setting: A consensus statement of the American society of Echocardiography and American College of Emergency Physicians," in *Journal of the American Society of Echocardiography*, Dec. 2010, vol. 23, no. 12, pp. 1225–1230, doi: 10.1016/j.echo.2010.10.005.
[70] J. Kobe, N. Mishra, V. K. Arya, W. Al-Moustadi, W. Nates, and B. Kumar, "Cardiac Output Monitoring: Technology and Choice," *Ann. Card. Anaesth.*, vol. 22, no. 1, p. 6, Jan. 2019, doi: 10.4103/ACA.ACA_41_18.
[71] L. J. Montenij, W. F. Buhre, J. R. Jansen, C. L. Kruitwagen, and E. E. De Waal, "Methodology of method comparison studies evaluating the validity of cardiac output monitors: A stepwise approach and checklist," *British Journal of Anaesthesia*, vol.

116, no. 6. Oxford University Press, pp. 750–758, Jun. 19, 2016, doi: 10.1093/bja/aew094.
[72] L. J. Montenij, W. F. Buhre, J. R. Jansen, C. L. Kruitwagen, and E. E. De Waal, "Methodology of method comparison studies evaluating the validity of cardiac output monitors: A stepwise approach and checklist," *British Journal of Anaesthesia*, vol. 116, no. 6. Oxford University Press, pp. 750–758, Jun. 19, 2016, doi: 10.1093/bja/aew094.
[73] G. F. Reed, F. Lynn, and B. D. Meade, "Use of Coefficient of Variation in Assessing Variability of Quantitative Assays," *Clin. Diagn. Lab. Immunol.*, vol. 9, no. 6, p. 1235, Nov. 2002, doi: 10.1128/CDLI.9.6.1235-1239.2002.
[74] T. K. Koo and M. Y. Li, "A Guideline of Selecting and Reporting Intraclass Correlation Coefficients for Reliability Research," *J. Chiropr. Med.*, vol. 15, no. 2, pp. 155–163, Jun. 2016, doi: 10.1016/j.jcm.2016.02.012.
[75] P. E. Shrout and J. L. Fleiss, "Intraclass correlations: Uses in assessing rater reliability," *Psychol. Bull.*, vol. 86, no. 2, pp. 420–428, Mar. 1979, doi: 10.1037/0033-2909.86.2.420.
[76] X. Han, "On Statistical Measures for Data Quality Evaluation," *J. Geogr. Inf. Syst.*, vol. 12, no. 03, pp. 178–187, 2020, doi: 10.4236/JGIS.2020.123011.
[77] R. O. Mada, P. Lysyansky, A. M. Daraban, J. Duchenne, and J. U. Voigt, "How to Define End-Diastole and End-Systole?: Impact of Timing on Strain Measurements," *JACC Cardiovasc. Imaging*, vol. 8, no. 2, pp. 148–157, Feb. 2015, doi: 10.1016/J.JCMG.2014.10.010.
[78] N. Benyounes *et al.*, "Left Ventricular End Diastolic Volume and Ejection Fraction Calculation: Correlation between Three Echocardiographic Methods," *Cardiol. Res. Pract.*, vol. 2020, 2020, doi: 10.1155/2020/8076582.
[79] D. Medvedofsky *et al.*, "Three-dimensional echocardiographic quantification of the left-heart chambers using an automated adaptive analytics algorithm: Multicentre validation study," *Eur. Heart J. Cardiovasc. Imaging*, vol. 19, no. 1, pp. 47–58, Jan. 2018, doi: 10.1093/ehjci/jew328.
[80] V. Mor-Avi *et al.*, "Real-Time 3-Dimensional Echocardiographic Quantification of Left Ventricular Volumes. Multicenter Study for Validation With Magnetic Resonance Imaging and Investigation of Sources of Error," *JACC Cardiovasc. Imaging*, vol. 1, no. 4, pp. 413–423, Jul. 2008, doi: 10.1016/J.JCMG.2008.02.009.
[81] F. M. Asch *et al.*, "Automated Echocardiographic Quantification of Left Ventricular Ejection Fraction Without Volume Measurements Using a Machine Learning Algorithm Mimicking a Human Expert," *Circ. Cardiovasc. Imaging*, vol. 12, no. 9, p. 9303, Sep. 2019, doi: 10.1161/CIRCIMAGING.119.009303.
[82] C. LA, L. A, and H. AM, "A critical review of the ability of continuous cardiac output monitors to measure trends in cardiac output," *Anesth. Analg.*, vol. 111, no. 5, pp. 1180–1192, 2010, doi: 10.1213/ANE.0B013E3181F08A5B.
[83] P. Vignon *et al.*, "Diagnostic ability of hand-held echocardiography in ventilated critically ill patients," *Crit. Care*, vol. 7, no. 5, p. R84, Oct. 2003, doi: 10.1186/CC2360.
[84] K. Y, Y. K, I. T, I. Y, S. M, and O. Y, "Clinical comparison of an echocardiograph-derived versus pulse counter-derived cardiac output measurement in abdominal aortic aneurysm surgery," *J. Cardiothorac. Vasc. Anesth.*, vol. 26, no. 2, pp. 223–226, Apr. 2012, doi: 10.1053/J.JVCA.2011.07.011.
[85] L. J. Montenij *et al.*, "Arterial pressure waveform analysis versus thermodilution cardiac output measurement during open abdominal aortic aneurysm repair: A prospective observational study," *Eur. J. Anaesthesiol.*, vol. 32, no. 1, pp. 13–19, 2015, doi: 10.1097/EJA.0000000000000160.

XII. Appendix A

LVivo tracings compared with AS tracings

As the results show in Tables 5 & 6, the AS quantification software overestimates the EDV and SV compared to 2DCPA and LVivo. However, AS measurements compared to 3DE HM measurements do not indicate that AS overestimates any parameters. Since it is well-known from previous studies that 2DE underestimates cardiac volumes compared to 3DE, this is an interesting observation. Therefore, it is relevant to investigate what causes the AS software to calculate higher values than the other 2DE quantification software, especially LVivo software since it is also a fully automatic quantification software. The first and most obvious explanation for this overestimation could be that the AS software has a broader trace of the ED endocardial border and therefore measures bigger volumes. The second explanation could be that the AS software algorithm contains an enlargement factor. However, the manufacturer has not disclosed the AS software, so its inner workings are unknown. To investigate these possible explanations, we need to look more closely at the data. Therefore, we devised the following approach: count the number of pixels of the endocardial tracing in the ED frame for both LVivo and AS tracing. Unfortunately, neither software packages (AS & LVivo) support the export of DICOM files. Therefore, the analysis required a different approach. We used the following:

1. Calculate the scaling factor of an AS SE image vs LVivo SE image.
2. Calculate the length of the left ventricle in the number of pixels from the apex until the basis of the mitral valve.
3. Calculate the width of the left ventricle in the number of pixels on the level of (1) 2/5, (2) 3/5 and (3) 4/5 length of the horizontal line determined in step two.
4. The difference in length and widths (3) of the left ventricle for AS and LVivo measurements is calculated, with the factor calculated in step one taken into account.

A small tool was developed in MatLab for this assessment.
To better understand these four steps, they are elaborated below.

Step 1. Determination of Scaling factor

The exported video of the LVivo quantification was a screen recording (Figure 27 A) which gave a signification smaller visualization of the A4CH view than the exported video from AS (Figure 27 B). To make an equivalent comparison of the tracing, the influence of the image size should be eliminated. Therefore, a scaling factor was determined by measuring the diameter of the white circle in the top left corner of the AS image and LVivo image, see Figure 27. This circle displays the angle of the transmitted ultrasound beam and is, therefore, a constant factor for each image and should ideally be equal in size for both LVivo and AS. This step is repeated three times to determine the intra-observer variability of the factor determination.

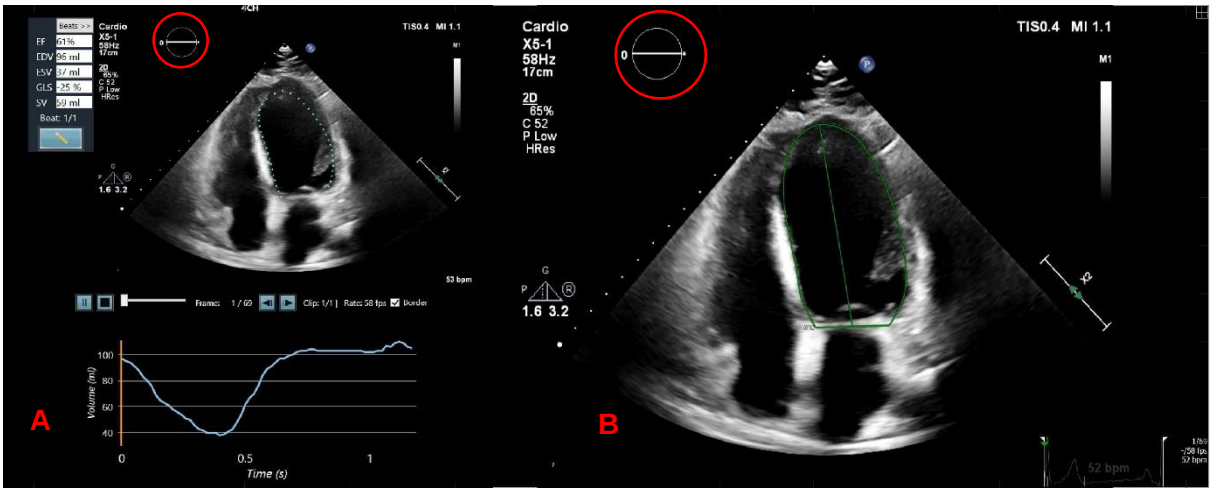

Figure 27. Example of an SE image quantified with A) Lvivo software; B) AS software. The red circle indicates the object in both images, which is used for calculating the scaling factor.

Step 2. Calculation of the longitudinal length
Calculation of the longitudinal length of the LV cavity is done differently for the LVivo image and the AS image. For example, the LVivo calculation consisted of four steps, see Figure 28A:

1) The investigator marks the highest point (close to the apex) of the parabola shaped tracing.
2) The left lower point and right lower point of the tracing are marked by the investigator.
3) The middle point between the left and right points is calculated
4) The length in number of pixels is automatically calculated between the highest point and the middle point

The AS calculation was more straightforward because the AS software visualizes a vertical line that represents the length of the LV cavity, see Figure 28 B. So, the top and bottom of this line are marked by the investigator. The length of the line is calculated in the number of pixels.

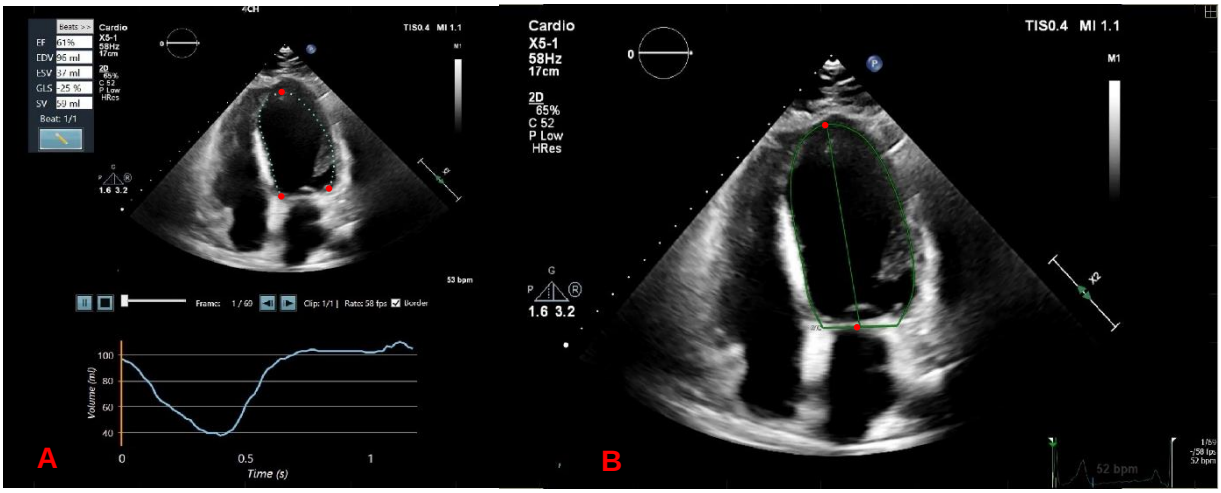

Figure 28. Example of how the longitudinal length of the LV cavity in the LVivo SE image (A) or the AS SE image (B) is calculated in step 2.

Step 3 Calculation of tracing width
Based on the length of the longitudinal line, three additional lines are drawn by the software in the image, on 2/5th, 3/5th and 4/5th length of the longitudinal line, see Figure 29. Finally, the investigator marks the intersections of the three lines with the endocardial border tracing of both the LVivo or AS software. In this way, the width is calculated on three different levels of the LV.

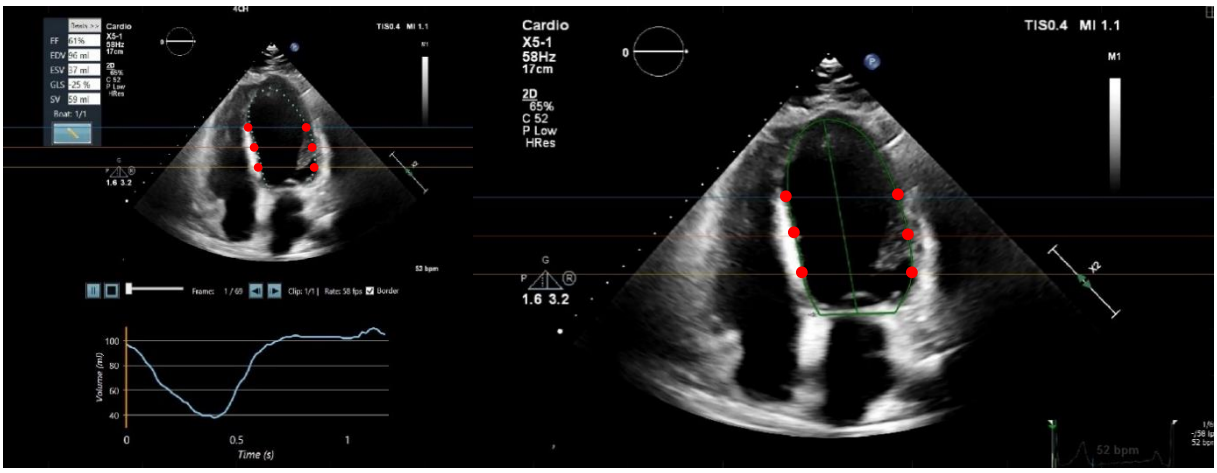

Figure 29. Example of how the width of the LV cavity is calculated for the Lvivo SE image (A); or the AS SE image (B)

Step 4 Difference in length and width of the tracing
Taking into account the scaling factor that is calculated in step one, the ratio for the longitudinal line and the width lines was calculated as:

$$Ratio\ (\%) = \frac{(number\ of\ pixels\ LVivo\ \times scaling\ factor) - number\ of\ pixels\ AS}{number\ of\ pixels\ AS} \times 100\%$$

The results show that AS makes a longer tracing of the endocardial border reflected by a significant ($p<0.05$) mean factor of -13.57% for the longitudinal line. Furthermore, are AS tracings also wide reflected by significant mean factors of -4.20%, -18.20% and -6.02% for the $2/5^{th}$, $3/5^{th}$ and $4/5^{th}$ line, respectively. This explains why the accuracy of the AS is not comparable with LVivo.

XIII. Appendix B

Effect of HHE image quality on quantification comparison between HHE and SE

This section investigates the effect of HHE image quality on the difference between HHE and SE quantification of SV and LVEF. Mean image quality is defined as the averaged image quality of one patient's three A4CH view recordings. Testing for normality with the Shapiro Wilkinson test showed a normal distribution, so Pearson's correlation coefficient (R) was used for correlation calculations. The analysed comparisons are listed below with corresponding scatterplots and correlation coefficients. To visualize the linear relationship between image quality and the absolute difference between SE and HHE for LVEF or SV, a regression line with the corresponding regression coefficient (R^2) is plotted.

SV - SE vs HHE (AS)
A4CH HHE image quality vs absolute difference in SV between SE (AS) and HHE (AS), shown in figure 30. R = 0,165 (p = 0,342)
LVEF - SE vs HHE (AS)
A4CH HHE image quality vs absolute difference in LVEF between SE (AS) and HHE (AS), shown in figure 31. R = -0,242 (p = 0,161)
SV- SE vs HHE (LVivo)
A4CH HHE image quality vs absolute difference in SV between SE (LVivo) and HHE (LVivo), shown in figure 32. R = 0,351 (p = 0,045)
LVEF – SE vs HHE (LVivo)
A4CH HHE image quality vs absolute difference in LVEF between SE (LVivo) and HHE (LVivo), shown in figure 33. R = 0,190 (p = 0,290)

Results show that only comparison of HHE A4CH image quality with the absolute difference of SV between SE and HHE (LVivo) shows a significant correlation. However, this correlation is weak. Hence, no relationship was found between image quality and the performance of HHE for LVEF or SV quantification compared to SE. Therefore, we can conclude that the quantification of SV and LVF with either AS or LVivo is not affected by A4CH HHE image quality. Due to time limitations the analysis only focused on the correlation between the mean image quality of A4CH views of HHE and the difference in SV or LVEF values between SE and HHE when quantified with AS or LVivo. The same analysis based on A2CH would also have been interesting. Furthermore, it would also be interesting to select the top best 50% of HHE images based on quality and perform the statistical analysis, as described in the VIII. methods section, again. In such a way, it can be assessed if accuracy and precision improve compared to the results shown in the IX. Results section.

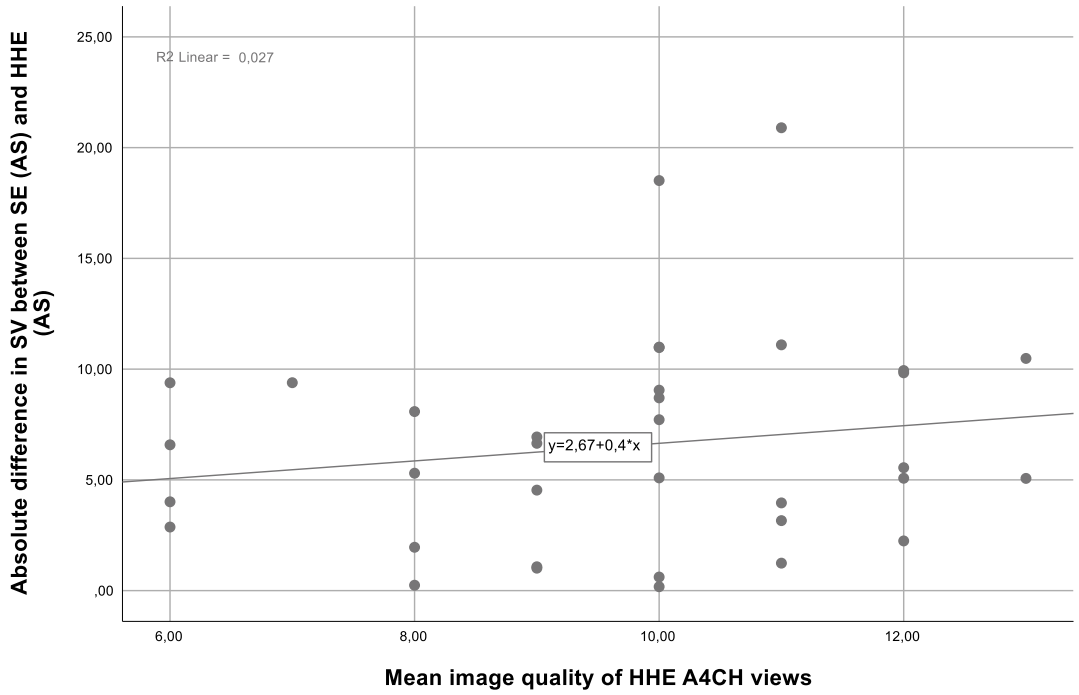

Figure 30. Scatterplot of the SV – SE vs HHE (AS) comparison.

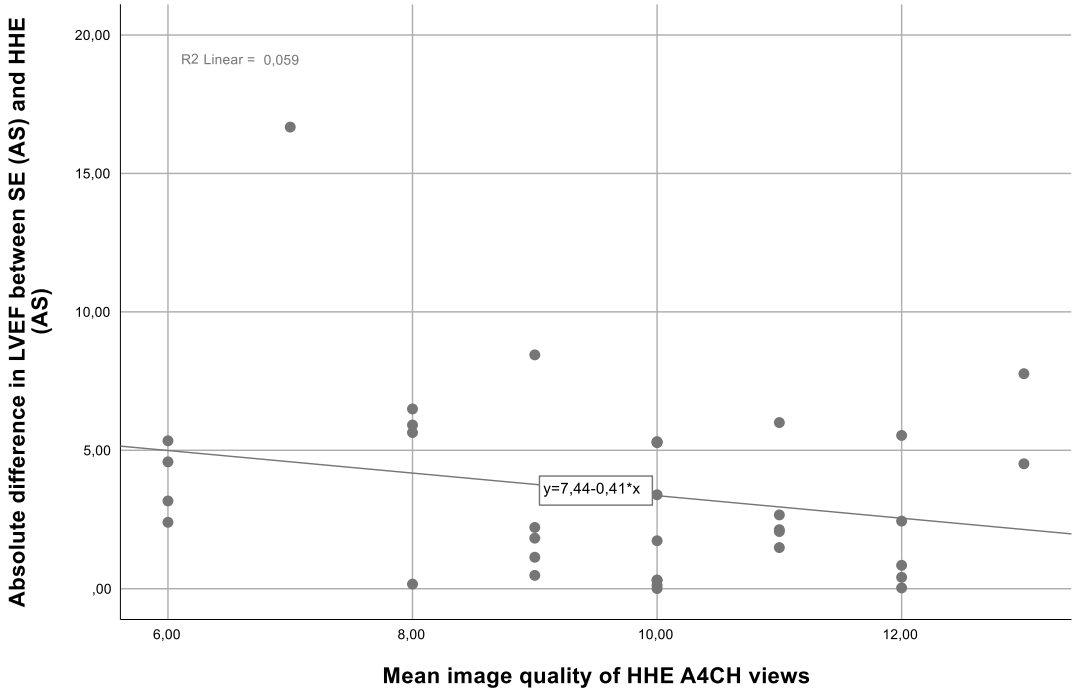

Figure 31. Scatterplot of the LVEF – SE vs HHE (AS) comparison.

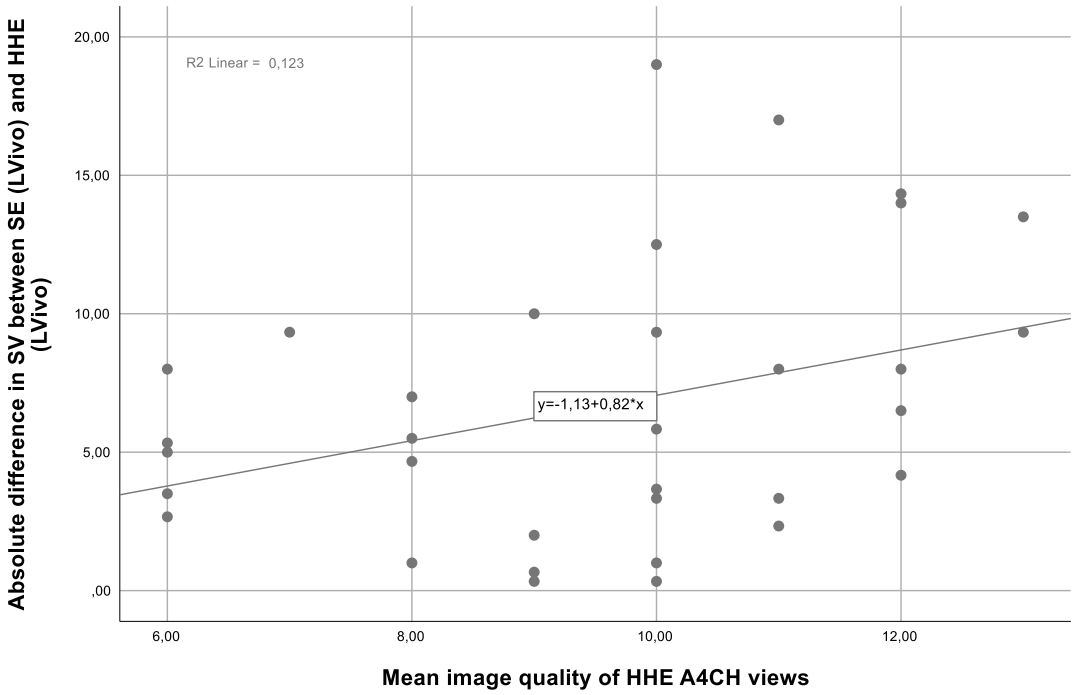

Figure 32. Scatterplot of the SV – SE vs HHE (LVivo) comparison.

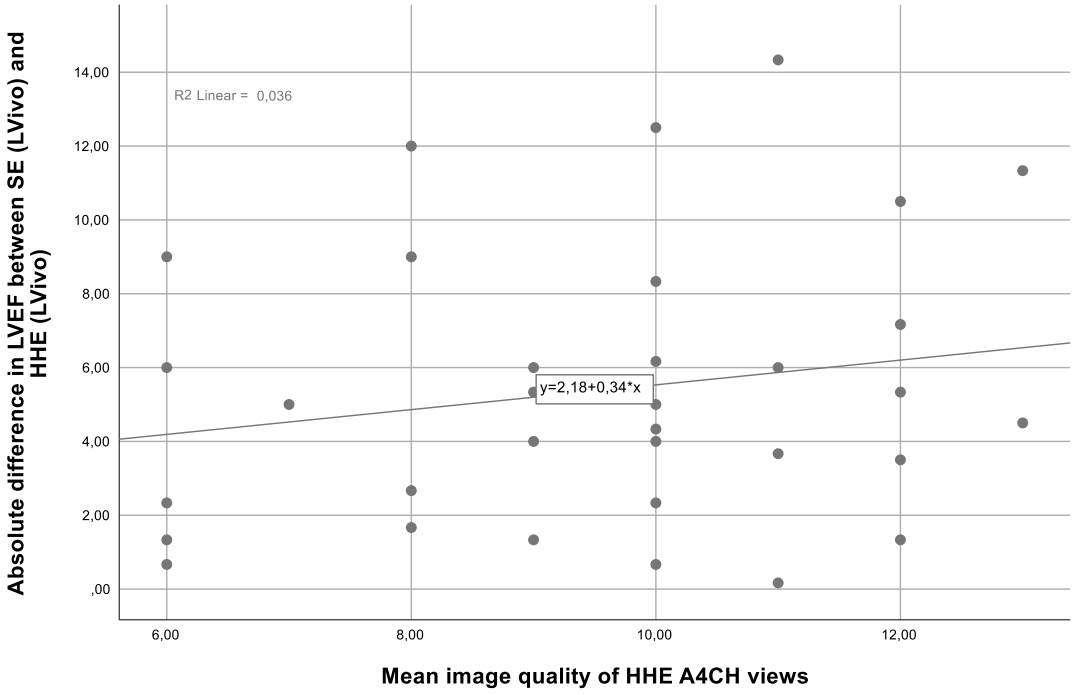

Figure 33. Scatterplot of the LVEF – SE vs HHE (LVivo) comparison.

XIV. Appendix C

LVivo™ - OPTIMAL SETTINGS

according to American Society of Echocardiography guidelines

Septal alignment
The interventricular septum should be parallel to the image plane.

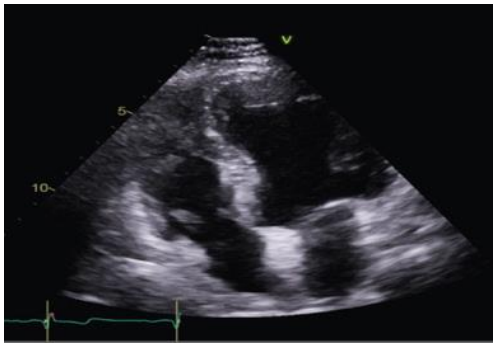

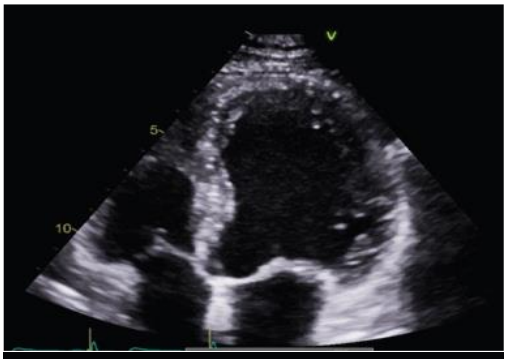

Endocardial visualization
At least 2/3 of the endocardium should be visualized.

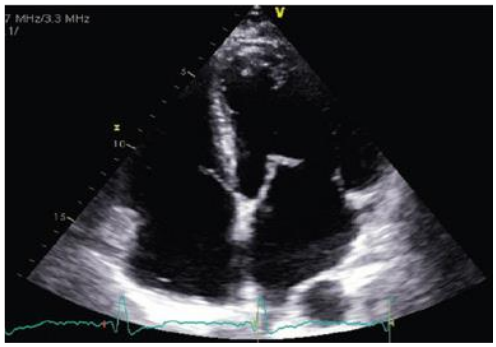

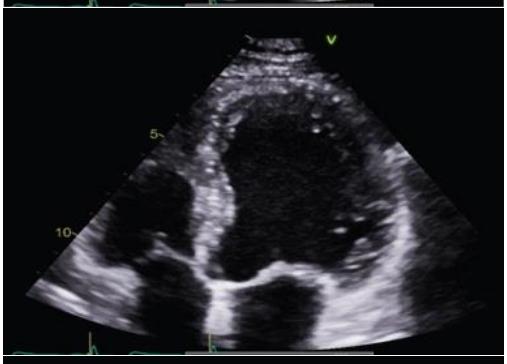

Depth
Proportion of LV-LA will be 2/3-1/3 (Optimum depth will be 14-18 cm).

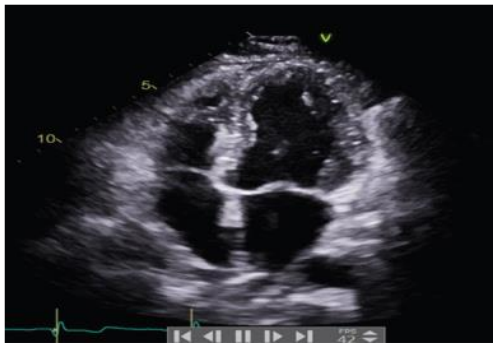

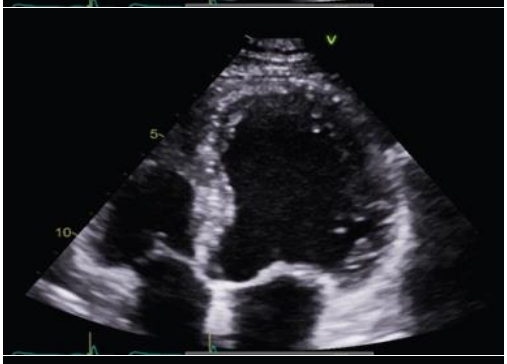

Avoiding foreshortening of the apex